THE UNIVERSITY OF TEXAS

LABORATORIES FOR ELECTRONICS AND RELATED SCIENCE RESEARCH

TUNNELING BETWEEN A METAL AND SILICON SEPARATED BY A POLYMER INSULATOR*

Technical Report No. 25

By

CARL W. WILMSEN**

WILLIAM H. HARTWIG+

September 15, 1966

*Supported in part by the Joint Services Electronics Program under Research Grant AF-AFOSR 766-66, the National Aeronautics and Space Administration Grants 8-11235 and NGR-44-012-043.

**Graduate Student, Candidate for Ph.D. degree in Electrical Engineering

+Professor of Electrical Engineering

ABSTRACT

This research investigates tunneling between a metal and silicon separated by an insulator (MIS structure) and develops a model describing the MIS current-voltage characteristics. Analysis shows that any model for MIS tunneling must consider the density of surface states and the formation of a depletion or accumulation layer in the silicon. The model shows that the electric field in the insulator controls the MIS current while the charge distribution in the silicon determines the insulator field.

For the experimental results presented in this report a polymerized silicone film formed the insulator. After establishing the technique of forming the polymer, metal - insulator - metal (MIM) junctions enabled study of the electrical properties of the polymer and characterization of MIM tunneling currents. The MIM characteristics permitted comparative analysis with MIS structures.

The experimental MIS curves on both N and P type silicon show the exponential dependence of current on voltage and they indicate that the mechanisms for MIM and MIS tunneling are quite similar. An asymmetric saturation of the MIS tunneling occurs. This is shown to be caused by the formation of a depletion layer on the semiconductor which forms

after completely charging the surface states. Experimental evidence verifies this model. The distinct roles played by the surface states, the depletion layer, insulator thickness, temperature and the work function of the field plate metal appears in the analysis.

TABLE OF CONTENTS

TABLE OF CONTENTS (Continued)

LIST OF ILLUSTRATIONS

LIST OF ILLUSTRATIONS (Continued)

LIST OF ILLUSTRATIONS (Continued)

LIST OF ILLUSTRATIONS (Continued)

LIST OF PLATES

CHAPTER I

Introduction

A. Tunneling Through an Insulating Barrier

Tunneling is the quantum mechanical phenomenon which allows electrons or holes to pass through an energy barrier. This differs from classical mechanics which requires the electron or hole to jump over the barrier (Schottky emission).[8] Fig. 1 illustrates these two processes.

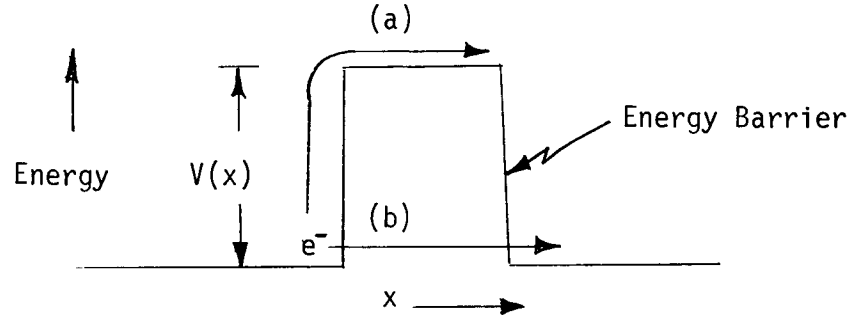

Figure 1. The two methods of overcoming a potential barrier.
(a) The electron must gain energy to jump the barrier (Schottky emission).
(b) The electron passes through the barrier (tunneling).

For the case of tunneling, consider a wave packet (an electron or hole) traveling toward a potential barrier. Schrödinger's time-independent wave equation[9a] describing the wave traveling in the x direction is:

$$(1)\quad \frac{d^2\psi}{dx^2} + K\left[E - eV(x)\right]\psi = 0$$

Where E is the expectation value or average of the total electron energy and V(x) describes the shape of the potential barrier. The wave packet

is of finite length and therefore is a summation of sine waves. To simplify the problem assume that the sum of all the wave packets striking the barrier takes the form of a single frequency sine wave of infinite extent.[10, 11] If the average energy of the wave striking the barrier is less than the barrier height then the wave will be partially reflected and partially transmitted. Fig. 2 illustrates the form of the solution.

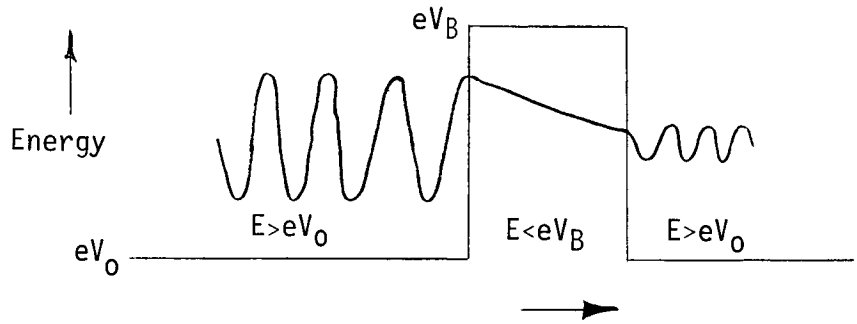

Figure 2. Form of the solution to Schrödinger's equation.

If V (x) is a constant as shown in Fig. 2 then the solution to Schrödinger's equation is a sine wave on both sides of the barrier; within the barrier, the solution is a decaying exponential of the form:

$$(2)\quad \psi \propto \exp\left[\alpha\,(E - eV_B)^{1/2}x\right]_{eV_B > E}$$

If V (x) is not a constant, which is the case for externally applied bias and solid dielectrics, then no closed solution of Schrödinger's equation can be found.[12] An approximate solution commonly used, appears below.[13] Starting with Schrödinger's equation

$$(3)\quad \psi'' + \frac{2m}{\hbar^2}\left[E - eV(x)\right]\psi = 0,$$

where the primes indicate differentiation with respect to x.

(4) and assuming $\psi = A(x) \exp\left(\frac{i}{\hbar} S(x)\right) = \exp\left(\frac{iW}{\hbar}\right)$,

where $W = S + \frac{\hbar}{i} \ln A$,

one obtains by substituting Eq. (4) into Eq. (3);

$$(5)\quad (S')^2 + \frac{2\hbar}{i} S' \frac{d}{dx} (\ln A) - \hbar^2 \left[\frac{d}{dx} \ln A\right]^2 + 2m \left[E - eV(x)\right] = -S'' - \frac{\hbar^2}{i} \frac{d^2}{dx^2} (\ln A).$$

Noting the identities:

$$(6)\quad \frac{d}{dx} (\ln A) = \frac{A'}{A}$$

$$(7)\quad \frac{d}{dx} \frac{(A')}{A} = \frac{AA'' - (A')^2}{A^2},$$

and substituting them into Eq. (5) and equating real and imaginary parts yields the following two equations:

$$(8)\quad (S')^2 - 2m\,(E - eV(x)) = \hbar^2 \frac{A''}{A} \qquad \text{(real parts)}$$

$$(9)\quad 2A'S' + AS'' = 0 \qquad \text{(imaginary parts)}.$$

Eq. (9) is a form of the continuity equation which when solved yields:

$$(10)\quad A = K (S')^{-1/2} \quad \text{where K is a constant}$$

Substituting Eq. (10) into Eq. (8) gives:

$$(11)\quad (S')^2 = 2m\left[(E - eV(x)\right] + \hbar^2 \left[\frac{3}{4} \left(\frac{S''}{S'}\right)^2 - 1/2 \left(\frac{S'''}{S'}\right)\right].$$

Eq. (4) is a solution to the initial Schrödinger equation if Eq. (11) is satisfied. However, only an approximate solution of Eq. (11) is possible. The commonly used WKB approximation appears below.

Expanding S in powers of $\hbar^2$ gives:

$$(12)\quad S = S_0 + \hbar^2 S_1 + \hbar^4 S_2 + \ldots$$

$$S' = S_0' + \hbar^2 S_1' + \ldots$$

$$S'' = S_0'' + \hbar^2 S_1'' + \ldots \quad .$$

Substituting Eq. (12) into Eq. (11)

$$(13)\quad (S_0' - \hbar^2 S_1' + \ldots)^2 = 2m\,(E - V(x)) + \hbar^2 \left[\frac{3}{4}\left(\frac{S_0'' + h^2 S'' + \ldots}{S_0' + hS_1' + \ldots}\right)^2 - \frac{1}{2}\left(\frac{S_0''' + h^3 S_1''' + \ldots}{S_0' + hS_1' + \ldots}\right)\right]$$

Arbitrarily dropping terms in $\hbar^2$ and higher, Eq. (13) becomes:

$$(14)\quad (S')^2 = (S_0')^2 = 2m\left[E - eV(x)\right].$$

$$(15)\quad \text{Thus } S_0' = \left[2m\,(E - eV(x))\right]^{1/2},$$

$$(16)\quad \text{and } S_0 = \pm \int \left[2m\,(E - eV(x))\right]^{1/2} dx.$$

Substituting Eq. (16) back into the assumed solution of Eq. (4), yields for the solution inside the barrier:

$$(17)\quad \psi \simeq \text{constant} \exp\left[-\frac{1}{\hbar} \int \left[2m\,(eV(x) - E_x)\right]^{1/2} dx\right]$$

This exponential term is called the transmission coefficient, $D(E_x)$.

To find the current tunneling from one side of a barrier, the number of electrons which inpinge upon the barrier per second is multiplied by the transmission coefficient, $D(E_x)$.[9c]

$$(18)\quad dJ_x = ev_x D(E_x) dN = ev_x\, D(E_x)\, n(v_x)\, dv_x$$

where:

J_x = current density in the x direction

e = electronic charge

v_x = velocity in the x direction

$D(E_x)$ = transmission coefficient

$n(v_x)$ = probability density function

$n(v_x)\, dv_x = dN$ = the number of electrons per unit volume with velocity between v_x and $v_x + dv_x$.

In terms of the Fermi function,[14] f(E),

$$(19)\quad n(v_x) = \frac{4\pi m^2}{h^3} \int_0^\infty f(E)\, dE_t$$

where: $E_t = 1/2\ mv_t^2$, $v_t^2 = v_x^2 + v_y^2$.

Therefore the current tunneling from one side of the barrier is:

$$(20)\quad J_x = \frac{4\pi em}{h^3} \int_0^{E_m} D(E_x)\, dE_x \int_0^\infty f(E) dE_t$$

where $E_m = E_{max}$ = the maximum electron energy in the electrode.

For the case of two metals separated by a thin insulator, there is tunneling from both sides of the barrier.[14, 15] The net current is the sum of the two currents.

$$(21)\quad J_x = \frac{4\pi em}{h^3} \int_0^{E_m} D(E_x) dE_x \int_0^\infty \left[f(E) - f(E + eV)\right]\, dE_t$$

where the energy of the second electrode has been shifted by an external bias voltage, V.

The general form of Eq. (21) suffices for most authors[14-22] as the starting point for the derivation of the tunneling current of a thin MIM sandwich. The main difference between the various tunneling analyses is in the approximation of the transmission coefficient, $D(E_x)$. The two basic methods of approximation are found in the works of Simmons[20] and Stratton.[18] Hartman[19] compared these works for asymmetric trapezoidal barriers and finds "surprisingly good agreement between them." Simmons' tunneling equation is explicit in the physical parameters of the tunneling junction while the constants of Stratton's equation only imply these parameters.

The equations of both Simmons and Stratton have been found by a number of authors to adequately describe tunneling through oxide films.

Stratton's equation more closely describes the experimental Al-polymer-Al tunneling characteristics of this research. An analytical expression describing MIM tunneling is desired in order to conveniently compare voltage-current characteristics of MIS with MIM junctions. Since there exist no physical criteria upon which to choose one tunneling equation over another, Stratton's equation is selected as the analytical expression to describe the observed tunneling through the polymer. This is not to say that Stratton's equation is more correct than other tunneling equations, but rather that the manner in which the transmission coefficient is approximated more closely describes the tunneling parameters of the polymer film. An outline of Stratton's MIM tunneling equation appears below.

Stratton starts with Eq. (22) which is a form of Eq. (21),

$$(22)\quad J = \frac{4\,em}{h^3}\int_0^{\infty}\left[f_1(E) - f_2(E)\right]dE\int_0^{E} D(E_x)dE_x,$$

$$(23)\quad \text{where } D(E_x) = \exp\left[-\alpha\int_{x_1}^{x_2}\left[\Phi(x,V) + E_F - E_x\right]^{1/2}dx\right],$$

x_1 and x_2 are the values of x where $(x) = E_x$ (the classical turning points),

f_1 and f_2 are Fermi functions,

E_F = the Fermi energy measured from the bottom of the valance band

$\phi(x,V)$ = the barrier energy profile measured from the Fermi level, E_F.

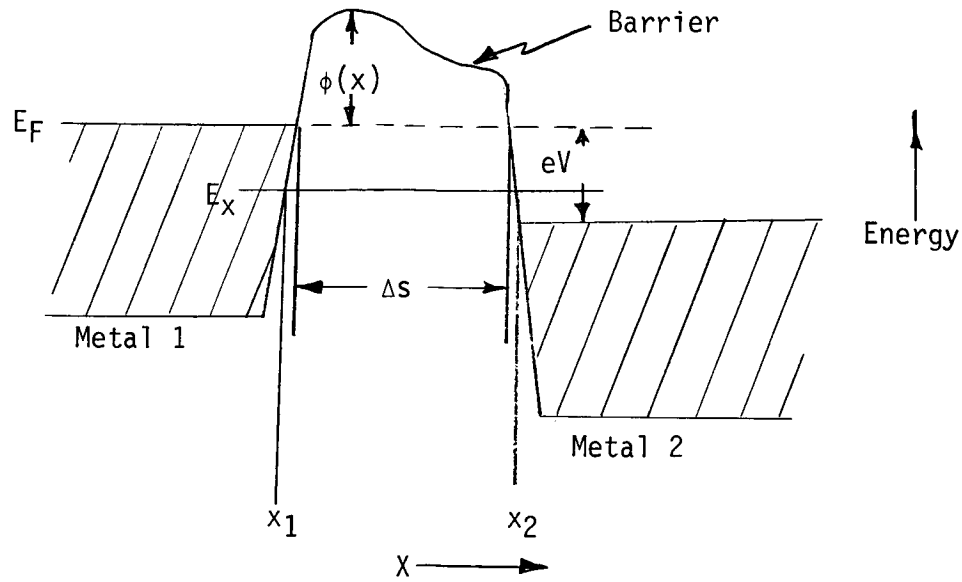

Figure 3. Arbitrary barrier between two metals.

Integrating the first integral of Eq. (22) by parts leads to:

$$(24)\quad J = \frac{4\pi em}{h^3} kT \int_0^\infty D(E_x) \ln\left\{\frac{1 + \exp\left[(E_F - E_x)/kT\right]}{1 + \exp\left[(E_F - E_x - qV)/kT\right]}\right\} dE_x$$

At this point Simmons and Stratton agree.[19]

The barrier profile follows $\phi_o(x)$ at zero bias and $\phi(x,V) = \phi_o + \frac{eVx}{L}$, when an external bias, V, appears across an insulator of thickness L. Stratton assumes that the electrons near the Fermi level dominate the tunneling current. Therefore the exponent of the transmission coefficient can be expanded in powers of ε_x, where $\varepsilon_x = |E_F - E_x|$. Thus,

$$(25)\quad \ln D(E_x) = b_1 + c_1\varepsilon_x + f_1\varepsilon_x^2 + \ldots \text{, where}$$

ε_x is small and only the first two terms need be retained. Substituting Eq. (25) into Eq. (24) and integrating yields:

$$(26)\quad J_x = \frac{B\pi c_1 kT}{(c_1 kT)^2 \sin(\pi c_1 kT)} \exp(-b_1)\left[1-\exp(-c_1 V)\right]$$

$$B = 4\pi em\,(kT)^2/h^3$$

b_1 and c_1 are functions of the applied voltage, V, and are approximated by a power series with respect to V.

$$(27)\quad b_1(V) = b_{10} - b_{11}\,V + b_{12}\,V^2 + \ldots$$

$$c_1(V) = c_{10} - c_{11}\,V + c_{12}\,V^2 + \ldots$$

$b_1(V)$ is now approximated by the first three terms of the power series of Eq. (27) and $c_1(V)$ is assumed constant (i.e., $c_1 = c_{10}$). Substituting these approximations into Eq. (27), J_x becomes:

$$(28)\quad J_x \simeq J\,\frac{2\pi c_{10}kT}{\sin(\pi c_{10}kT)}\exp(b_{11}V - b_{12}V^2)\left[1-\exp(-c_{10}V)\right]$$

For barriers which are symmetrical with respect to the center of the insulator, i.e. $x = \frac{L}{2}$, $b_{11} = \frac{c_{10}}{2}$ and Eq. (28) simplifies to Eq. (29),

$$(29)\quad J_x = J_o\,\frac{2\pi c_{10}kT}{\sin(\pi c_{10}kT)}\exp(-b_{12}V^2)\sinh\left(\frac{c_{10}V}{2}\right).$$

Chapter III compares this equation with experimental data. On page 47, note that theory and experiment agree over four decades of current.

Eq. (29) is now examined to obtain the temperature dependence of the tunneling current. Since b_{10}, c_{10} and J_o are independent of temperature, Eq. (29) can be written in the form shown in Eq. (30) if the applied voltage is held constant.

$$(30)\quad J_x\Big|_{V=\text{const}} = J(T) = J(0)\,\frac{\pi c_{10}kT}{\sin(\pi c_{10}kT)}\,.$$

Note that $J_o \neq J(0)$.

Representing the sine as a power series, Eq. (30) becomes:

$$(31)\quad J_x(T) = J(0)\left[1 + \frac{1}{6}(\pi c_{10}kT)^2 + \ldots\right].$$

Approximating $J_x(T)$ with the first two terms of Eq. (31) yields,

$$(32) \quad J_x(T) \simeq J(0) + \gamma T^2.$$

Simmons[20] finds this same result.

B. Review of Previous MIS Investigation

Relatively few investigations of tunneling between a semiconductor and a metal have been reported in the literature. The early works[23-25] were primarily concerned with explaining experimentally observed rectification in plate rectifiers of Cu-CuO_2 or of selenium. More recent works[2-7] seek to utilize the phenomenon of tunneling to observe impurity states in the semiconductor or to explore the band structure of semimetals and degenerate semiconductors. This section reviews these investigations to establish the present understanding of MIS tunneling.

A. H. Wilson[23] (1932) proposed a tunneling model to explain rectification. His model envisioned the metal separated from the semiconductor by a thin insulating region. The current flows only by the tunneling mechanism. An unlimited number of electrons tunnel from the metal into the semiconductor since the metal is an infinite source. However, the finite number of electrons in the semiconductor conduction band limit the number of electrons tunneling from the semiconductor into the metal. Mott[24] (1939) pointed out that Wilson's model predicted the opposite polarity of rectification than was experimentally observed. For the same reason Wilson's model does not explain MIS tunneling saturation. Miss C. C. Dilworth[25] (1948) theoretically investigated a metal-semiconductor rectifier with a thin insulating barrier in addition to the Schottky barrier. She assumed the electrons of the semiconductor and the metal could readily communicate through the insulator by the tunneling

mechanism. She considers the diode equation,

$$J = \sigma\left[\frac{2\pi Nek(\phi+V)}{\varepsilon}\right]1/2 \quad (1 - e^{-eV/kT})\, e^{-e\phi/kT}$$

to hold for this case by adding the proper exponential tunneling communication terms to account for: (1) the voltage drop across the insulator, (2) the barrier height and (3) the barrier thickness. Four equations resulted--for strong and weak fields with high and low barriers. This model requires the metal to form rectifying contact with the semiconductor, otherwise the diode equation does not apply. The data of Chapter III violates this assumption, therefore this model does not apply to the present MIS tunneling. P. V. Gray[2] (1962) presented what he believed to be the first reported evidence of tunneling into a semiconductor through an oxide film. He investigates tunneling between impurity states and the metal. In a later expanded paper Gray[3] (1965) derives an equation for MIS tunneling current and conductance. These equations and their interpretation make strong demands upon the generally accepted tunneling concepts. An outline of these equations is given below.

Following the reasoning of Bardeen[26] and Harrison,[27] Gray arrives at an equation similar to Eq. (21).

$$(33)\quad J_x = \frac{m_t e}{2\pi h^3}\int_{-\infty}^{\infty} dE \int dE_t e^{-2K}\,(f_a - f_b)$$

Where $K = \int |k_x| dx$ - a form of the WKB approximation

m_t = effective mass k_x = wave vector in the x direction

E_t = transverse energy f_a and f_b = initial and final state occupation probabilities.

Assume the transmission coefficient, K, independent of applied voltage and energy and expand K in a MacLaurin series in terms of E_t yields:

$$K(E_t) = K(0) + E_t K'(0) + \frac{E_t^2}{2!} K''(0) + \ldots \quad .$$

To first order:

$$(34)\quad J_x = \frac{m_t e \exp(-2K)}{2\pi^2 \hbar^3} \int_{-e(V-V_b)}^{0} dE \int_{0}^{e(V-V_b)} dE_t \, e^{-2K' E_t} \quad .$$

Where $K' = \frac{\partial K}{\partial E_t}$ and V_b is the voltage required to bring the Fermi level of the metal coincident with the energy level of either the conduction band on the valence band of the semiconductor. The current, then, is approximately

$$(35)\quad J_x \simeq \frac{m_t e^2 \exp(-2K)}{4\pi\hbar^3 K'} \left\{ (V - V_b) \left[1 - e^{-2K' e(V-V_b)} \right] \right\}$$

and the conductance is

$$(36)\quad \frac{dJ_x}{dV} = G \simeq G_o \left[1 + (2K' e(V - V_b) - 1) \, e^{-2K' e(V - V_b)} \right]$$

Where $G_o = \frac{m_t e^2 \exp(-2K)}{4\pi\hbar^3 K'}$

K and K' are constants evaluated at $V = V_b$ and $E_t = 0$.

Equation (36) predicts a saturation of the conductance for both polarities of applied voltage. This is not consistent with experimental data, neither Gray's or that of this research. Fig. 4 gives the theoretical curves predicted by Eq. (36) with constant G_o and a slightly varying G_o. Fig. 5 shows Gray's experimental curves. Therefore, this theory predicts a near-ohmic behavior for MIS tunneling after a rise at the band edges. This result appears primarily by the assumption that the barrier parameters are independent of applied voltage. In MIM tunneling ohmic behavior at low voltages appears as predicted.[45] However, this ohmic region only extends to voltages of the order of 100 mv. The theoretical MIM tunneling equation

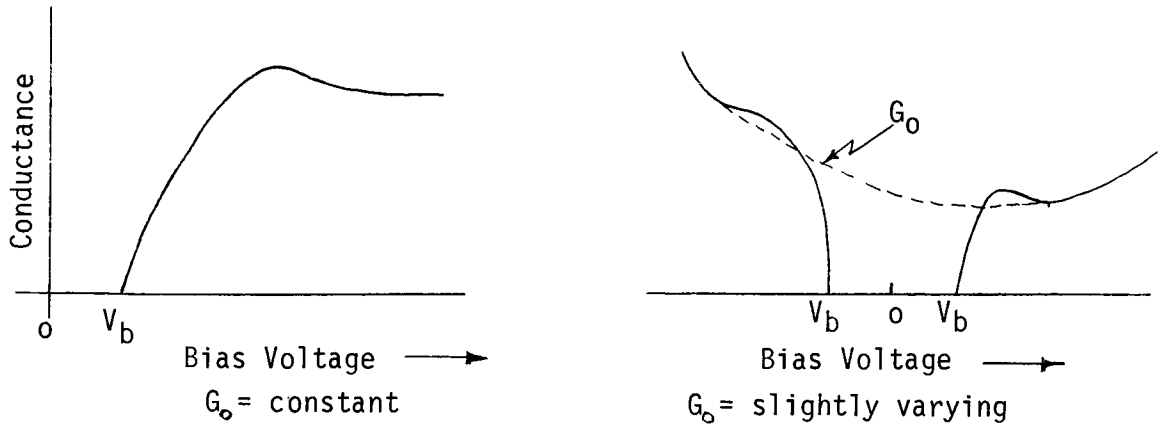

Figure 4. Theoretical curves from Gray (1965).

of Simmons predicts a vast increase in the tunneling conductance for small changes in the barrier height. Fig. 6 graphically illustrates curves calculated from Simmons[14, 18] tunneling equation.* Esaki and Stiles[7] (Mar. 1966) note that Gray made a serious mistake in the integration of Eq. (34). This is strong evidence that the theoretical work of Gray is not correct.

Esaki and Stiles[4, 7] (May 1965, Mar. 1966) observed tunneling from a metal to the various conduction and valence bands of single crystal Bi and Bi-Sb alloys at liquid helium temperatures. The conductance curves shown in Fig. 7 display considerable structure which Esaki and Stiles related to the sum of the conductance from the many hole and electron band edges. A large dip in the conductance shows the existence of the energy gap (10 - 15 millivolts). In a later paper Esaki and Stiles[5] (June 1966) theoretically analyze the energy gap conductance dip of evaporated films of degenerate SnTe, Fig. 8. They begin with a form of Eq. (21) and assume a trapezoidal barrier, i.e.

*Simmon's equations were used in this comparison, rather than Stratton's, due to their greater convenience.

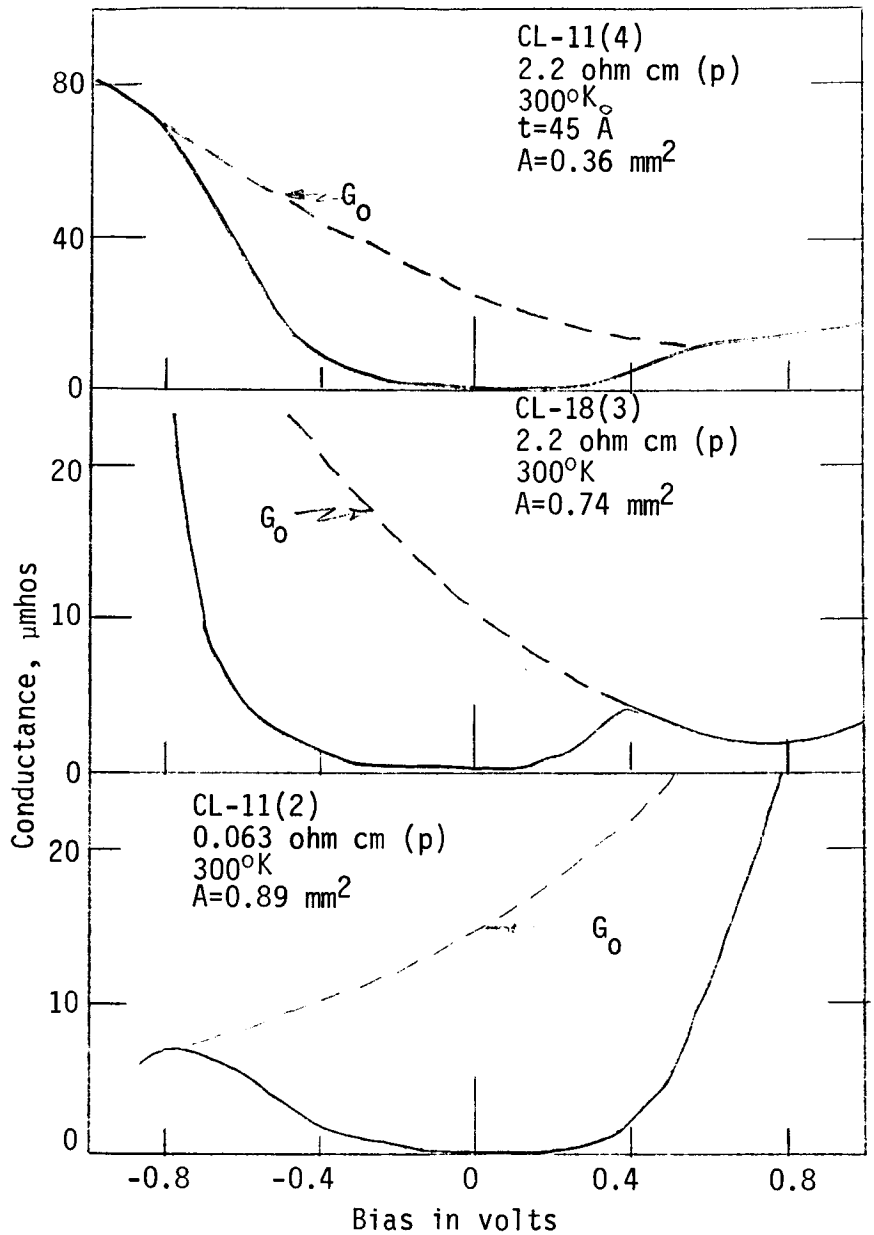

Figure 5. Gray's experimental curves.

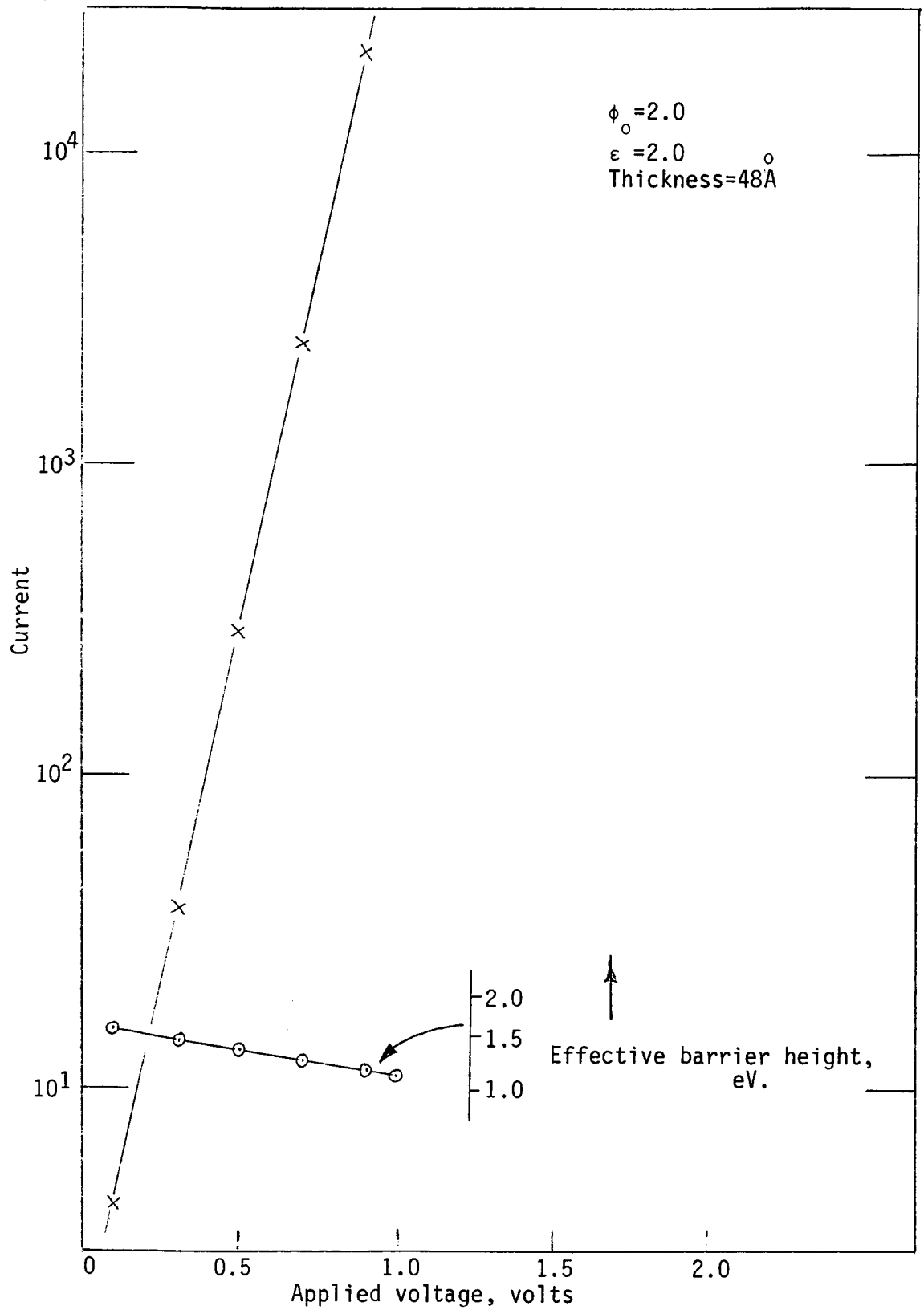

Figure 6. MIM tunneling current and barrier height as a function of applied voltage. (Calculated by Simmons equation[14])

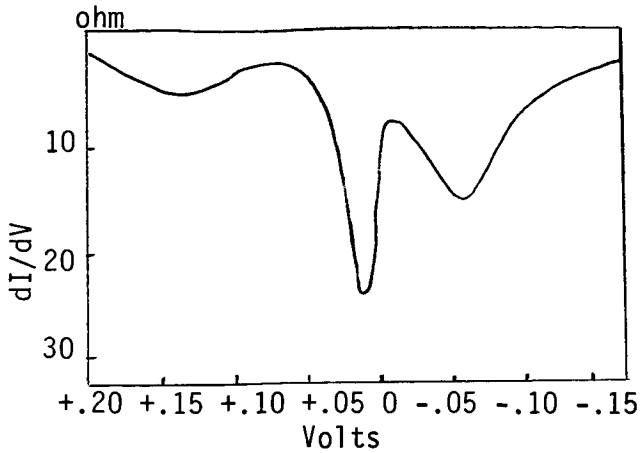

Figure 7. Tunneling into BiSn @ 2°K. (From Esaki and Stiles[7], March 1966)

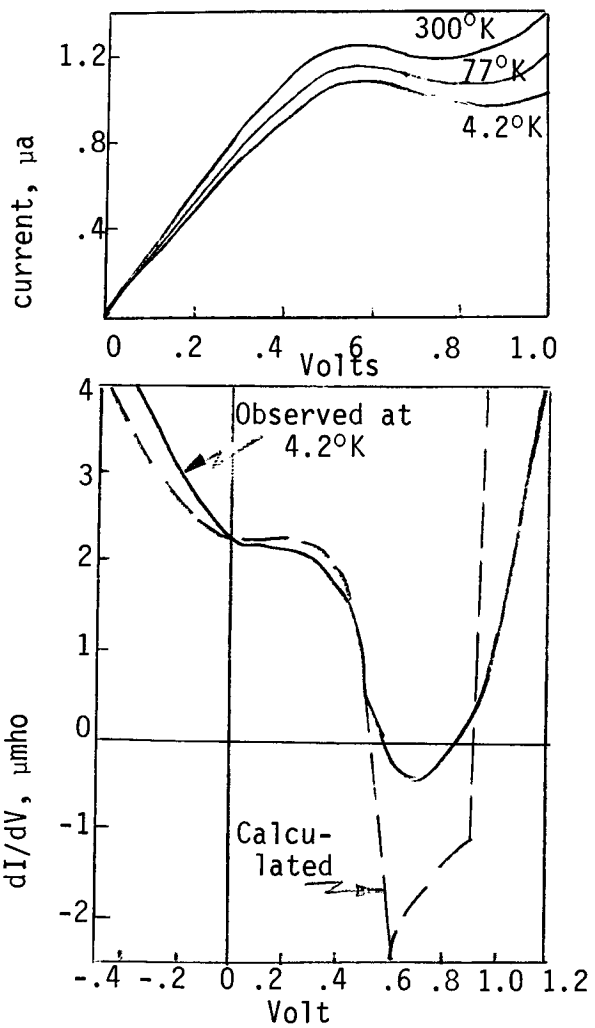

Figure 8. Tunneling into SnTe. (From Esaki and Stiles[5], June 1966)

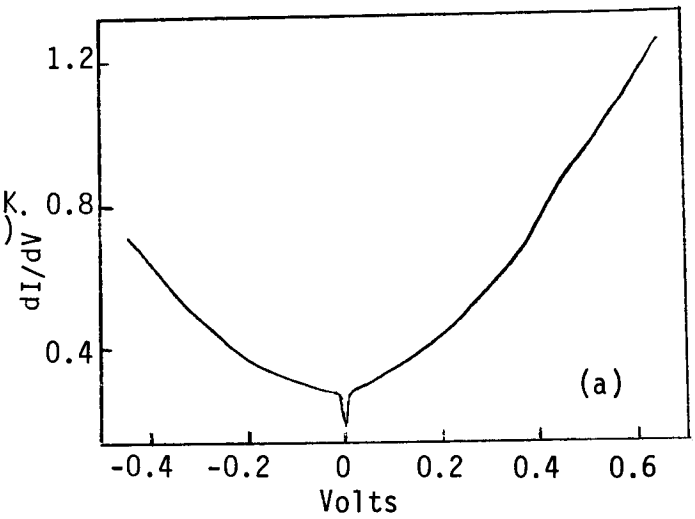

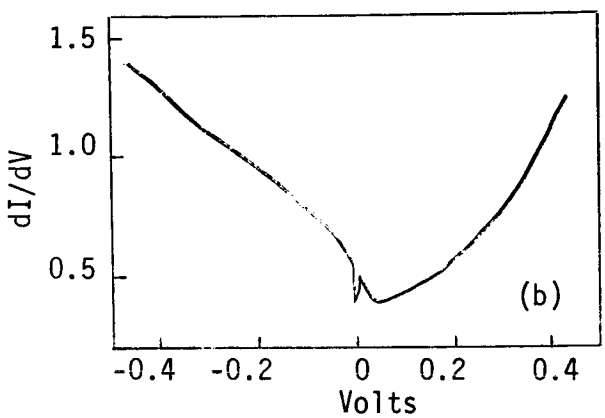

Figure 9. Tunneling into degenerate InSn, a) N-type, b) P-type. (From Chang, Esaki and Jona[6], July 1966)

$\phi(x,V) = eV_v - \frac{eVx}{L}$, where V_v is the barrier height at V = 0 and L is the insulator thickness. Without providing the intervening steps, they find that for relatively large voltage compared to the band gap, the current tunneling from the metal into the semiconductor is given by:

$$(37) \quad I_c = \text{const} \exp\left[\alpha\beta \left(\frac{eV}{2} - E_F - E_g\right)\right].$$

Their presentation makes no effort to verify the exponential behavior predicted by this equation or an earlier conjecture[7] that the conductance peaks "could be attributed" to band bending near the surface. They do not clarify which of the many conductance peaks are thought caused by band bending. Following the work of Esaki and Stiles, Chang, Esaki and Jona[6] (July 1966) report tunneling into degenerate InSb. The InSb curves of Fig. 9 shed no new light on the tunneling process. It appears that the results with these semimetals and degenerate semiconductors cannot be directly correlated to experiments with well-behaved semiconductor crystals such as the silicon used in the present research.

Three separate investigations report injection electroluminescence produced by tunneling through thin insulators. The first, Jaklevic et al[1] (Jan. 1963) used a variety of insulators on single crystal N-type CdS. V-I curves with a Au field plate show rectification properties similar to a Au - CdS contact with the Au positive for the easy direction of current flow. Only positive voltage produced luminescence. Jaklevic interprets the luminescence in terms of electrons tunneling from the valence band of the CdS into the metal, thus injecting holes into the CdS which recombine with conduction band electrons injected by the ohmic contact. Green light is emitted upon recombination. Jaklevic states

that although the experiments point to the mechanism of tunneling, little is known about the details of the process.

Fischer and Moss[30] (July 1964) produced the same results as Jaklevic. They used both evaporated and single crystal semiconductors (CdS, ZnTe, ZnSe, GaP). A wide band semiconductor replaced the field plate metal.

O'Sullivan and Malarkey[31] (Jan. 1965) duplicated Jaklevic's work but replaced the Au contact with a Au - Cr combination to achieve a stable high current contact. Current densities as high as 20,000 amps/ cm^2 were passed through the MIS structure. At high current density, the emission spectum narrowed to 35Å centered at 4900Å.

These three electroluminescent investigations utilized MIS tunneling but did not study the properties of tunneling. Current saturation was interpreted as rectification. The important role played by surface states, depletion and accumulation layers were not considered. Chapter II presents an MIS tunneling model that is compatible with the data presented in these papers.

Of the papers discussed in this section, only the works of Gray[2, 3] (Oct. 1962 and 1965) and Esaki[5] (June 1966) investigate the properties of MIS tunneling. Neither demonstrate the exponential nature of MIS tunneling nor do they investigate the role played by the charge distribution in the semiconductor. The present research addresses itself to these problems.

CHAPTER II

Theory of MIS Tunneling

A. Introduction

It is desired to find an analytical expression describing MIS tunneling. Stratton's MIM equation is a logical starting point since it closely describes the experimental MIM curves of this research (see page 46). This equation involves the basic elements of tunneling and differs from other tunneling equations mainly in the way the transmission coefficient is approximated. The experimental MIS structures are identical to the MIM structures except the base metal electrode is replaced by a silicon electrode. Many similarities are therefore expected between the tunneling characteristics of MIM and MIS junctions. However, the silicon electrode has properties different from those of the metal electrode. These properties may effect the tunneling process and must be examined in order to adapt Stratton's equation to MIS tunneling. The properties examined are the following:

1. Density of states function
2. Forbidden band
3. Conservation of momentum
4. Symmetry of the tunneling barrier
5. Space distribution of semiconductor surface charge .

The first four of these properties are discussed without taking into account the distribution of charge at the silicon surface. The discussion is qualitative and is intended to explore the differences in MIM and MIS

tunneling. It is found that Stratton's equation requires only slight modification in order to be adapted to MIS tunneling. The distribution of silicon surface charge is then considered. A model describing the effect of surface states, accumulation and depletion layers upon tunneling current is proposed. The model predicts an asymmetric saturation of the tunneling current which is dependent upon the conductivity type of the silicon. Following this, some of the parameters of MIS tunneling are discussed within the framework of the proposed model. Variation of these parameters provides a means of experimentally verifying the model.

Before proceeding to the analytical section, it is useful to examine the physical structure (Fig. 10) and energy diagram (Fig. 11) of a MIS tunneling junction.

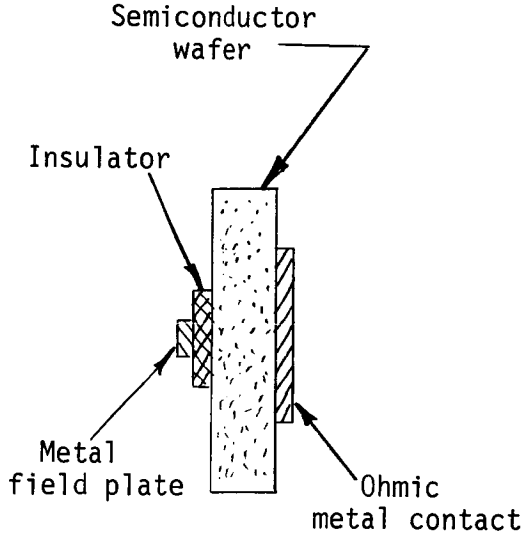

Figure 10. Physical structure of a MIS tunneling junction.

Chapter IV describes in detail the construction of the MIS junctions. However, the basic elements are shown in Fig. 10. A thin insulating film is formed on a silicon wafer. A small metal dot field plate is deposited

on the insulating film, and a large metal contact is deposited on the back of the silicon. Fig. 11 is the energy diagram for a MIS junction with a P-type silicon substrate.

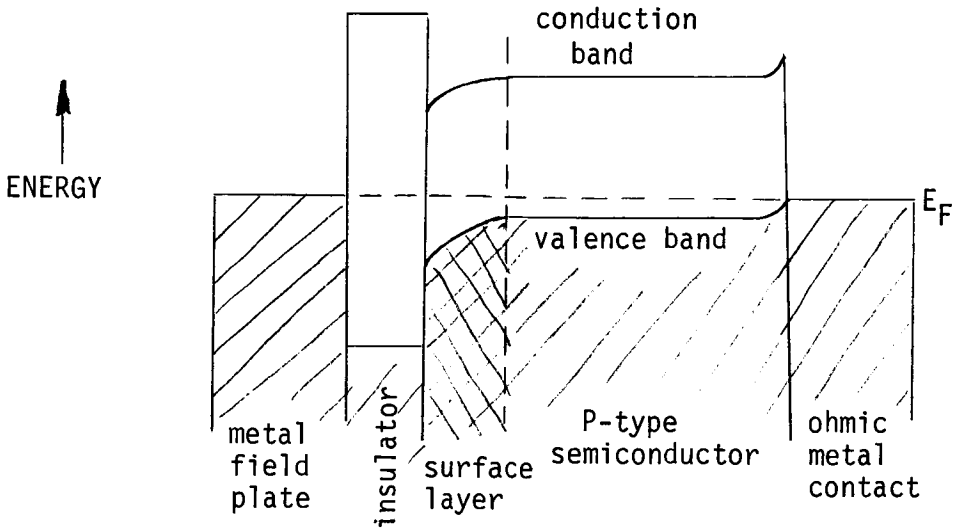

Figure 11. Energy diagram for MIS junction on P-type semiconductor.

The net effect of surface states on the energy structure is shown in Fig. 11 as an excess of donor states which raises the Fermi level at the surface. This is what is usually found on a chemically etched silicon surface.[32] The insulator is pictured as having a conduction and a valence band.[33,34,43] The forbidden band of the insulator is assumed large compared to that of silicon.

B. Adaptation of Stratton's Equation to MIS Tunneling

1. The Forbidden Band

The forbidden band of the perfect silicon lattice is void of allowed states. Electrons in the metal or the silicon cannot tunnel through the insulator until they lie opposite unoccupied energy states in the other electrode.[3, 5] Therefore, no current flows in the MIS system, illustrated in Fig. 12, until the metal is biased either + V_2 or -V_1

volts, assuming all the voltage drop is across the insulator. When $+V_2$ volts is applied to the metal, electrons in the valence band of the silicon tunnel into unoccupied states of the metal. At $-V_1$ volts, electrons at the Fermi level of the metal tunnel into the conduction band of the semiconductor.

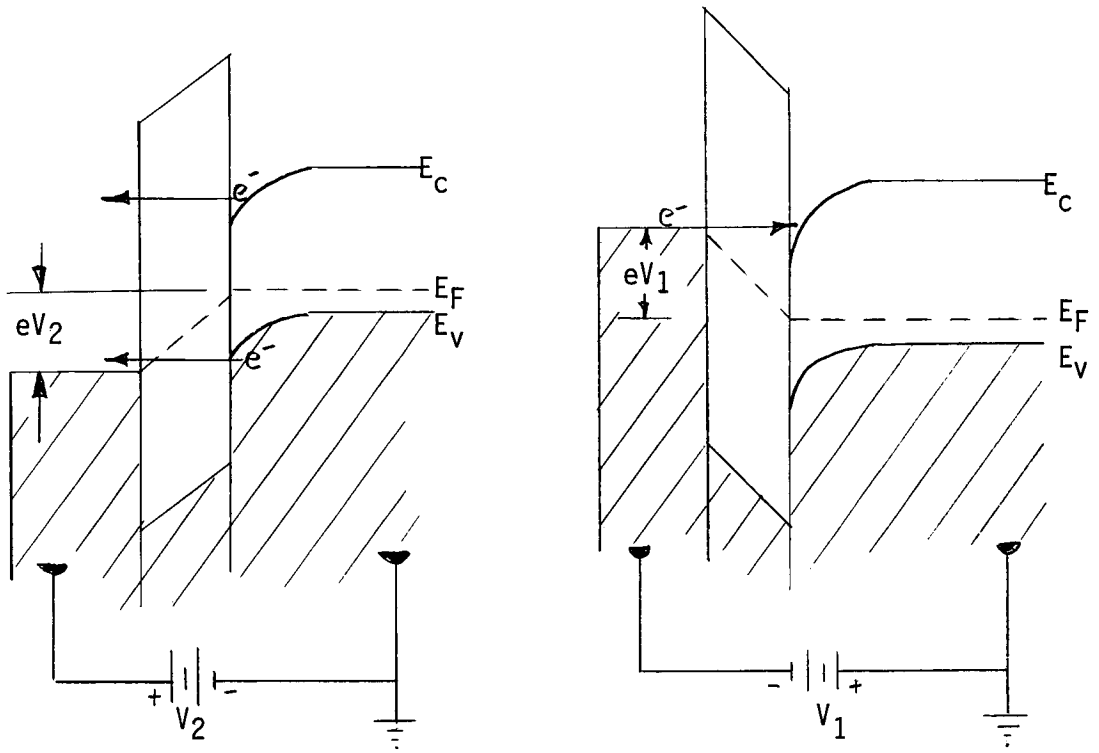

Figure 12. Tunneling between a P-type semiconductor and metal with (a) positive voltage, (b) negative voltage.

For positive voltage, electrons from the conduction band can also tunnel into the metal. However, since the semiconductor is P-type the concentration of conduction band electrons is low, especially at low temperatures. On N-type materials the situation is changed (Fig. 13). When the semiconductor is N-type, tunneling is dominated by metal-conduction band transitions, and the forbidden band does not introduce a large gap in the voltage-current characteristics. An N-type silicon is expected, therefore,

to appear more like a metal than P-type. To alter the tunneling equation to account for the effect of the forbidden band, V_A is replaced by $V_A - V_G$, where V_A is the applied voltage and V_G is the voltage required to bring the Fermi level of metal opposite tunneling states in the silicon.

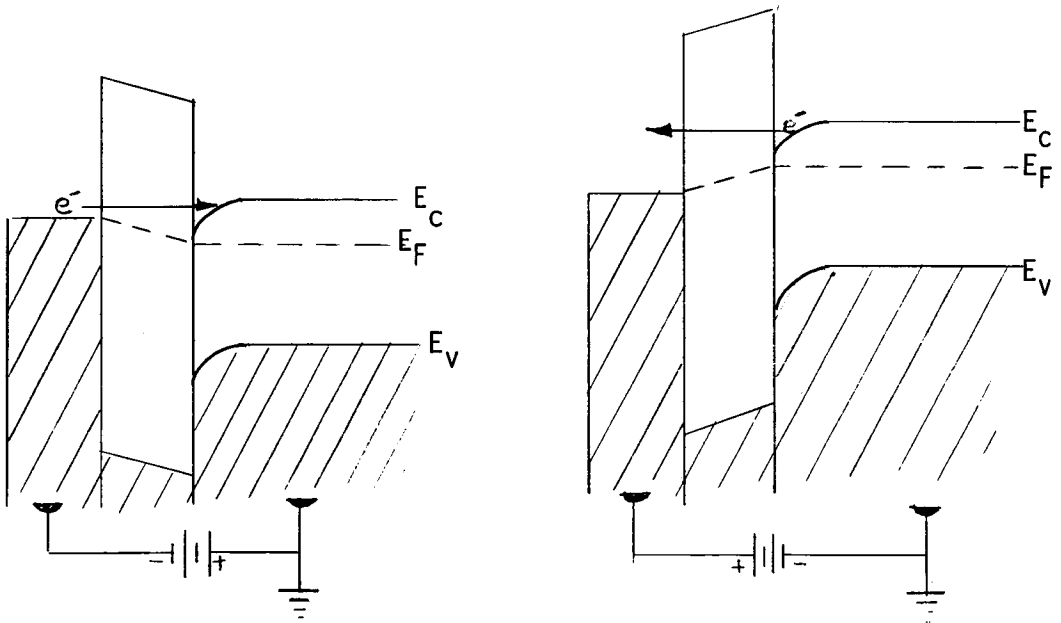

Negative Bias Positive Bias

Figure 13. Tunneling between an N-type semiconductor and a metal separated by a thin insulator.

2. Density of States

There is a large difference in the density of states distribution of a metal and a semiconductor (Fig. 14). However, the density of states function does not appear in the tunneling equation of Stratton,[18] Simmons,[14, 20] Hohm,[15] etc. Harrison[27] notes that this is a direct consequence of the application of the independent particle approach to tunneling. He goes on to state the independent particle model breaks down for tunneling into superconductors but that the model is expected to hold for tunneling into normal metals, semimetals, and semiconductors. Goldberg and Pollack[35] point out that even though the tunneling equations do not

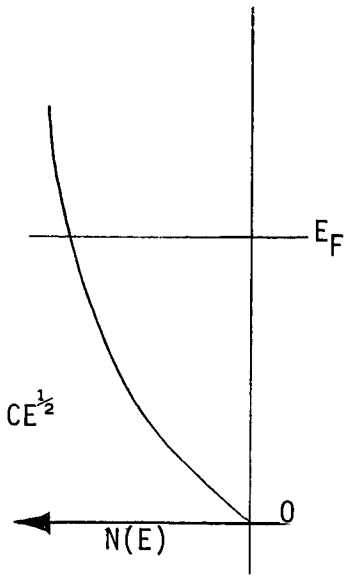

From Dekker[44] page 213

Density of States of a Metal

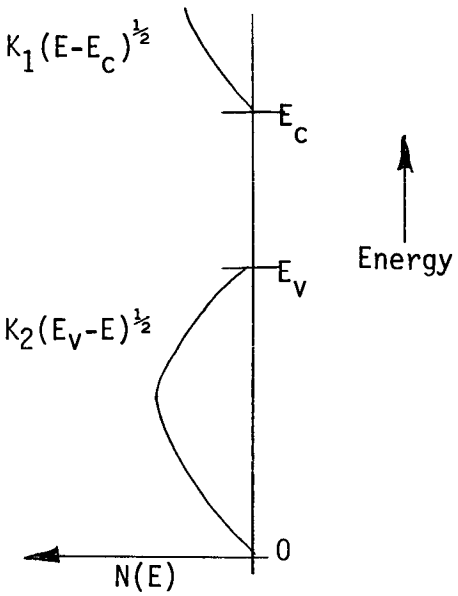

From Dekker[44] page 308

Density of States of a Semiconductor

Figure 14. Density of state functions.

contain the density of states explicitly, it is not correct to conclude that the density of states does not indirectly effect tunneling. Since the density of states is implied in the tunneling equation, it is assumed that no direct account of the density of states need be added to Stratton's equation in order to adapt it to MIS tunneling.

3. Conservation of Momentum

The rules for the conservation of momentum are also implied by the independent particle model since the matrix element for the tunneling transition goes to zero unless the transverse wave number, k_t, is the same for the initial and final states,[27] i.e., there is no force perpendicular to the direction of tunneling. However, transitions with the conduction band of the silicon do not conserve transverse momentum unless a phonon is also emitted or absorbed.[9d] Furthermore, the distribution of

of momentum for the semiconductor is considerably smaller than for a metal, i.e., the Fermi surface of the semiconductor is much smaller than that of the metal field plate[3, 5] (Fig. 15).

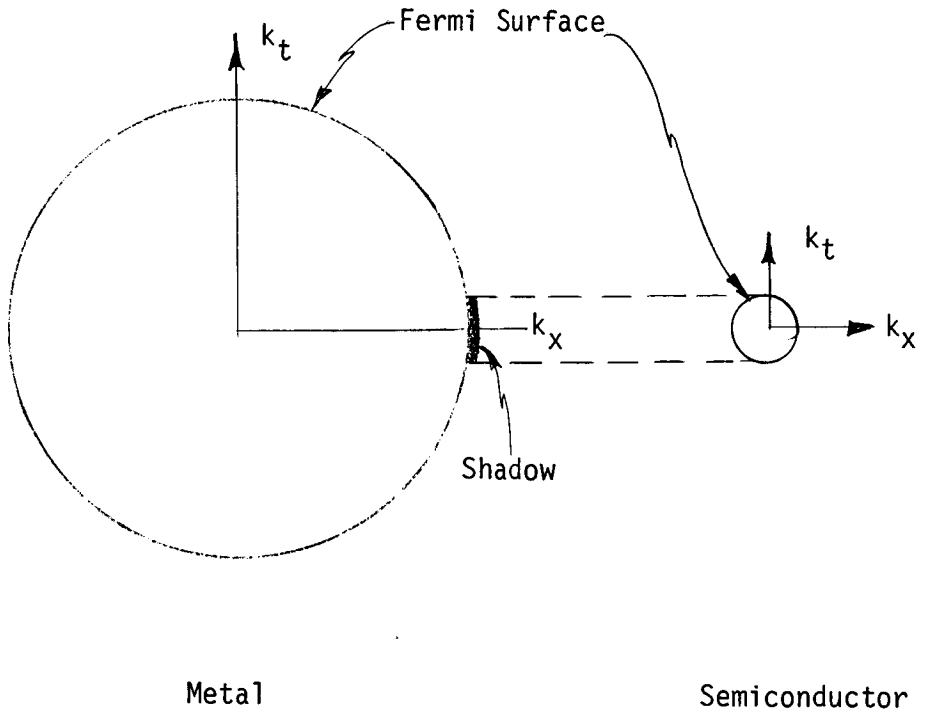

Figure 15. Relative size of the Fermi surface of metal and semiconductor (from Gray[3]).

Esaki[5] notes that the shadow cast by the semiconductor Fermi surface is always covered by the large shadow of the metal. Hence, electrons tunneling from the semiconductor into the metal can easily find an available site in the metal but electrons tunneling from the metal are restricted to a narrow region near the shadow cast by the semiconductor. This reduces the current but does not greatly alter the tunneling voltage-current characteristics. The restricting of the region of allowed momentum and the requirement of phonon cooperation have the effect of reducing the transmission coefficient, $D(E_x)$. Recall that Stratton[18] approximates the transmission coefficient with the power series:

$$\ln D(E_x) = b_1 + C_1 \varepsilon_x = b_{10} - b_{11}V + b_{12}V^2 + C_{10}$$

This same approximation should hold for MIS tunneling with the magnitude of the coefficients reduced. Moll[9] presents this same type of reasoning in examining tunnel diodes of silicon and germanium.

4. Symmetry of the Tunneling Barrier

The tunneling current between two electrodes separated by a thin insulator is dependent upon the energy barrier of the insulator. If the work function of the two electrodes are not equal, then the barrier is asymmetric. For MIM tunneling this results in a difference in the forward and reverse current. Simmon's[29, 60] (also Stratton[18] and Hartman[19]) investigated the asymmetry of these currents and found only small changes in the tunneling characteristics as shown in Fig. 16. No change is evident until the applied voltage exceeds the lower of the two work functions, i.e., $eV_A > \phi_1$, where V_A is the applied voltage and ϕ_1, and ϕ_2 are the work functions of the two metal electrodes such that $\phi_1 < \phi_2$.

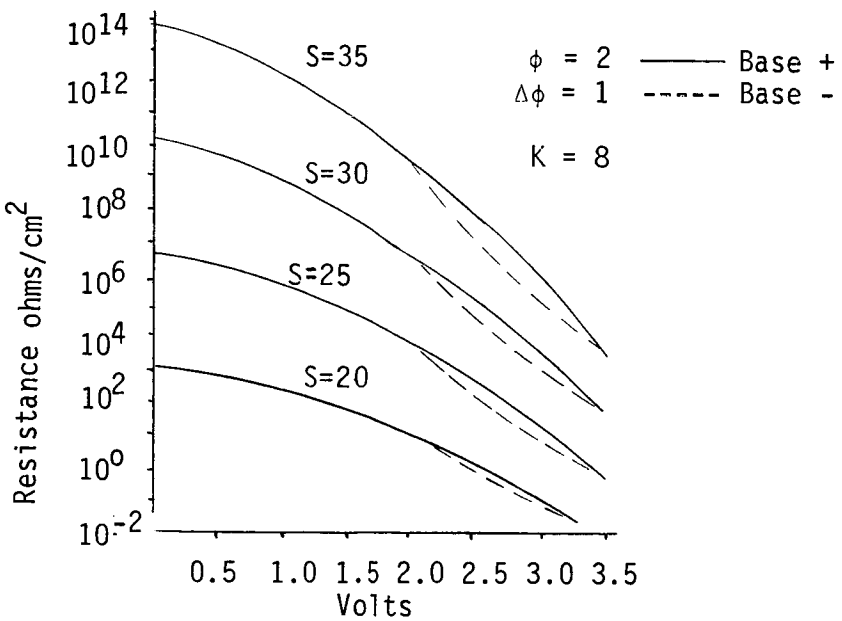

Figure 16. Current through an asymmetric tunneling barrier (from Simmons[60]).

This type of analysis is applicable to MIS tunneling with N-type silicon since the tunneling transitions are with the conduction band for both directions of current as shown in Fig. 13, page 22. However, on P-type silicon there are tunnel transitions with the valence band for positive voltage and with the conduction band for negative voltage, as shown in Fig. 12, page 21. In general the tunneling barrier is different for the two current directions and a current asymmetry should occur.

5. Summary

The semiconductor properties discussed above predict no major difference between MIM and MIS tunneling. The forbidden band shifts the tunneling curve to higher voltage and the momentum considerations reduce the magnitude of the current. Stratton's equation contains the primary principles of tunneling and describes the Al-polymer-Al V-I characteristics. Therefore, it is reasonable to apply his equation, in modified form, to MIS tunneling. When surface effects are not considered, Eq. (29) becomes:

$$(38)\quad J_X = J_o \frac{2\pi c_{10} kT}{\sin(\pi c_{10} kT)} \exp\left[-b_{12}(V_A - V_G)^2\right] \sinh\left[\frac{c_{10}}{2}(V_A - V_G)\right]$$

where b_{12} and c_{10} are smaller for MIS than for MIM.

The constants b_{12} and c_{10} are functions of the physical parameters of the insulator, i.e., dielectric constant, thickness and effective mass.[14, 15] Of particular importance is the dependence of b_{12} and c_{10} upon L^{-2} and L^{-1} respectively, where L is the thickness of the insulator. The tunneling current is therefore dependent upon the electric field in the insulator.[39,40,41] The importance of this fact is clearly seen in the following section which includes the effect of surface charge upon MIS tunneling.

C. The Effects of Surface Charge upon MIS Tunneling

The nature of surface charge at the silicon-silicon oxide interference has been intensively studied in the past few years by measuring the differential capacitance as a function of applied voltage.[32,36,37,38] The structure of the devices used in these experiments is identical to the MIS tunneling junction except the thickness of the insulator is so great that very little current flows. On silicon the surface states cause an N-shift in the surface energy. The surface states are filled up to the Fermi level. When negative voltage is applied to the metal field plate, mobile electrons are removed from the surface states. This continues until the supply of electrons from the surface states is exhausted. What happens when the negative bias voltage is increased still further depends upon the conductivity type of the silicon. For P-type silicon positive mobile holes move to the surface and form a surface accumulation region. For N-type silicon electrons from the conduction band are removed from the surface leaving positively charged donor ions. This is a depletion region. The electric field of the applied voltage is entirely within the insulator until the surface states are exhausted. Since the field lines terminate on charge, an increase in the negative bias will cause the field to penetrate the bulk N-type silicon but not P-type where a surface accumulation layer has formed. For positive voltage the opposite effect occurs, i.e., electrons fill up the surface states and then form an accumulation layer on N-type and a depletion layer on P-type silicon. The behavior of the electric field again follows the charge distribution. These phenomena are directly applicable to the case of MIS tunneling.

It is tempting to consider the MIS structure as a tunneling layer resistance in series with a depletion layer resistance. However, the resistance concept by itself is misleading and leads to an artificial representation of the processes involved. A model which considers the tunneling junction as a field dependent emitter and the depletion region as a collector is now proposed. The data presented in Chapter III not only shows that this model describes the current-voltage characteristics but it also predicts the changes caused by the variation of the parameters.

The concept of the majority carrier emitters is first developed, i.e., conduction band tunneling is by electrons, while valence band tunneling is by holes. Hole tunneling as compared to electron tunneling shows a marked similarity.

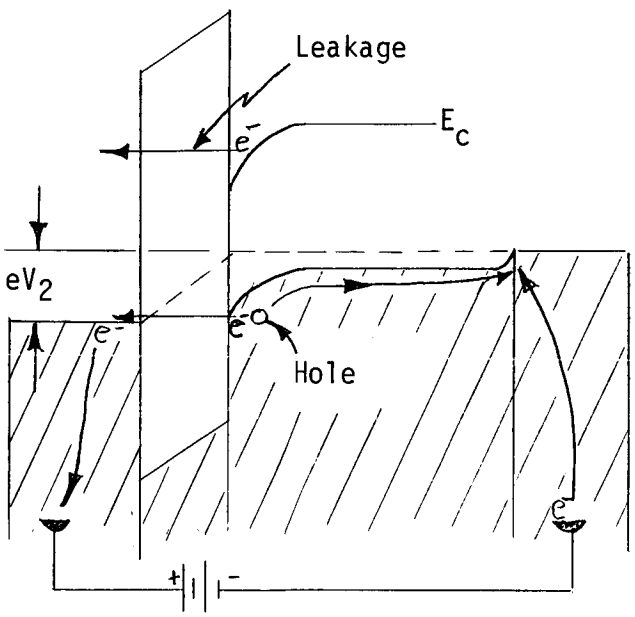

Figure 17. Current in a P-type MIS structure.

If electrons from the valence band of the semiconductor are considered to tunnel into empty states in the metal, then the electron enters the metal and traverses the external circuit to the ohmic contact metal, (Fig. 17). When the electrons leave the valence band, they leave

holes behind. The holes are then moved by the semiconductor's surface and bulk fields (major conduction) and recombine with the electrons in the space charge region at the ohmic metal contact. The energy barrier for the electrons is the conduction band edge of the insulator. However, the electron tunneling from the semiconductor through the barrier to the metal is identical to a hole tunneling from the metal into the semiconductor, except the valence band edge of the insulator is the barrier for the hole. This concept envisions the metal-insulator-semiconductor surface is a hole emitter and the space charge region of the semiconductor is a collector. Any charged carrier which reaches the space charge region is collected and moved in the high field at the surface. This is analogous to a bipolar transistor in that there is an emitter and a collector. The resistance of the back biased collector diode is very high, yet any carrier reaching it from the emitter can easily move in the high field. Therefore, the concept of depletion layer resistance is not valid since the current is not determined by $I = \frac{V}{R}$, but rather by the emitter parameters. In a similar manner the current in the semiconductor space charge region is not strongly dependent upon the resistance of the region since it is a collector of holes emitted by the tunneling layer. The resistance of the region is not the important quantity but rather the potential drop across the layer. For the N-type semiconductor the above model also holds. The energy diagram for MIS on an N-type semiconductor is given in Fig. 18. Here the electron is the majority carrier and the current is carried by electrons around the entire circuit loop.

Tunneling current is dependent upon the electric field in the insulator.[14,15,45] The following is a discussion of how the field in the insulator of an MIS structure varies with applied voltage. The field

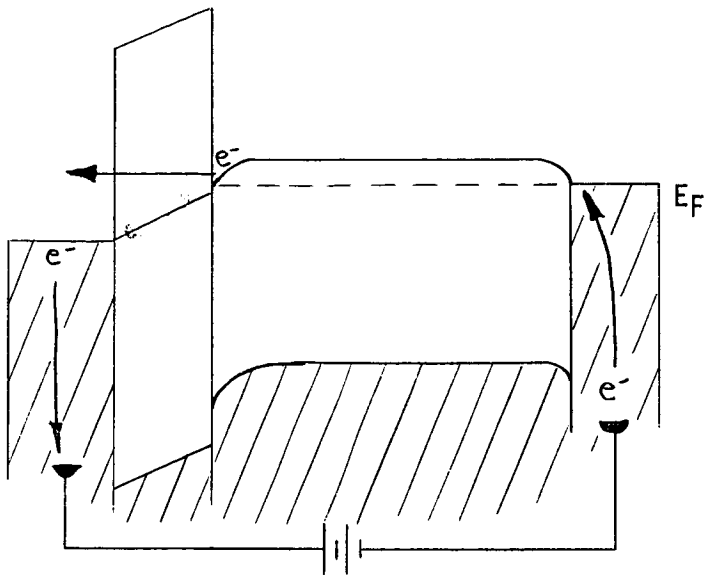

Figure 18. Current in an N-type MIS structure.

lines pass through the insulator and terminate on charges in the metal and semiconductor. The charge on the metal appears at the surface and does not penetrate the metal. The charge on the silicon, however, is more complex. Charge can build up in surface states and in a depletion or accumulation layer at the surface. The location of these charges determines the field in the insulator and hence the current-voltage relationship of the MIS structure. It is essential, therefore, that the general nature of charging of the surface states be established. The surface states in general can have any type of energy distribution. Silicon under normal ambient conditions has an excess of donor type surface states. These states are partially filled, and create an internal electric field.[46a] This internal field does not effect the tunneling consideration except where the tunneling barrier is altered by the field.

Fig. 19 illustrates the termination of electro-static field lines on charges of an N-type semiconductor with surface states.[46b] At zero bias the surface states which lie above the Fermi level are considered empty. If an external field is suddenly applied a large

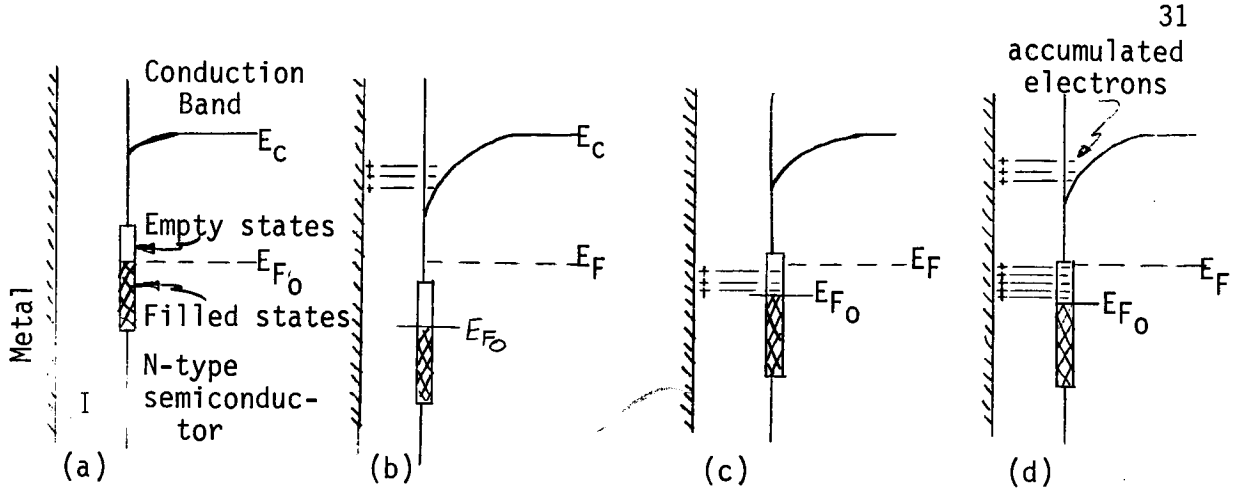

Figure 19. Shape of the conduction band and field line termination for N-type semiconductor with positive bias.
(a) No external field.
(b) Immediately following application of field.
(c) Steady state condition, low field.
(d) Steady state condition, high field.

accumulation region forms. Excess free electrons of this accumulated charge tend to fill up the surface states until equilibrium is reached. When enough bias is applied all of the surface states are filled. Any additional bias results in an increase in the charge collected in the accumulation region which is immediately adjacent to the surface. In both cases the charge in the semiconductor is at the surface and the field in the insulator is approximately proportional to applied voltage. In this case the semiconductor surface appears metallic. If the bias polarity is reversed then the surface state begins to empty. When the surface states are empty then negative charge is removed from the surface region of the semiconductor leaving immobile positive charge (ionized donors). Field lines now begin to terminate on bulk charges and the field penetrates into the bulk as illustrated in Fig. 20.

The above analysis can also be carried out on P-type semiconductor. The results are the same except the polarities are reversed.[46c]

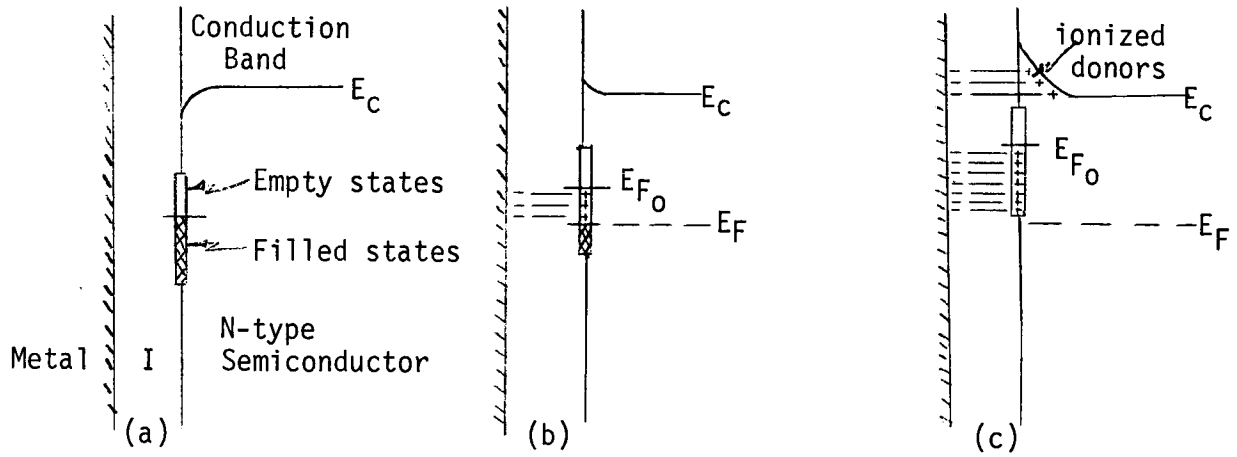

Figure 20. Shape of the conduction band and field line termination for N-type semiconductor with negative bias.
(a) no external field.
(b) small external field.
(c) large external field.

Fig's. 21 and 22 illustrate the energy diagrams for P-type silicon showing the field line terminations for externally applied bias. Therefore, the insulator field depends upon the charge distribution in the semiconductor. The charge distribution is a function of applied voltage and semiconductor conductivity type. In this model the insulator field, as a function of applied voltage, is predicted to be as shown in Fig. 23. The current emitted by the tunneling junction is dependent upon the insulator field. In the regions where the field is proportional to the applied voltage, the MIS current increases in the exponential manner described by the modified Stratton equation. When the depletion layer begins to form, the insulator field no longer increases or increases very slowly and the emitted current levels off. The current should level off with negative voltage on N-type silicon and with positive voltage on P-type as shown in Fig. 24.

When the depletion layer forms, minority carriers tend to collect at the surface in an inversion layer. The minority carriers are

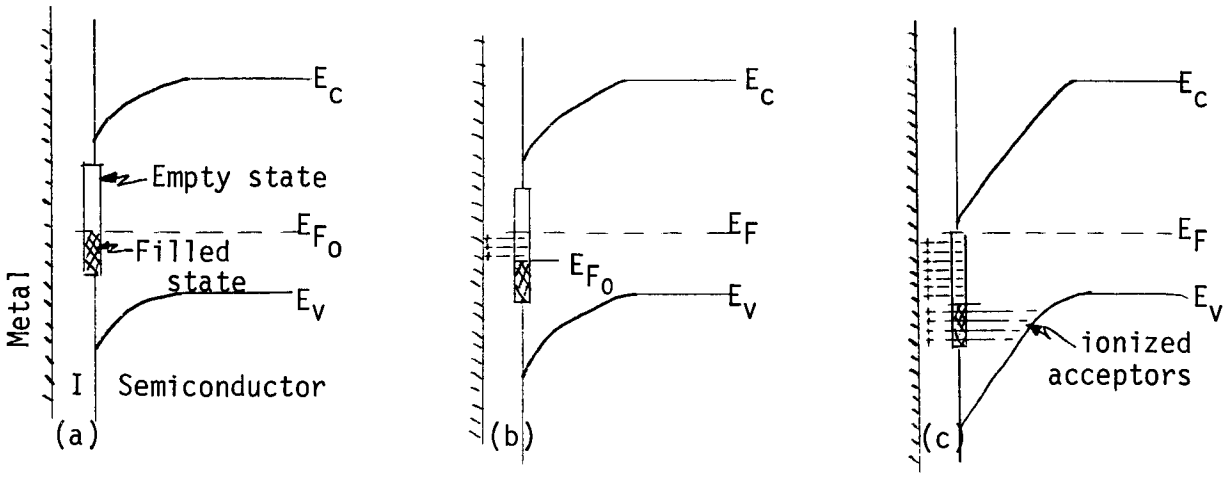

Figure 21. Shape of the energy bands and field line termination for P-type semiconductor with positive bias.
(a) no external field.
(b) small external field (surface states not completely full).
(c) large external field (surface states full).

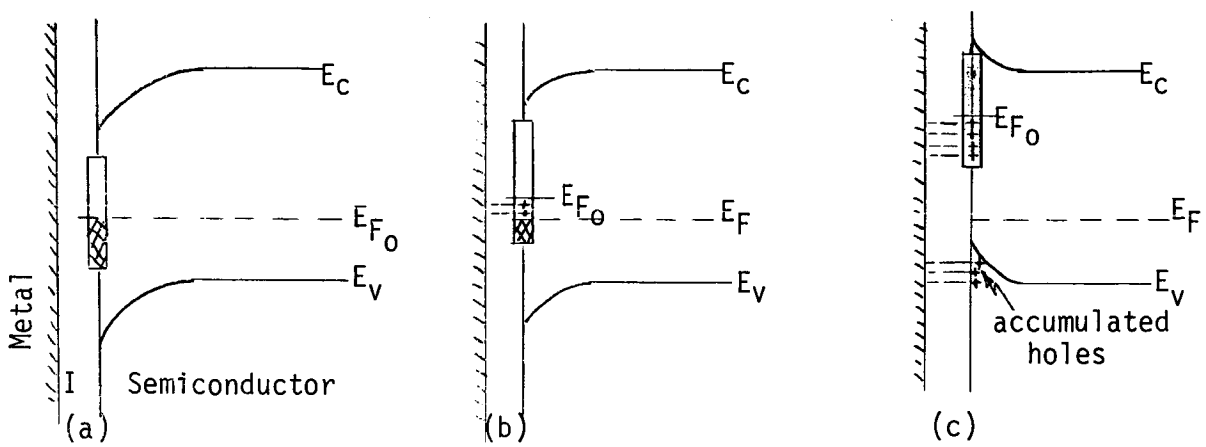

Figure 22. Shape of the energy bands and field line termination for P-type semiconductor with negative bias.
(a) no external field.
(b) small external field (surface states not completely empty).
(c) large external field (surface states nearly empty).

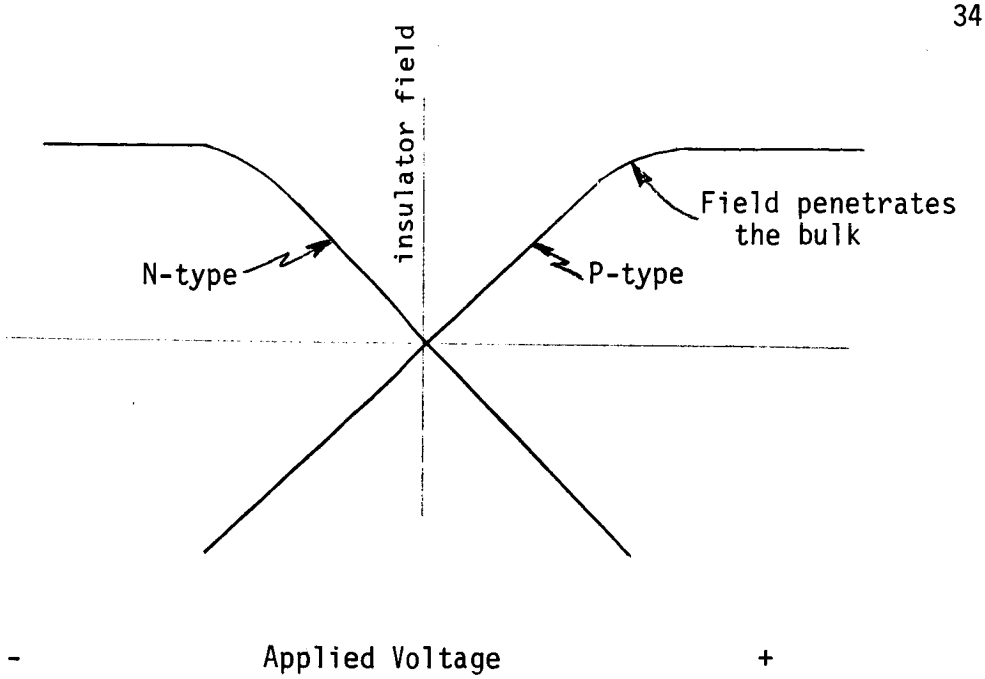

Figure 23. Electric field in the insulator as a function of applied voltage.

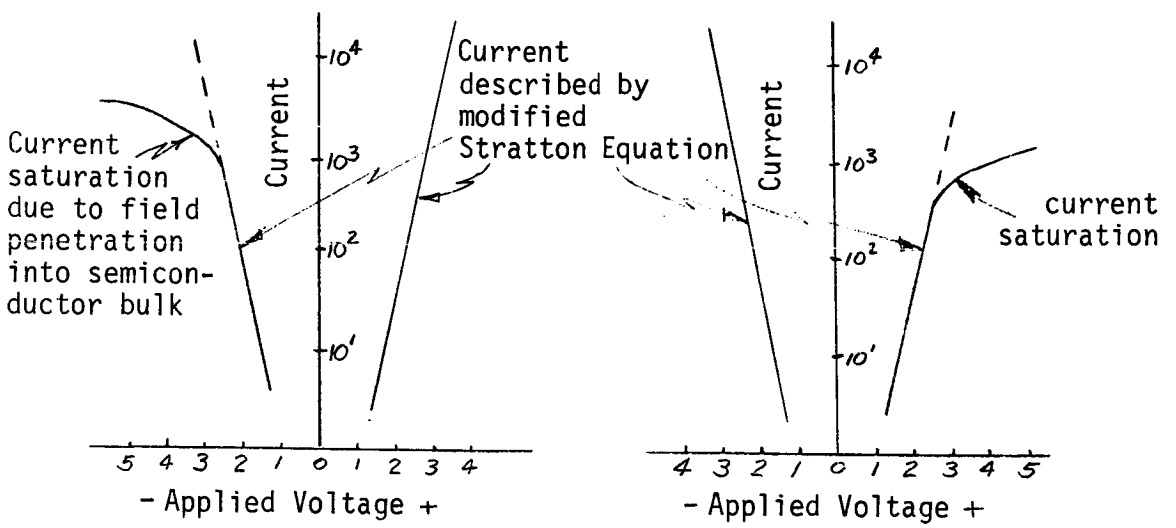

Figure 24. Current-voltage characteristics described by the proposed model.

mobile and add to the tunneling current. However, minority carriers are not expected to greatly effect the insulator field since they are of low density and readily leak (tunnel) through the insulator.

In the summary the behavior of metal-silicon tunneling is explained in terms of the surface states of the silicon. The high density of surface states gives the silicon a metal-like surface. When an external voltage is applied, charge accumulates in the surface states. The electric field lines terminate on this accumulated surface charge, therefore, the insulator field is proportional to the applied voltage. As the external bias is increased, charging of the surface continues until the surface states are exhausted. Further increase in the applied voltage creates either an accumulation layer or a depletion layer in the silicon depending upon the conductivity type of the silicon and polarity of the applied voltage. If an accumulation layer forms, then the insulator field does not penetrate the silicon bulk and continues to increase. Therefore, the tunneling current increases in an exponential manner as before. If a depletion layer forms, then the field lines terminate on ionized dopant states in the bulk. The field now penetrates the bulk and the field in the insulator levels off and approaches a constant. As a result the tunneling current also levels off. The field penetration occurs with positive voltage on P-type silicon and negative voltage on N-type.

D. Tunneling Parameters

1. Introduction

The model proposed in section C agrees well with experimentally observed current-voltage characteristics. However, examination of the tunneling parameters provides further verification of the model and adds

insight into the MIS tunneling process. The insulator thickness, work function of the field plate metal and the temperature are the parameters considered in this section. The variation of the insulator thickness and field plate metal are simple problems of electrostatics. Variation of the temperature provides only qualitative discussion since both the properties of the silicon and the tunneling current are dependent upon temperature.

2. Work Function of the Metal Field Plate

When two electrodes of different work functions, which are electrically connected, are brought into proximity there is a charge transfer between them in order to bring the system into equilibrium.[47a] When equilibrium is reached the Fermi levels of the two electrodes are coincident. Fig. 25 illustrates the energy profile of N-type semiconductor without surface states and a large work function metal, i.e., $\phi_m > \phi_{s/c}$. In this case, electrons leave the semiconductor and enter the metal. A positive charge builds up in the semiconductor.

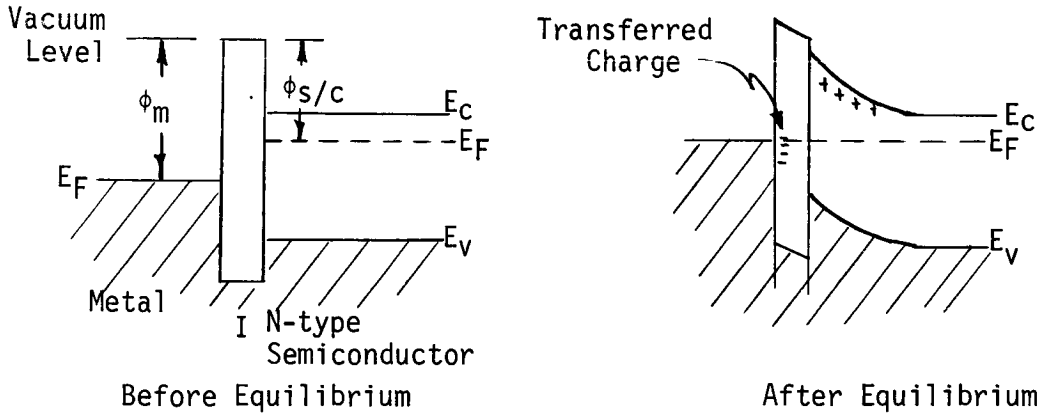

Figure 25. Charge transfer from a large work function metal to an N-type semiconductor without surface states.

This is the condition for a rectifying contact if the insulator were not present. If the work function of the metal is less than that of the

semiconductor, i.e., $\phi_m < \phi_{s/c}$, then electrons leave the metal and collect on the semiconductor surface. This is the condition for an ohmic contact and is illustrated in Fig. 26.

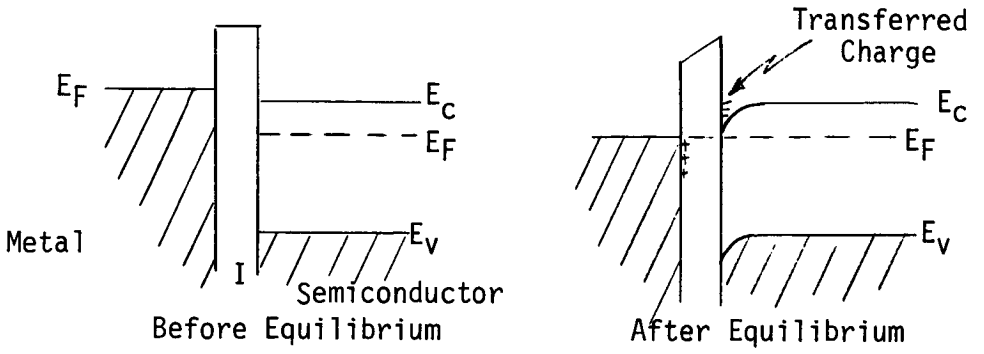

Figure 26. N-type semiconductors--low work function metal, no surface states.

Real surfaces contain many surface states which accommodate the transferred charge. A high work function ($\phi_m > \phi_{s/c}$) field plate metal empties some of the surface states while a low work function metal, $\phi_m < \phi_{s/c}$, fills some of the states. On a MIS junction on N-type silicon, increasing the metal work function has the effect of reducing the voltage required to empty the remaining surface states. Hence, the current saturation level is reduced. The opposite effect occurs on P-type silicon since the number of unfilled states determines the point of saturation. Fig. 27 shows the expected results.

The amount of charge transferred between two electrodes is determined by Gauss' law:

$\int_S \bar{E} \cdot d\bar{A} = \frac{Q_T}{\varepsilon}$, where Q_T is the transferred charge, and E is the field created by the difference in electrode work functions.

Therefore, $E = \left[\frac{\phi_{s/c} - \phi_m}{eL}\right] = \frac{\Delta\phi}{eL}$, where L is the insulator thickness and e is the electronic charge. Therefore:

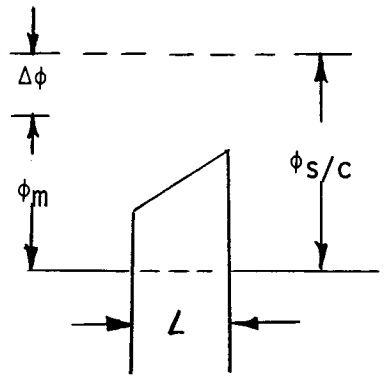

$$EA = \frac{Q_T}{\varepsilon} = \frac{\Delta\phi A}{eL}$$

$$\text{and } Q_T = \frac{\Delta\phi \varepsilon A}{eL} .$$

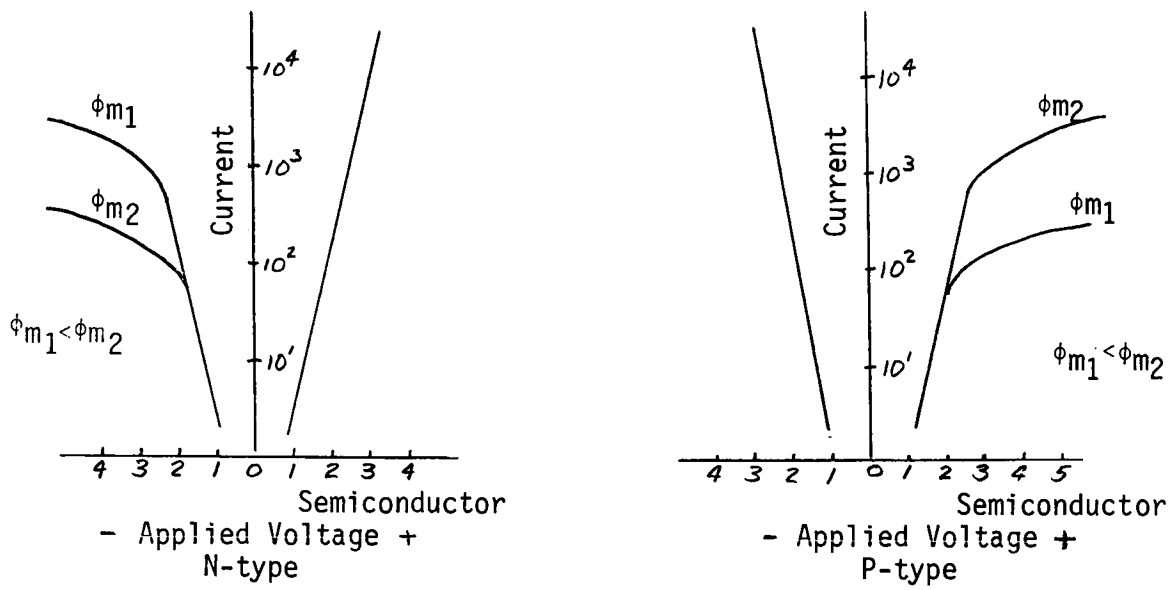

Figure 27. Predicted tunneling characteristics with high and low work function field plate metal.

For the purpose of example, it is useful to assume the published work function values and calculate the number of electrons transferred per unit area for several metals. Assuming an 80Å thick insulator:

Material	ϕ	$\phi_{s/c} - \phi_m$	$\frac{\phi_T}{eA} = N_T$
Si[48, 49]	4.0ev	-	-
Al[50]	3.7	0.3ev	0.6×10^{12} electrons/cm^2
Sn[50]	4.1	-0.1	-0.2×10^{12}
Au[50]	4.6	-0.6	-1.2×10^{12} ,

A surface state density of approximately 4×10^{12} states/cm^2 is calculated in Chapter III. The above metals alter the number of states by a factor of 5 to 30%.

In the next section it is shown that the insulator field at current saturation depends upon $\Delta\phi$, i.e.

$$E = \frac{Q_s}{\epsilon A} + \frac{\Delta\phi}{eL} .$$

The tunneling current is approximately an exponential function of the electric field. Therefore:

$$I_{sat} \simeq A \exp(\alpha E) = A \exp\left[\alpha \left(\frac{Q_s}{\epsilon A} + \frac{\Delta\phi}{eL}\right)\right]$$

$$I_{sat} \simeq B \exp\left(\frac{\alpha\Delta\phi}{eL}\right)$$

where I_{sat} is the saturated current level and $B = A \exp(\alpha Q_s/\epsilon A)$. Hence, the saturated current level is approximately an exponential function of $\Delta\phi$.

3. Insulator Thickness

The point at which the tunneling current levels off is dependent upon the maximum charge collected in the surface states. The field in the insulator terminates on this change. The charge, Q, and field, E, are related by Gauss' law:

$$\int_S \bar{E}.d\bar{A} = \frac{Q}{\varepsilon}$$

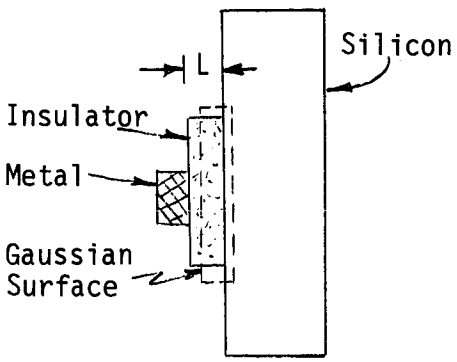

Only the area perpendicular to the semiconductor surface has a net electric field. Therefore,

$$EA = \frac{V_Q A}{L} = \frac{Q}{\varepsilon}$$

Where V_Q is the voltage required to completely ionize the surface states; Q is the charge collected at the surface; L is the insulator thickness and A is the area of the contacting metal. Hence:

$$V_Q = \frac{QL}{\varepsilon A} .$$

However, the charge, Q, is dependent upon the insulator thickness since the field plate metal and the silicon transfer charge in order to aline the Fermi level. The amount of transferred charge, Q_T, was found in the previous section. The total charge, Q, is the sum of the unpreturbed charge, Q_S, and the transferred charge. $Q = Q_S + Q_T$. The voltage at saturation then is:

$$V_Q = \frac{(Q_S + Q_T)L}{\varepsilon A} = \frac{L}{\varepsilon A}\left(Q_S + \frac{\Delta\phi\varepsilon A}{eL}\right) = \frac{LQ_S}{\varepsilon A} + \frac{\Delta\phi}{e}$$

and $$E = \frac{V_Q}{L} = \frac{Q_S}{\varepsilon A} + \frac{\Delta\phi}{eL} .$$

However, for small thickness changes the field at saturation is approximately independent of insulator thickness. For this case the voltage, V_Q, increases linearly with insulator thickness but the value of the saturated

current is independent of insulator thickness since it is controlled solely by the insulator field. The expected tunneling curves are given in Fig. 28.

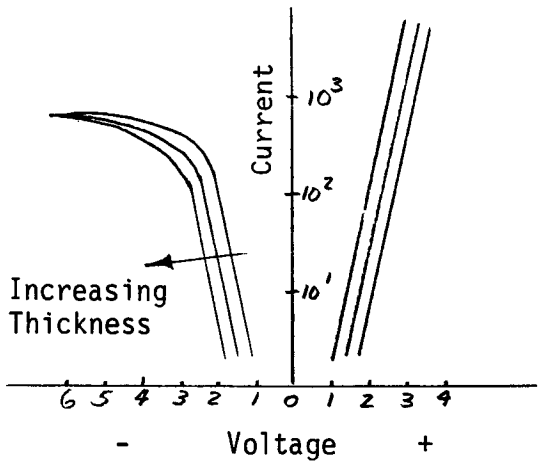

Figure 28. Predicted variation of the tunneling characteristics with insulator thickness, $\Delta\phi << 1$.

4. Temperature

MIM tunneling current decreases as the square of the absolute temperature. The temperature dependence of MIS tunneling is expected to be stronger since the tunneling transition requires phonon cooperation. Temperature also effects the properties of the silicon surface and bulk. These factors complicate the analysis of the temperature dependence of the MIS current. For simplicity, the case of constant surface charge is examined. For this case the voltage required to fill or empty the surface states remains constant with temperature but the saturated current level is reduced due to the decreased tunneling efficiency. This case is illustrated in Fig. 29. Deviations from this simple model can be attributed to changes in the surface states.

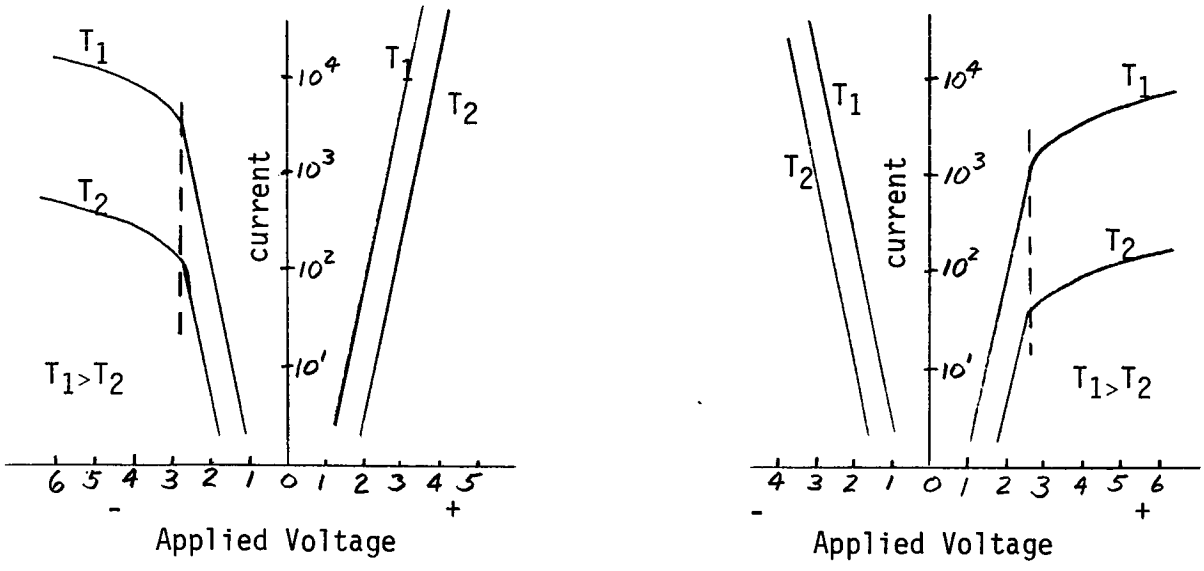

Figure 29. Predicted effect of temperature upon V-I characteristics (no silicon temperature effect).

CHAPTER III

MIS Experimental Data

A. Introduction

This chapter presents experimental data which verifies the proposed MIS tunneling model. First the experimental curves compare reasonably well with Stratton's MIM and modified MIS tunneling equations. Note the exponential nature and the asymmetric saturation of MIS current. Systematic variation of experimental techniques eliminated technique as the source of the current saturation. The formation of depletion and accumulation layers on MIS tunneling junctions appears in the C-V curves. The above experiments establish the basic properties of the proposed MIS model. Added verification of the model results from variation of the insulator thickness, work function of the field plate metal, and temperature.

The initial exploratory experiments established the techniques of constructing and testing the MIS devices. Devices or sets of devices were constructed to demonstrate particular properties of MIS tunneling. Therefore, most of the samples were not subjected to a complete series of tests and the following curves came from different samples. Of thirty-nine MIS samples constructed, twenty-seven exhibited tunneling. The other twelve had thick insulators and provided capacitance-voltage (C-V) characteristics. All of the tunneling samples tested had the characteristics shown in the following data. A slow aging of the samples occurred,

so measurements began immediately after removal of the specimen from the vacuum chamber. An evaporated aluminum field plate produced a more electrically stable device than did other metals such as Au and Sn.

The V-I data was taken with the bridge[51] described in Appendix I. The bridge was thoroughly analyzed and tested before using it to test experimental devices. Measurement of fixed carbon resistors of values from 10K ohms to 680 meg ohms tested the reliability of the bridge. The bridge leakage conductance was approximately 10^{-9} mhos (1000 meg ohms). A check of the leakage current of the bridge always preceded testing of the MIS samples. The leakage current was subtracted from the total current to obtain the true sample current.

B. Comparison of Theoretical Model with Experimental Data

The experimental approach of this research studies MIM tunneling and then replaces one of the metal electrodes with a silicon electrode. The difference in the resulting MIM and MIS curves arises from the properties of the silicon. Fig. 30 gives V-I curves for a number of different MIM tunneling junctions. These curves resemble those of Fisher et al[45] and Christy.[52] They illustrate the general exponential character of MIM tunneling and the strong dependence of current on thickness. Fig. 31 shows an expanded MIM tunneling curve; the insulator thickness is 80Å. The small X's mark a fit of Stratton's equation.[18] The values of the constants, $b_{12} = 1.0$ and $C_{10} = 16.4$, are close to those used by Stratton to fit the Al - Al_2O_3 - Al tunneling curves of Fisher and Giaever.[45] Stratton's fit requires $b_{12} = 1.11$ and $C_{10} = 12.6$. The excellent agreement for the polymer insulator over four decades of current indicates Stratton's equation to be adequate for MIM tunneling and suitable as the basis for MIS tunneling.

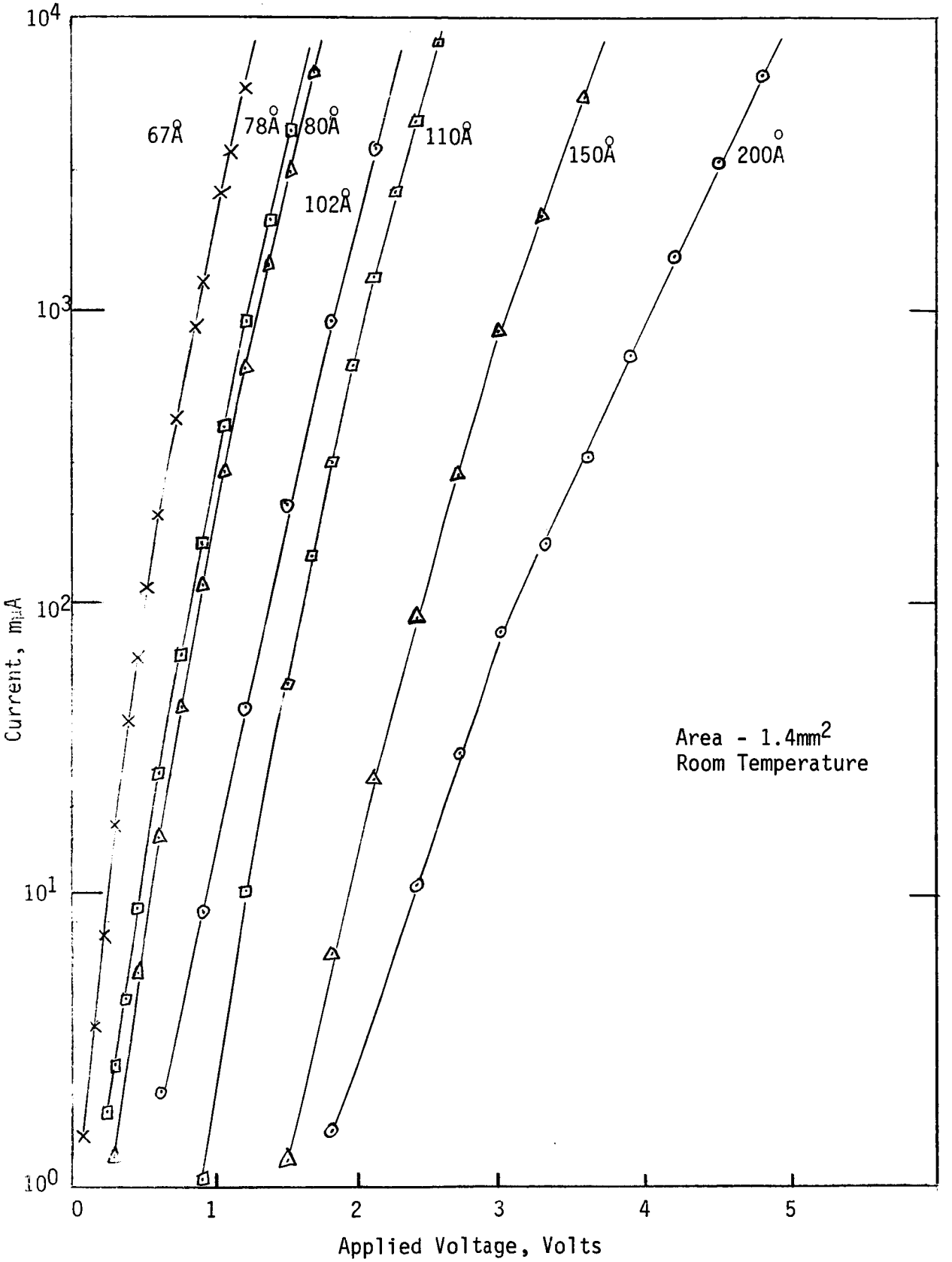

Figure 30. Metal-polymer metal current-voltage characteristics, seven different polymer thicknesses.

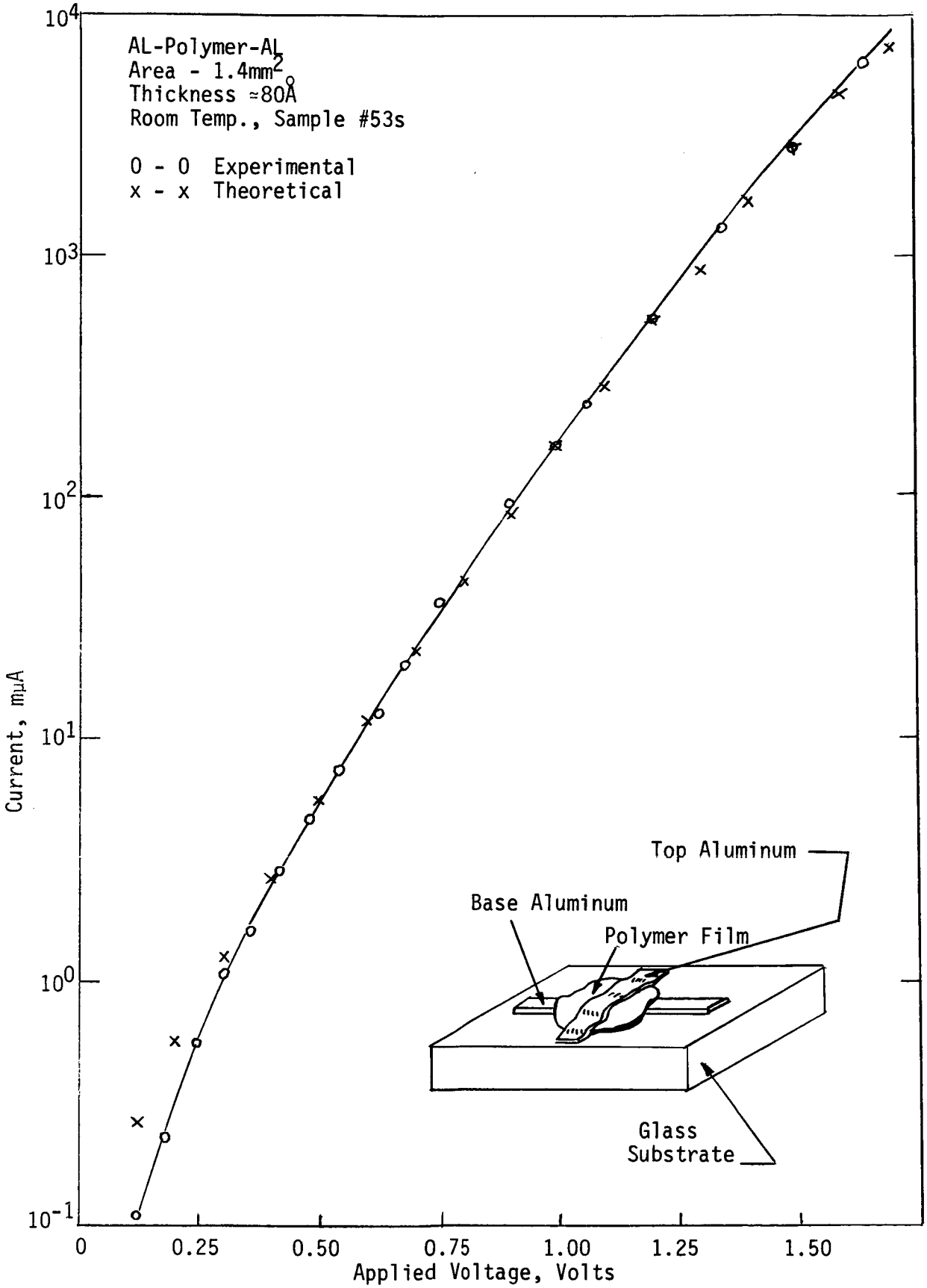

Figure 31. Fit of Stratton's MIM equation to Al-polymer-Al sample.

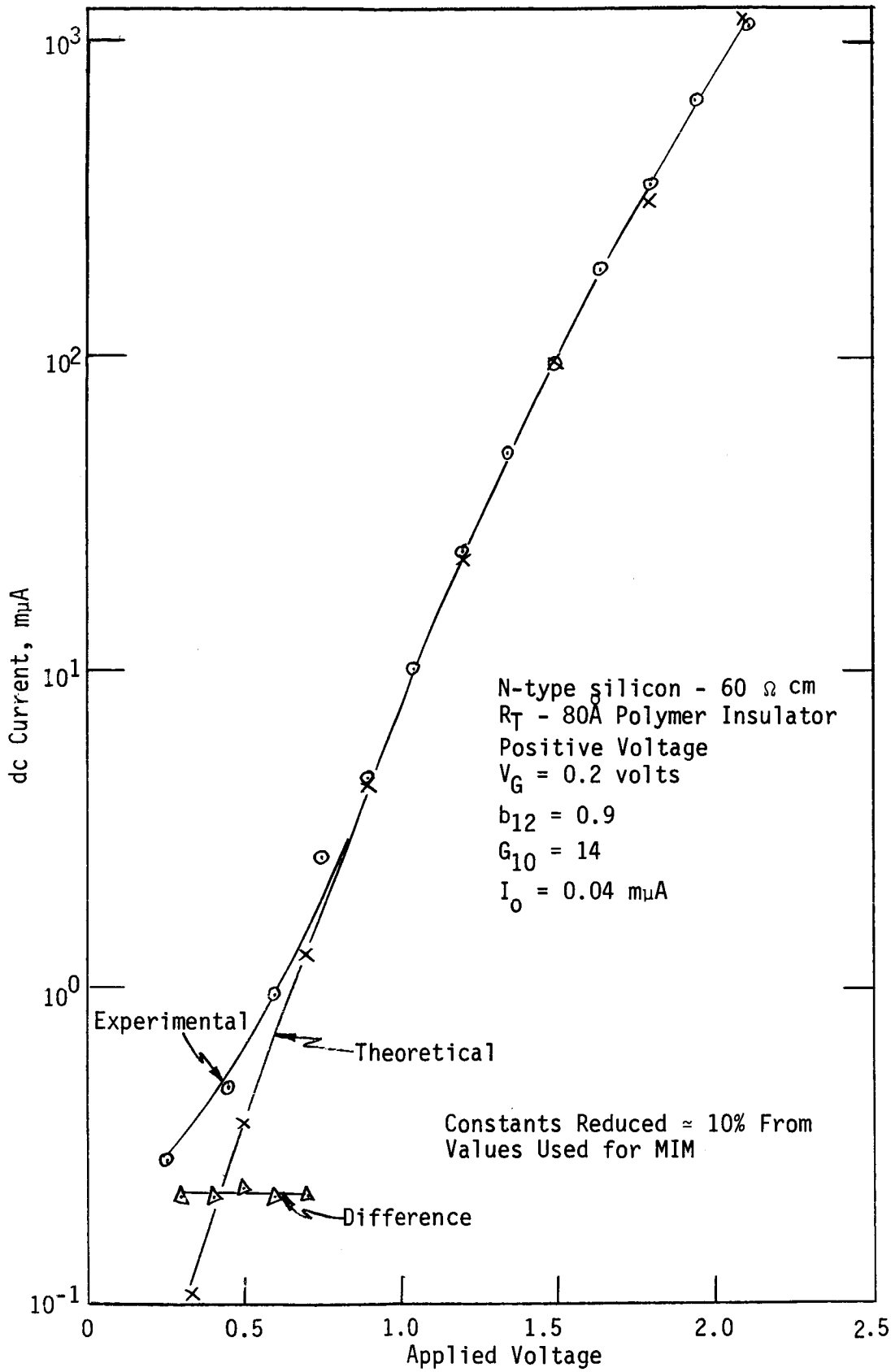

Figure 32. Comparison of experimental MIS curve and Stratton's modified equation.

Eq. (38) of Chapter II modifies Stratton's equation by taking into account the properties of the silicon. Only two modifications seem necessary: 1) reducing the constants, and 2) replacing the applied voltage, V_A, by $V_A - V_G$. N-type silicon substrates compare readily with Eq. (38) (Fig. 32) since they are more metal-like than P-type. Fig. 32 is for positive voltage on N-type silicon with an 80Å thick polymer insulator. Calculations from Eq. (38) give the small X's. The constants used for the MIS curve are approximately 10% smaller; $b_{12} = 0.9$, $C_{10} = 14$, $V_G = 0.2$ volts. Very good agreement is achieved with these minor modifications. The experimental and theoretical curves of Fig. 32 coincide except for low voltage. The constant difference at low voltage may be the fault of the equation or a fixed leakage current. From the close agreement of the two curves it is felt that the rules which govern MIM tunneling also govern MIS tunneling. This is the first published evidence of the exponential nature of MIS tunneling and the first direct comparison of MIM and MIS current. It is significant that MIM and MIS tunneling are described by the same basic equation.

Fig's. 33 and 34 present tunneling current curves for N- and P-type silicon for both voltage polarities. The X's again represent points calculated from Stratton's modified equation shown in Fig. 32. For P-type V_G changes to 0.55 volts but the constants b_{12} and C_{10} remain the same as for N-type. The agreement is remarkable. No major difference appears except an asymmetric saturation of the current which depends upon the conductivity type of the silicon. On N-type the current saturation occurs with negative voltage and with positive voltage on P-type. The proposed field penetration model predicts this result. The onset of saturation is quite sharp and little deviation from the exponential tunneling occurs

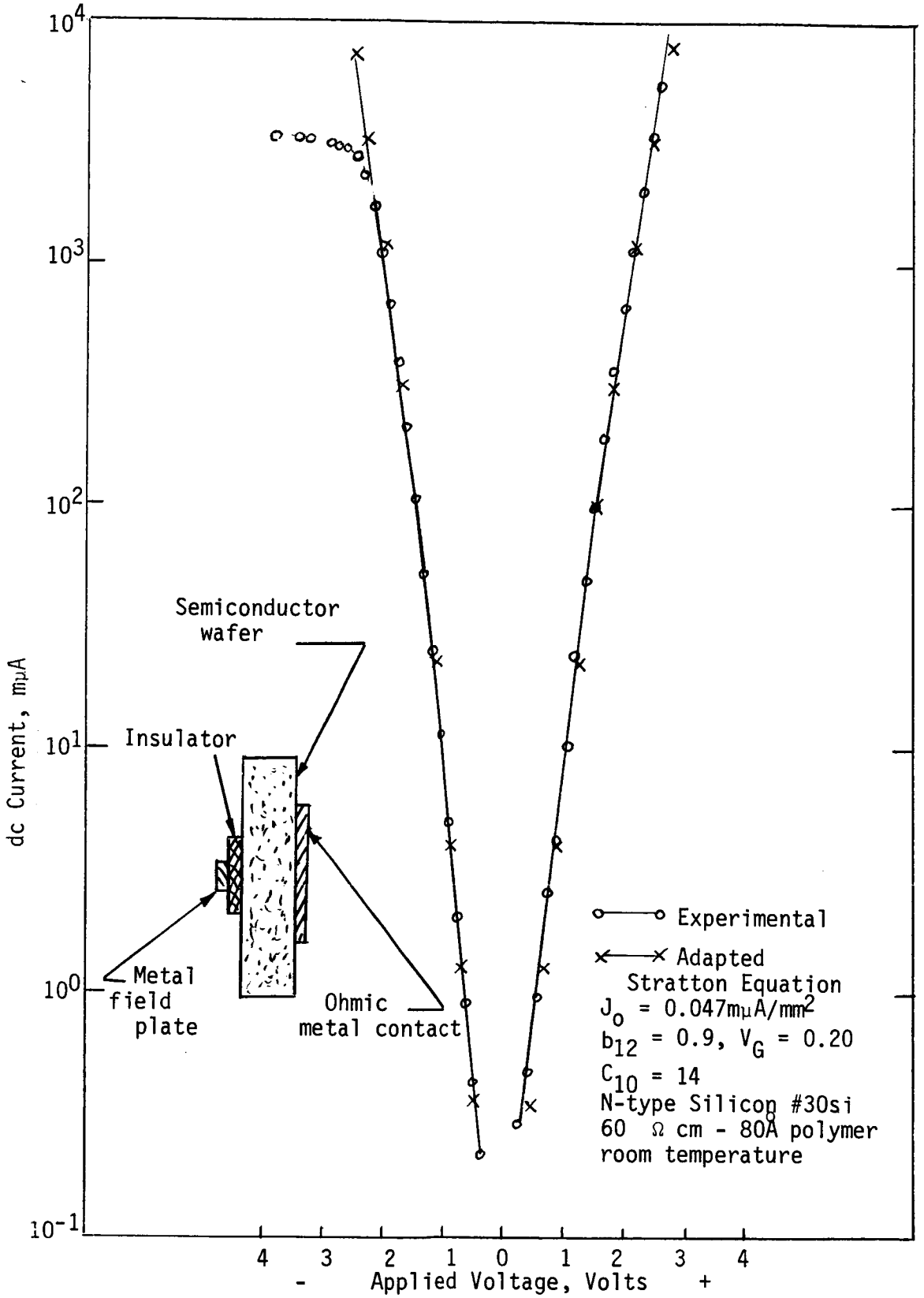

Figure 33. Theoretical and experimental N-type MIS current-voltage characteristics.
Negative voltage indicates semiconductor reverse bias.

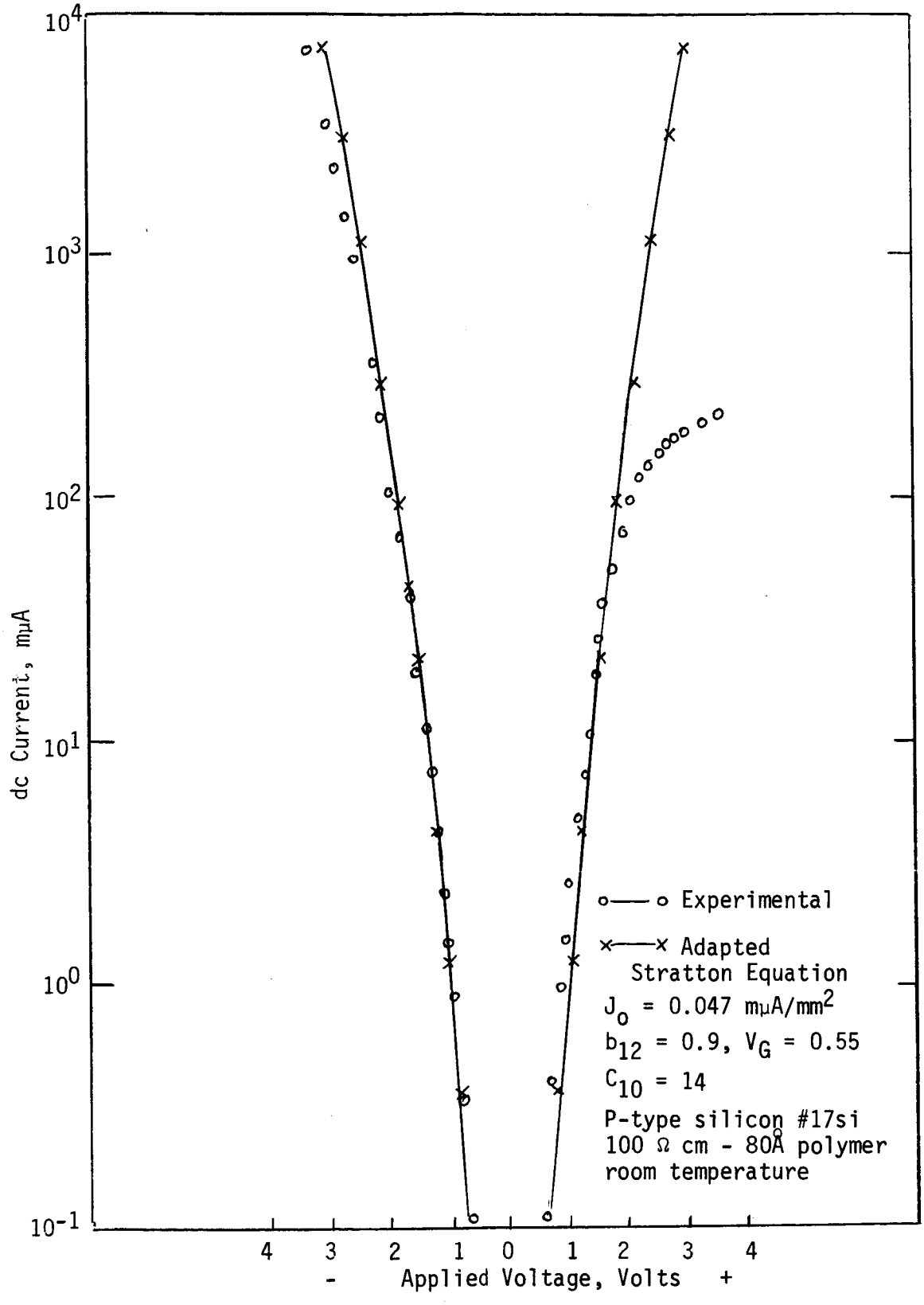

Figure 34. Theoretical and experimental P-type MIS current-voltage characteristics.
Positive voltage indicates semiconductor reverse bias.

until saturation begins. This is compatible with the model which requires complete ionization of the surface states before field penetration.

Experimental anomalies could cause the current saturation. To eliminate this possibility, three causes are investigated: 1) saturation of the measuring technique; 2) a large series resistance (either internal or external to the MIS structure); and 3) pin holes in the insulator which could allow small metal silicon diodes to be formed. If the measuring technique or a large series resistor is the cause of current saturation, then the saturation would occur with both voltage polarities and with MIM junctions, therefore eliminating case 1 and 2 by inspection. The field plate metal of Fig's. 33 and 34 is vapor deposited aluminum. To test the Al - silicon contact, aluminum was deposited directly on both N- and P-type silicon. On N-type a low resistance ohmic contact was formed. The Al - P-type silicon formed a diode with the V-I characteristics shown in Fig. 35. This diode had a large short circuit photo current, 1.7μA in the light of a 40 watt incandescent bulb at three cm. The V-I curve is continuous through the origin and does not display the symmetry of the MIS curve of Fig. 34. No photovoltaic effects occurred with the MIS samples. This evidence eliminates the possibility of metal bridges dominating the conduction through the insulator.

The polymer film MIS samples are now compared with the work of Gray.[2,3,51] Fig's. 36 and 37 give both semi-log and linear scale conductance curves for N- and P-type silicon. A set of Gray's linear scale conductance curves appear in Fig. 5 (page 13). The linear scale curves compare very closely in shape which indicates that Gray's conductance curve would also display the exponential character of tunneling. The semi-log graphs clearly reveal the exponential character of MIS tunneling

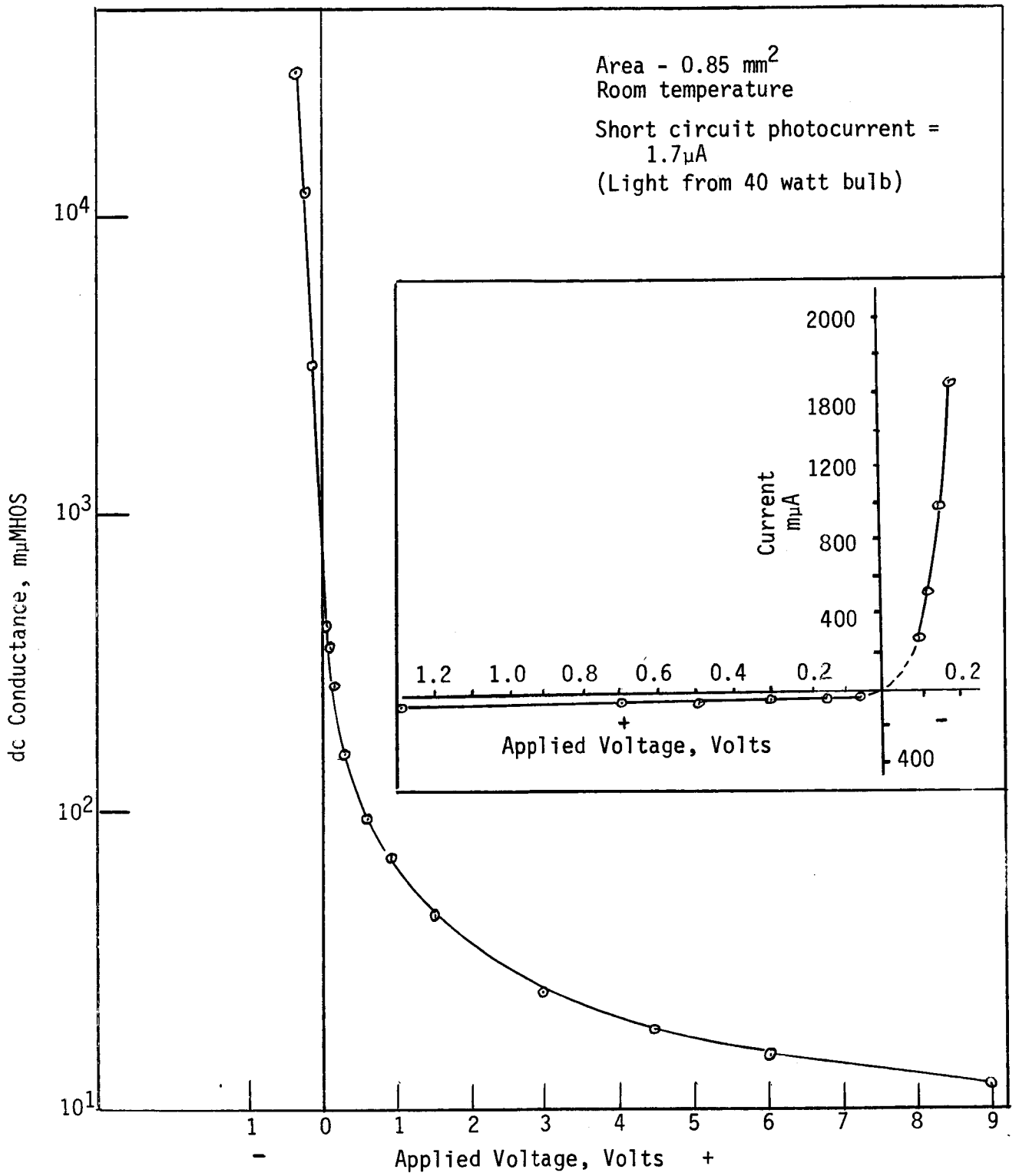

Figure 35. Aluminum - P-type silicon diode.

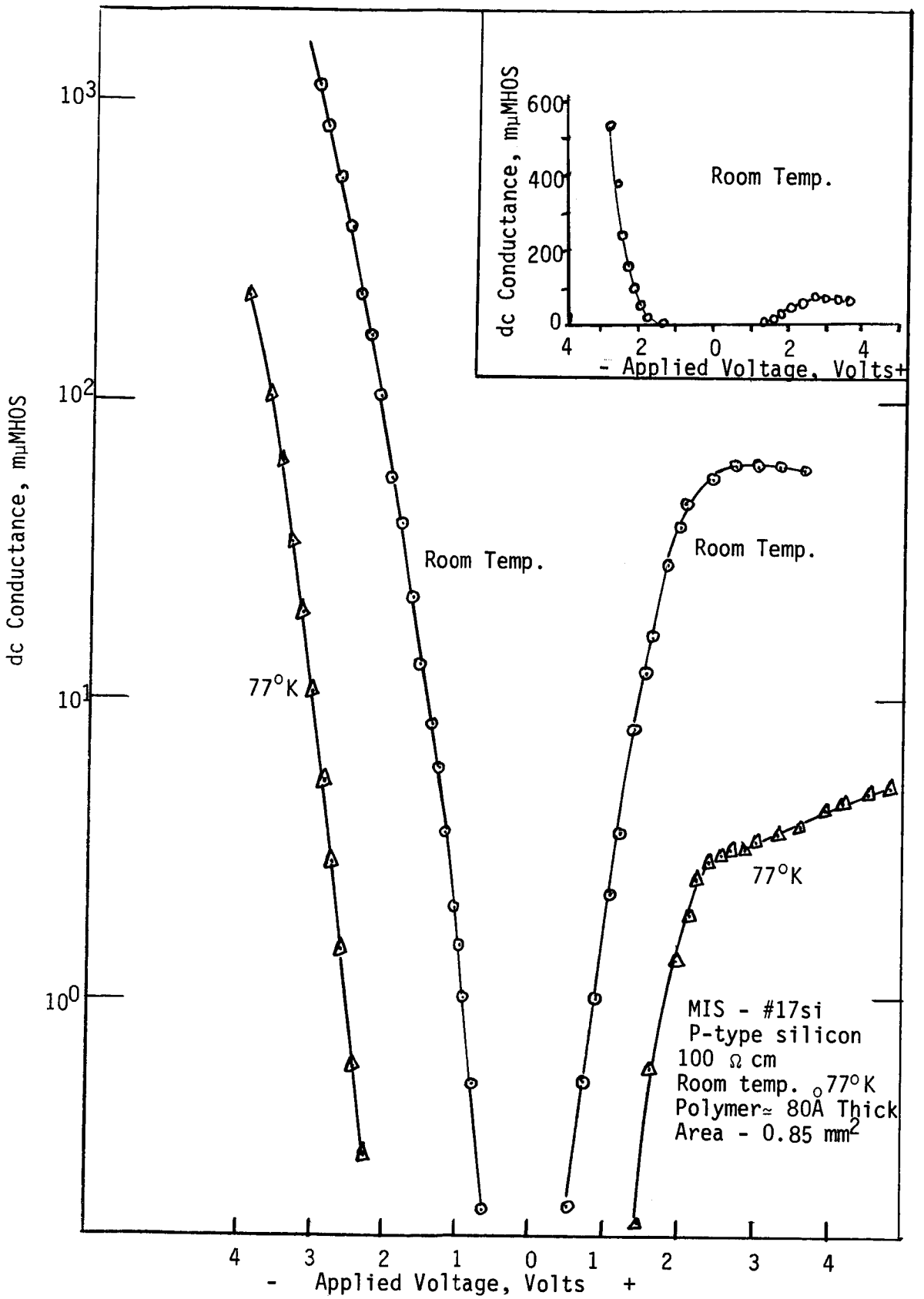

Figure 36. P-type MIS tunneling conductance.
Positive voltage indicates semiconductor reverse bias.

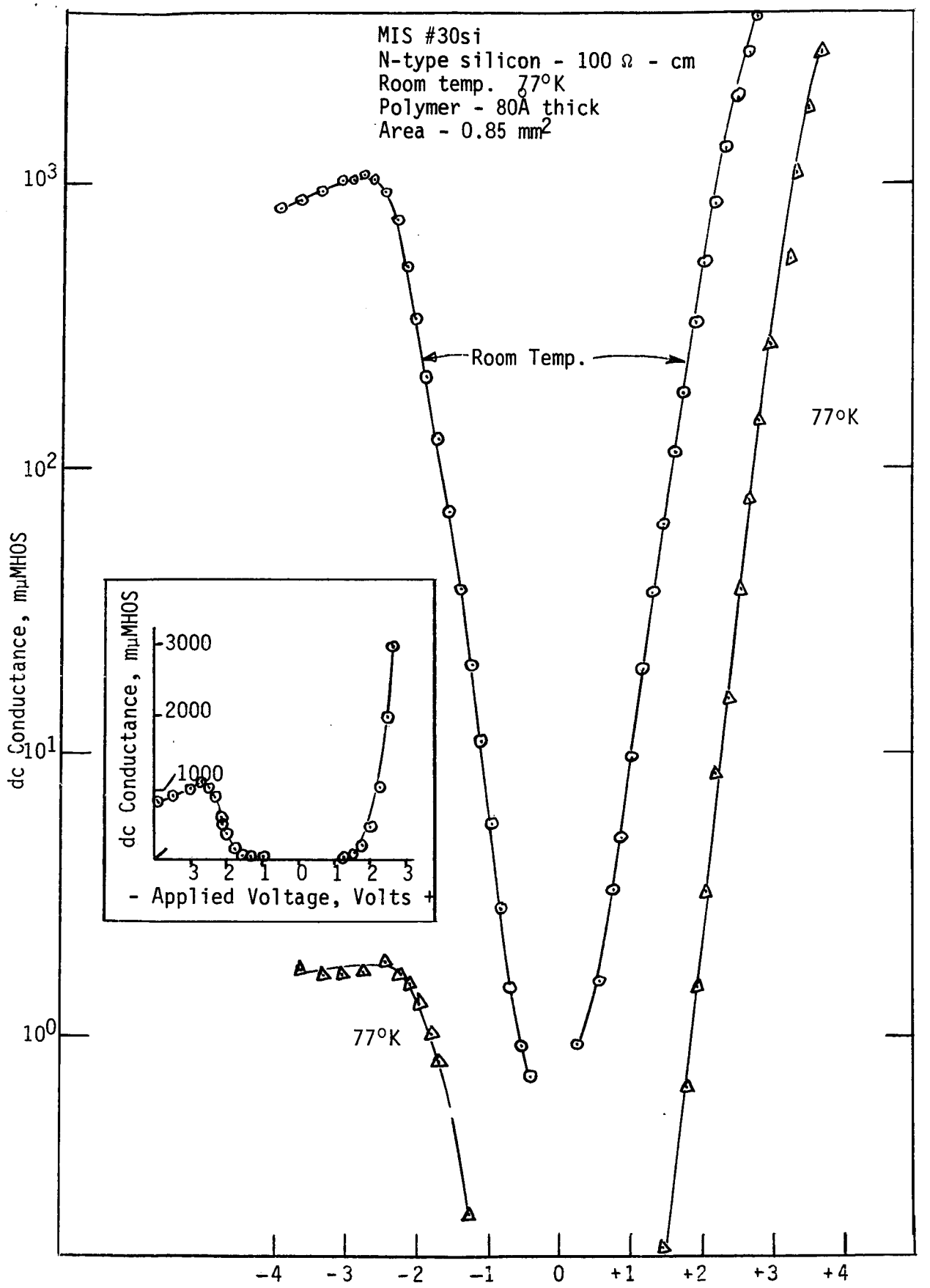

Figure 37. N-type MIS tunneling conductance.

Negative voltage indicates semiconductor reverse bias.

and suggest that another mechanism causes the saturation. Linear scale graphs do not demonstrate that fact.

The general effect of decreased temperature appears in Fig's. 36 and 37, i.e., the current decreases and the voltage at the onset of saturation depends little on temperature. This is in agreement with the model. A more detailed discussion of the temperature dependence comes later. The samples of Fig's. 36 and 37 were tested to less than four volts which provides investigation of only the first 1.5 to 2 volts of saturation. Higher voltage testing might damage the samples before other tests could be performed. However, one sample tested to 11.4 volts (Fig. 38) exhibited no damage or change in the saturation characteristics. In the saturation region the electric field in the insulator does not increase since the field penetrates the bulk semiconductor. Therefore, the MIS structure can withstand very high applied voltage when in the saturation region. If the insulator supported the entire voltage of the above sample, then the field strength of the insulator would exceed $\frac{11.4v}{100\text{Å}} = 1.14 \times 10^7$ volts/cm. This unusually high field strength adds evidence that the field penetrates the bulk.*

The model proposed in Chapter II requires that depletion and accumulation layers form on the silicon surface when external bias is applied. The fact that the layers do form with thick insulator devices is well documented.[32,36,37,38] However, for a thin insulator, the charge partially leaks off, i.e., tunnels through the insulator.[55] Therefore, the analysis must show that the depletion and accumulation layer also form with thin insulator devices. Fig's. 39 and 40 show capacitance vs

*Polyethylene[53] - 5×10^6V/cm, teflon[53] - 8×10^6V/cm are examples of the field strength of other materials.

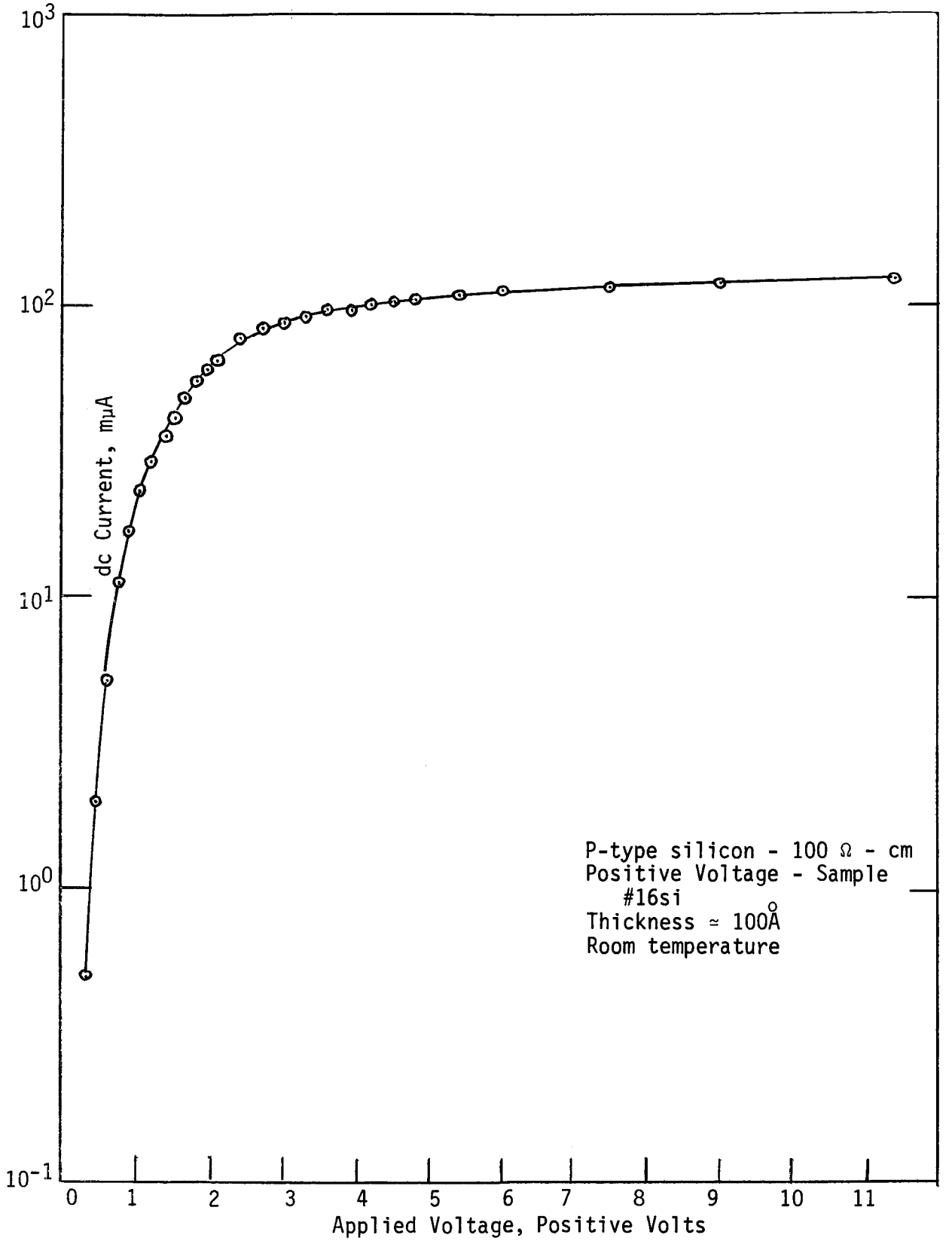

Figure 38. Saturation at high voltage.

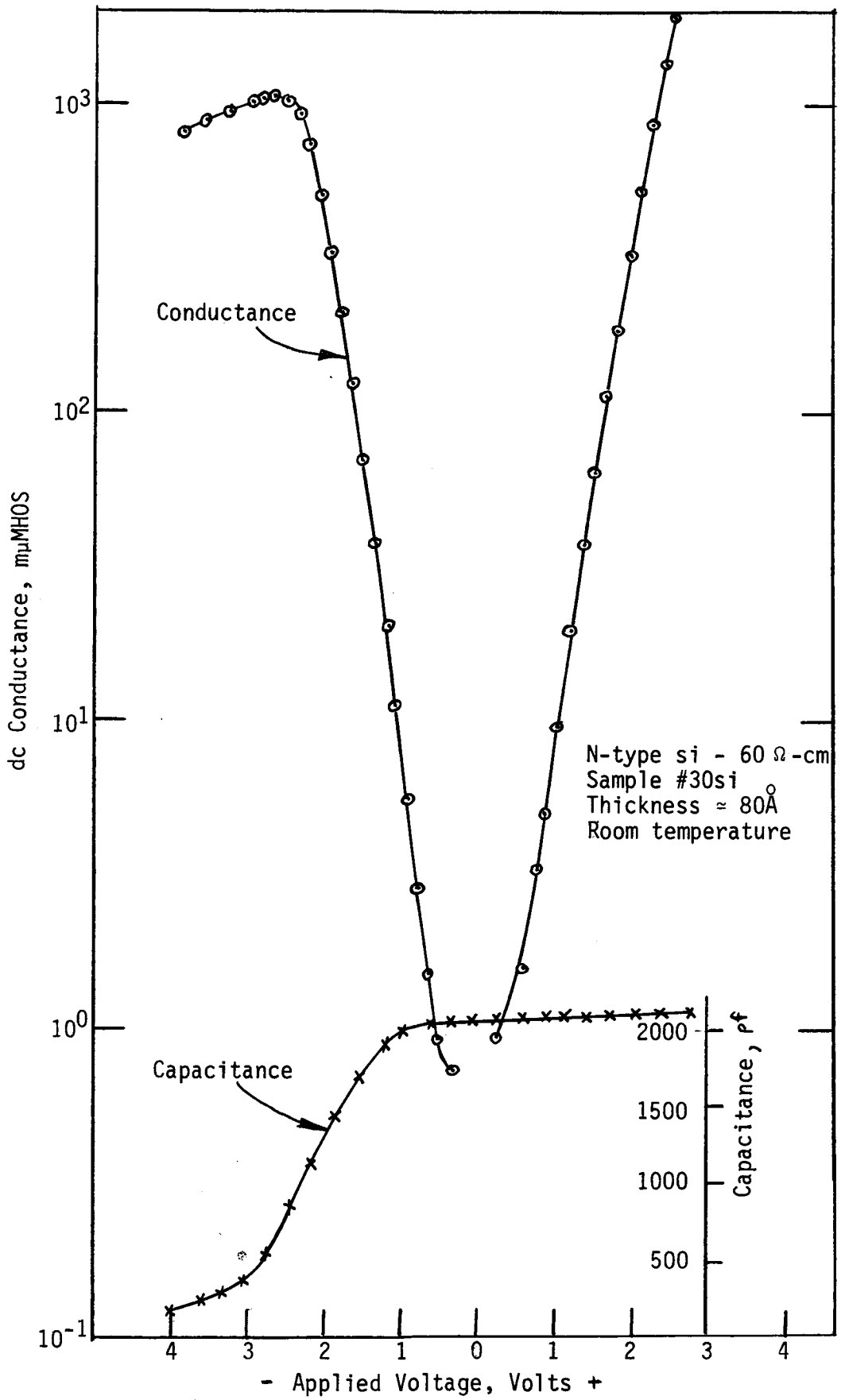

Figure 39. Depletion layer formation on N-type Silicon. Negative voltage indicates semiconductor reverse bias.

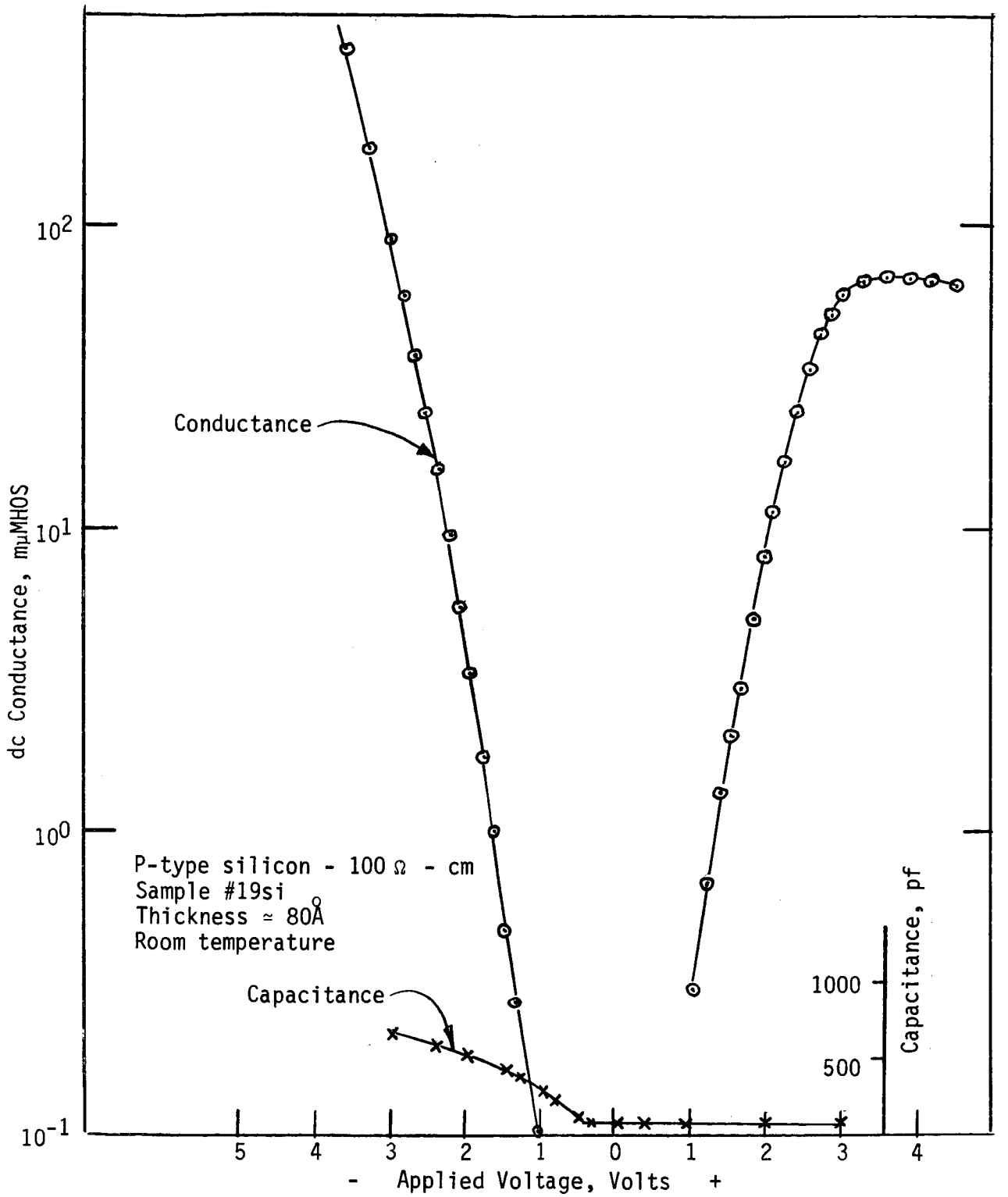

Figure 40. Accumulation layer formation on P-type silicon. Positive voltage indicates semiconductor reverse bias.

voltage and current vs voltage curves for N- and P-type silicon. The insulator thickness of these two samples is approximately 80Å. The capacitance curve of Fig. 39 clearly demonstrates the formation of a depletion layer on the N-type silicon by the sharp decrease in capacitance for negative voltage. The depletion layer forms before the current saturates. The accumulation layer is maintained with positive voltage even though a current up to 10 μA flows. The formation of an accumulation layer for negative voltage on P-type silicon is seen in the capacitance curve of Fig. 40. The capacitance does not rise as sharply as with thick insulators. This probably results from tunneling leakage of the accumulated charge. For zero bias voltage the P-type silicon surface is already depleted by an internal field. However, empty surface states remain and must fill up before the external field penetrates the bulk.

The following basic properties of the proposed MIS tunneling model are therefore established:

(a) MIS tunneling is exponential in nature and similar to MIM tunneling.

(b) Current saturation occurs with only one voltage polarity and is a separate mechanism from tunneling.

(c) Depletion and accumulation layers form on the silicon surface with thin insulators.

The model verification continues by experimentally varying the tunneling parameters and comparing the results within the concept of the proposed model.

C. Variation of Parameters

1. Insulator Thickness

Chapter II showed that the electric field at the onset of current saturation depends little on insulator thickness. This model predicts the applied voltage at saturation to increase linearly with insulator thickness but the saturated current level to remain constant. To test these properties, three samples with different insulator thickness were constructed on N-type silicon with an aluminum field plate. The thickness of the three samples came from assuming a linear film formation rate of 6.7Å/min. This linear formation rate was determined from tests on MIM junctions formed under the same polymerization conditions. The insulator thickness of the MIS sample tested are 80, 100 and 120 Å. The V-I Characteristics of these samples appear in Fig. 41. Note that the tunneling current decreases for increased insulator thickness but the saturated current level remains approximately constant. To assign the point of saturation, the V-I curves are extrapolated beyond saturation as shown in Fig. 42 and the voltage drop across the silicon surface, V_S is determined by $V_s = V_A - V_I$, where V_I is the voltage required to produce the extrapolated current curve and is considered the voltage drop across the insulator. V_S, V_I and E_I are plotted as a function of applied voltage in Fig. 43. The voltage drop, V_s, across the silicon surface is zero until saturation; it then increases in direct proportion to the applied voltage. The extrapolation of V_s in Fig. 43a, back to $V_s = 0$ serves as the value of applied voltage at which saturation begins, i.e. $V_A = V_Q$. V_Q is the voltage required to fully charge the surface states. The insulator voltage and field increase linearly with applied but level off and approach a constant when saturation is reached.

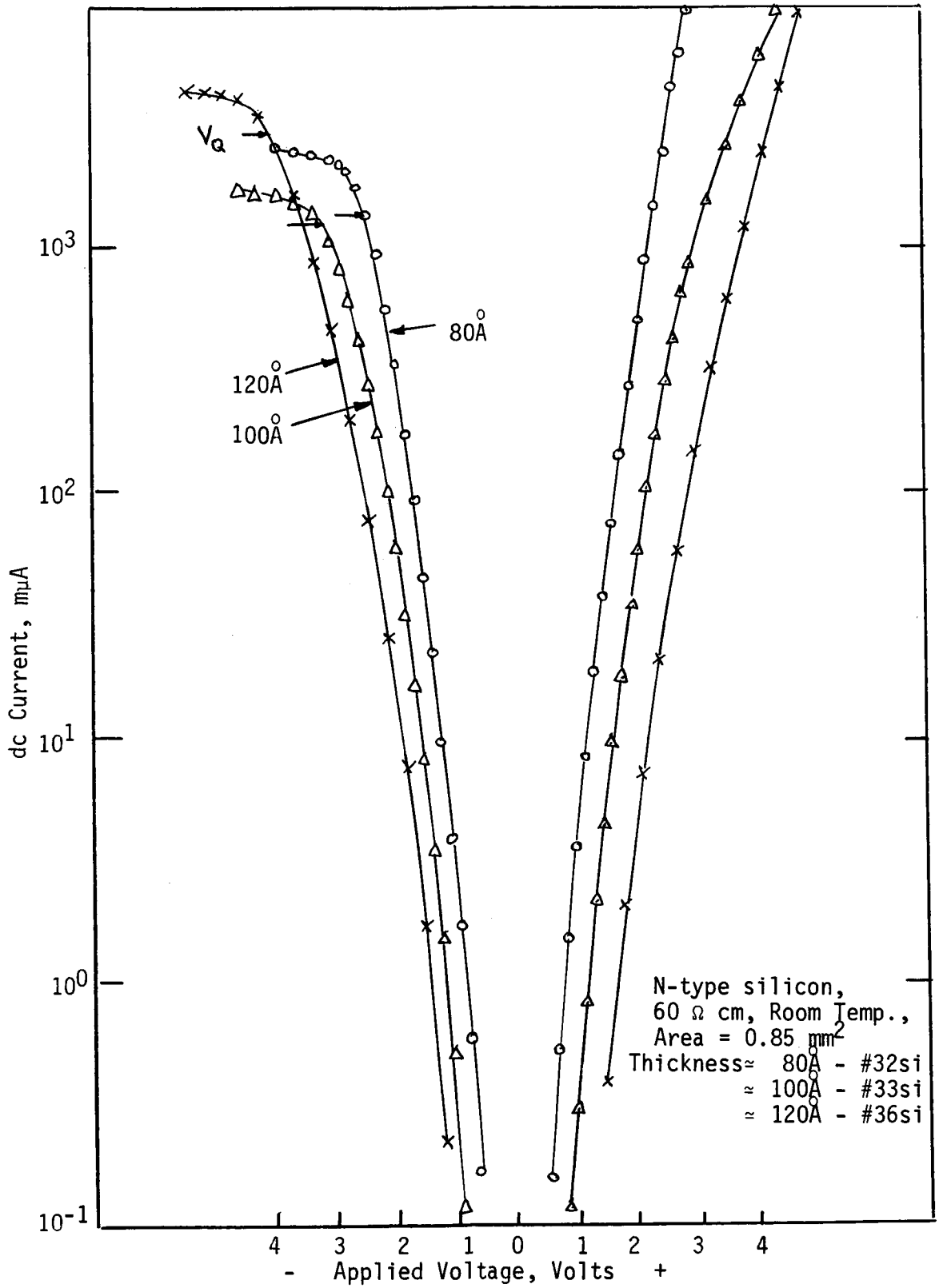

Figure 41. N-type MIS tunneling for three polymer thicknesses.

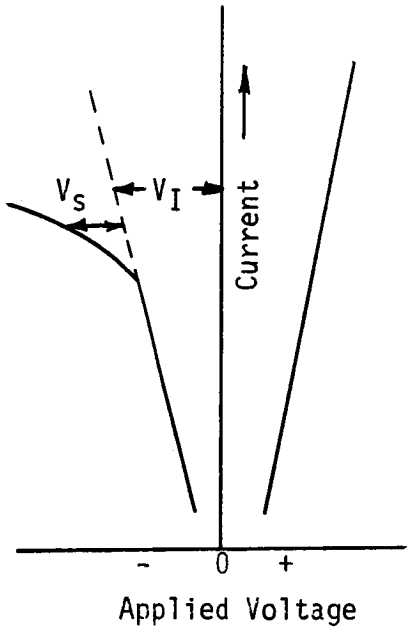

Figure 42. Method of determining V_s.

Fig. 44 shows the voltage at saturation, V_Q, to increase linearly with insulator thickness, and the field $E_Q = \frac{V_Q}{L}$ holds approximately constant. The current at $V_A = V_Q$ is also approximately constant as shown in Fig. 45. Fig. 45 also shows the exponential dependence of MIS tunneling current upon insulator thickness for V_A = constant $< V_Q$. For comparison, current vs thickness also appears for MIM tunneling.

The surface state density is often calculated from capacitance - voltage data. Tunneling saturation provides a new method of calculating surface state density since the electric field at current saturation relates to the surface states by:

$$\frac{Q}{eA} = \frac{\varepsilon E}{e} = N,$$

Where: N is the density of surface states

E is the field at saturation.

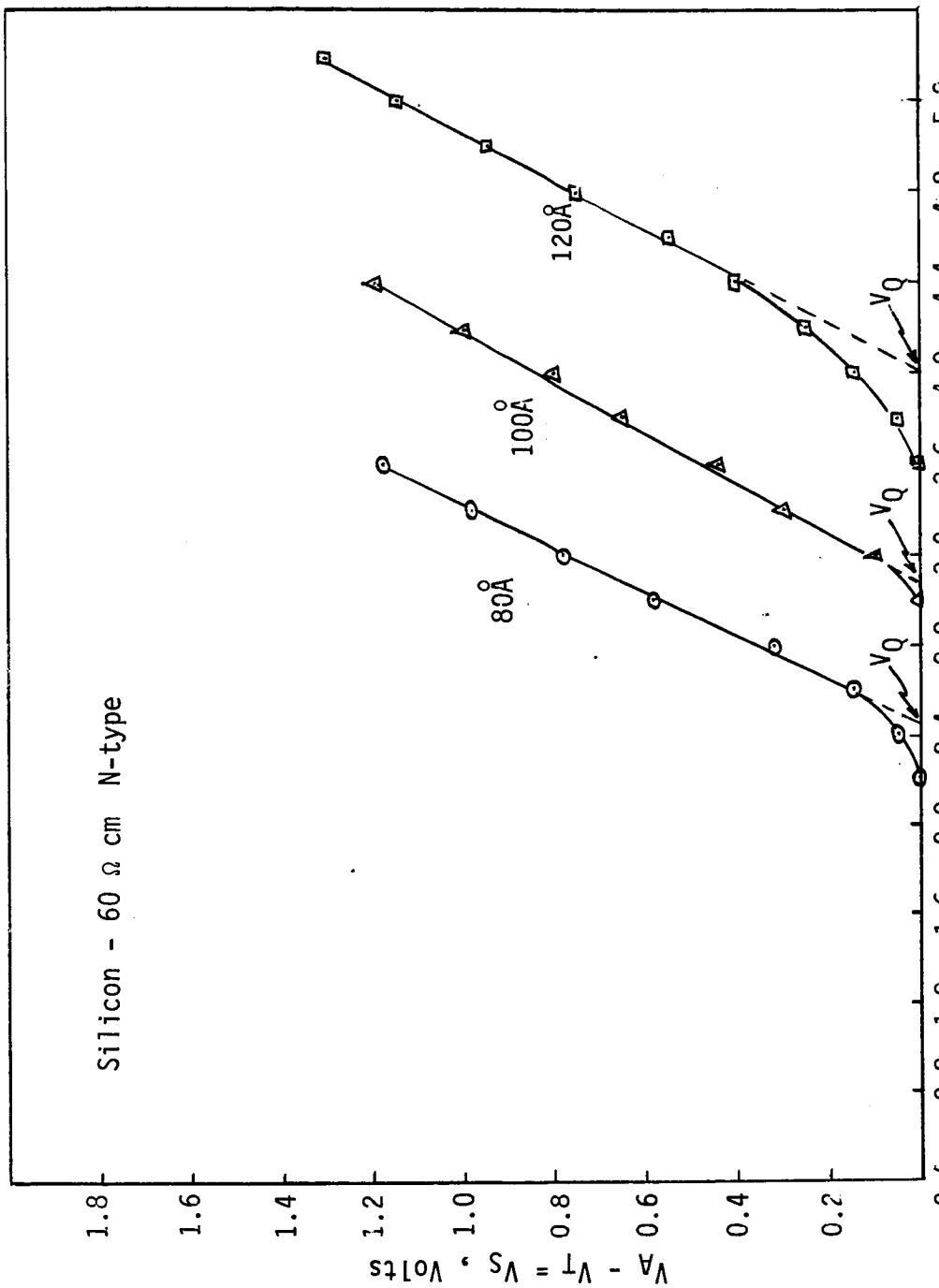

Figure 43a. Voltage drop across the semiconductor for samples of Fig. 42.

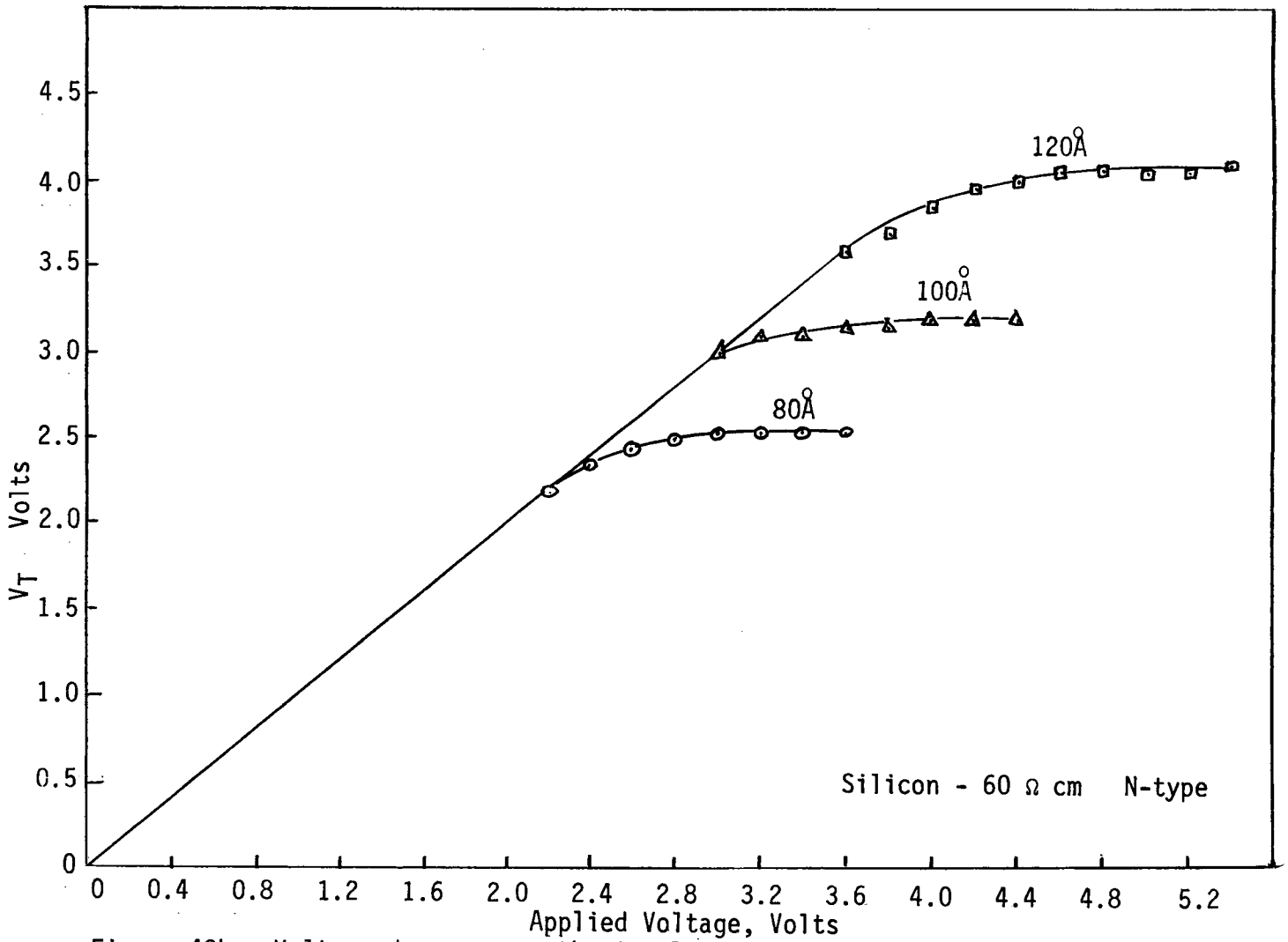

Figure 43b. Voltage drop across the insulator for samples of Fig. 42.

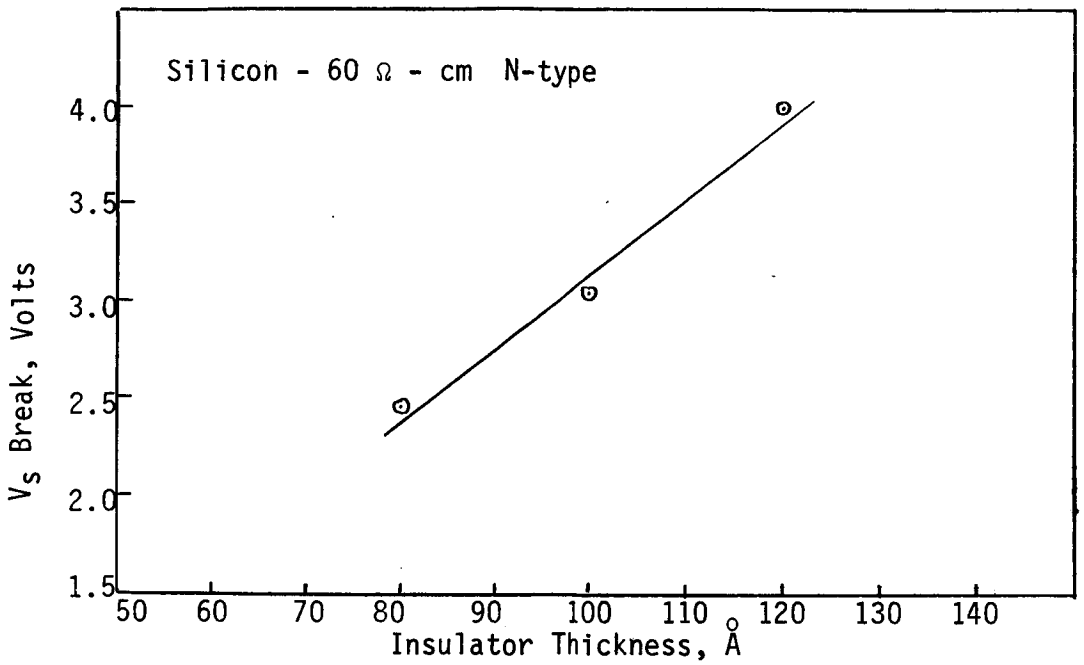

Figure 44a. Saturation voltage versus insulator thickness for samples of Fig. 42.

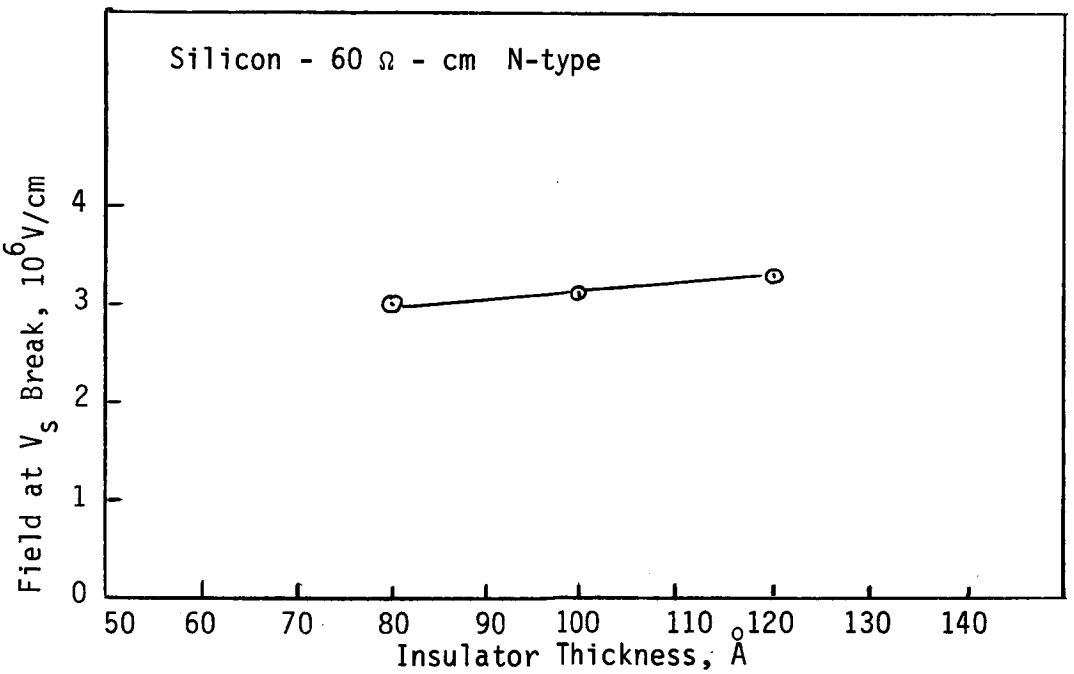

Figure 44b. Field at saturation versus thickness for samples of Fig. 42.

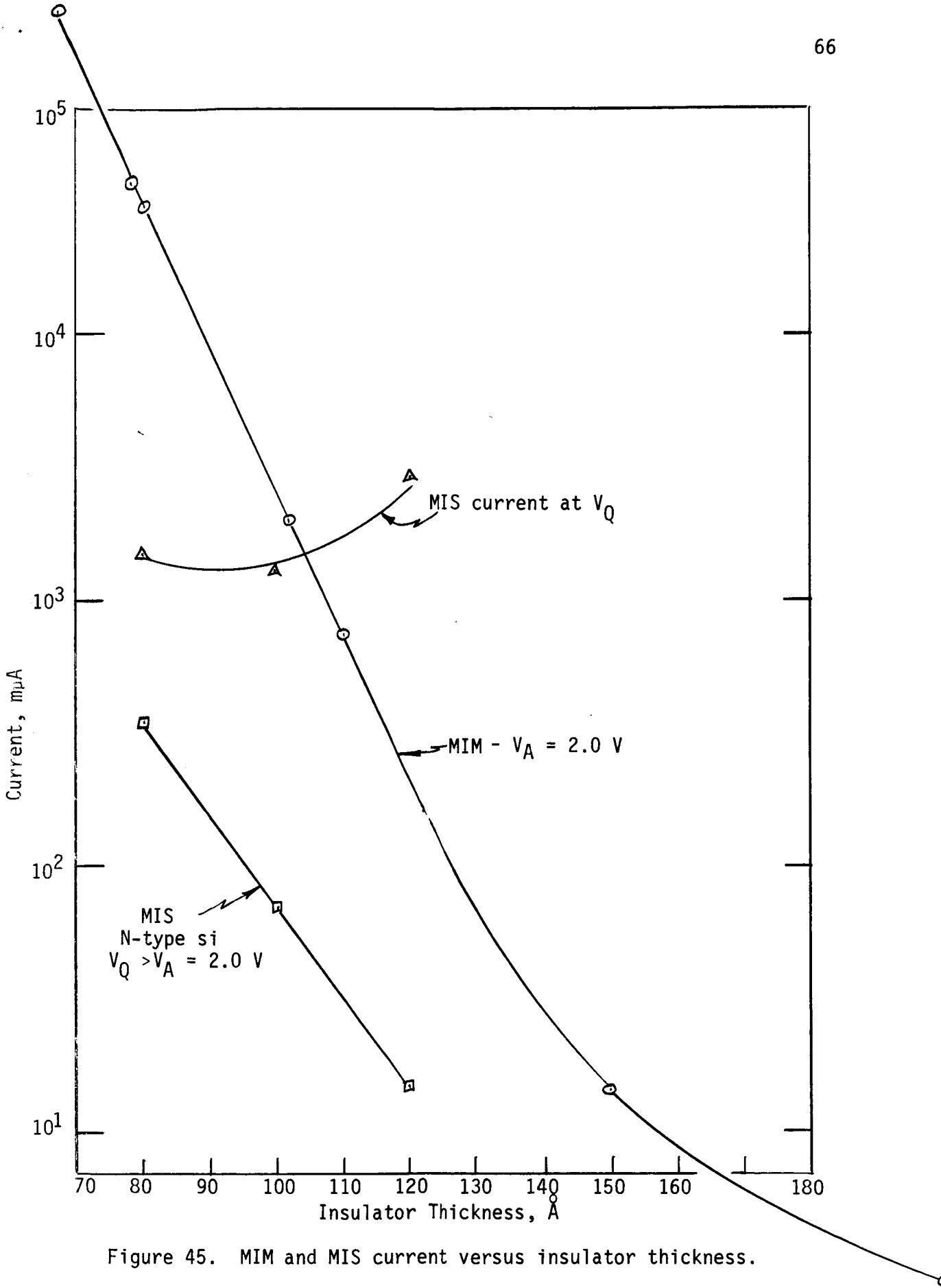

Figure 45. MIM and MIS current versus insulator thickness.

From Fig. 44b, $E_Q \simeq 3 \times 10^6$ volts/cm.

$$N = \frac{(2.8)\ (8.85 \times 10^{-14}\ f/cm)\ (3 \times 10^6\ V/cm)}{1.6 \times 10^{-19}\ coul/state}$$

$$N = 4.7 \times 10^{12}\ states/cm^2.$$

By the capacitance method with data from Fig. 39,

$$N = \frac{Q}{eA} = \frac{CV}{eA} = \frac{(2.05 \times 10^{-9} f)\ (2.3\ Volts)}{1.6 \times 10^{-19}\ coul/state)\ (0.85 \times 10^{-2} cm^2)}$$

$$N = 3.5 \times 10^{12}\ states/cm^2$$

The density of states calculated by the tunneling method is 34% larger than the value calculated from the C-V curve. This may be caused by multiply-charged sites but these sites would probably be evident in both experimental methods. In any event, it is clear that tunneling saturation may be utilized as a method of studying semiconductor surface states.

2. Field Plate Work Function

The amount of charge transferred between the field plate metal and the silicon depends upon the difference in work function of the two electrodes. N-type silicon transfers electrons to a large work function field plate, thus remvoing charge from the surface states. As a result the proposed MIS tunneling model predicts the current level at saturation to decrease exponentially with the difference in the silicon and metal work functions. To test this property, several N-type MIS samples were made using different work function[50] field plate metals; aluminum (ϕ = 3.7 ev), tin (ϕ = 4.1 ev), and gold (ϕ = 4.6 ev). The V-I curves of Fig. 46 for these metals show the effects of the work function upon current level at saturation.

Some experimental difficulty occurred in testing of the gold samples. The current appeared very erratic and all three samples tested broke down with small positive voltage. Note in Fig. 46 that the gold curve is shifted to high voltage. The reasons for this anomaly are not known although it may be associated with the high temperature required to evaporate the gold. The heat may have affected the polymer insulator.

The curves of Fig. 46 are offset and do not lend themselves to the type of analysis used with the variation of insulator thickness. To obtain useful information concerning the effect of work function upon MIS tunneling, the d c conductance is plotted in Fig. 47. These conductance curves reach a definite maximum. Plotting these maxima as a function of $\Delta\phi$ results in the approximate straight line of Fig. 48. Therefore, the experimental anomalies do not mask the dependence of the current saturation upon the density of filled surface states and implies that the saturation depends upon the surface states and not other tunneling parameters.

3. Temperature

Fig's. 36 and 37 show the general effect of reduced temperature on MIS tunneling characteristics. The tunnel efficiency decreases but the voltage at saturation holds approximately constant. To examine the effect of temperature upon the point of saturation, the voltage drop across the semiconductor surface, V_s, is plotted as a function of applied voltage at 296 and 77°K. Fig. 49 illustrates two P-type samples. These curves demonstrate the approximate invariance of the point of saturation. This is in agreement with the simple case discussed in Chapter II.

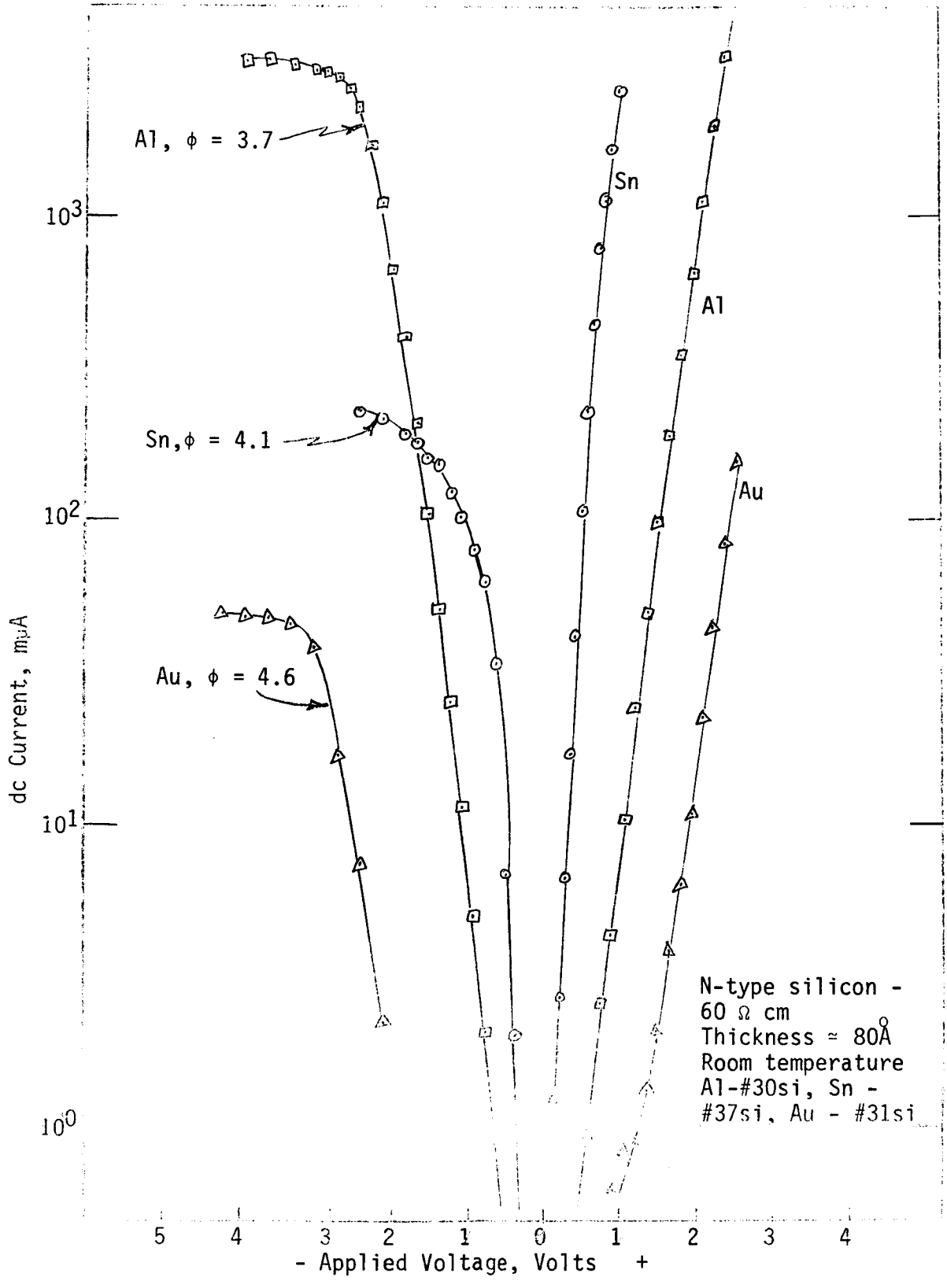

Figure 46. Effect of field plate work function on V-I characteristics.

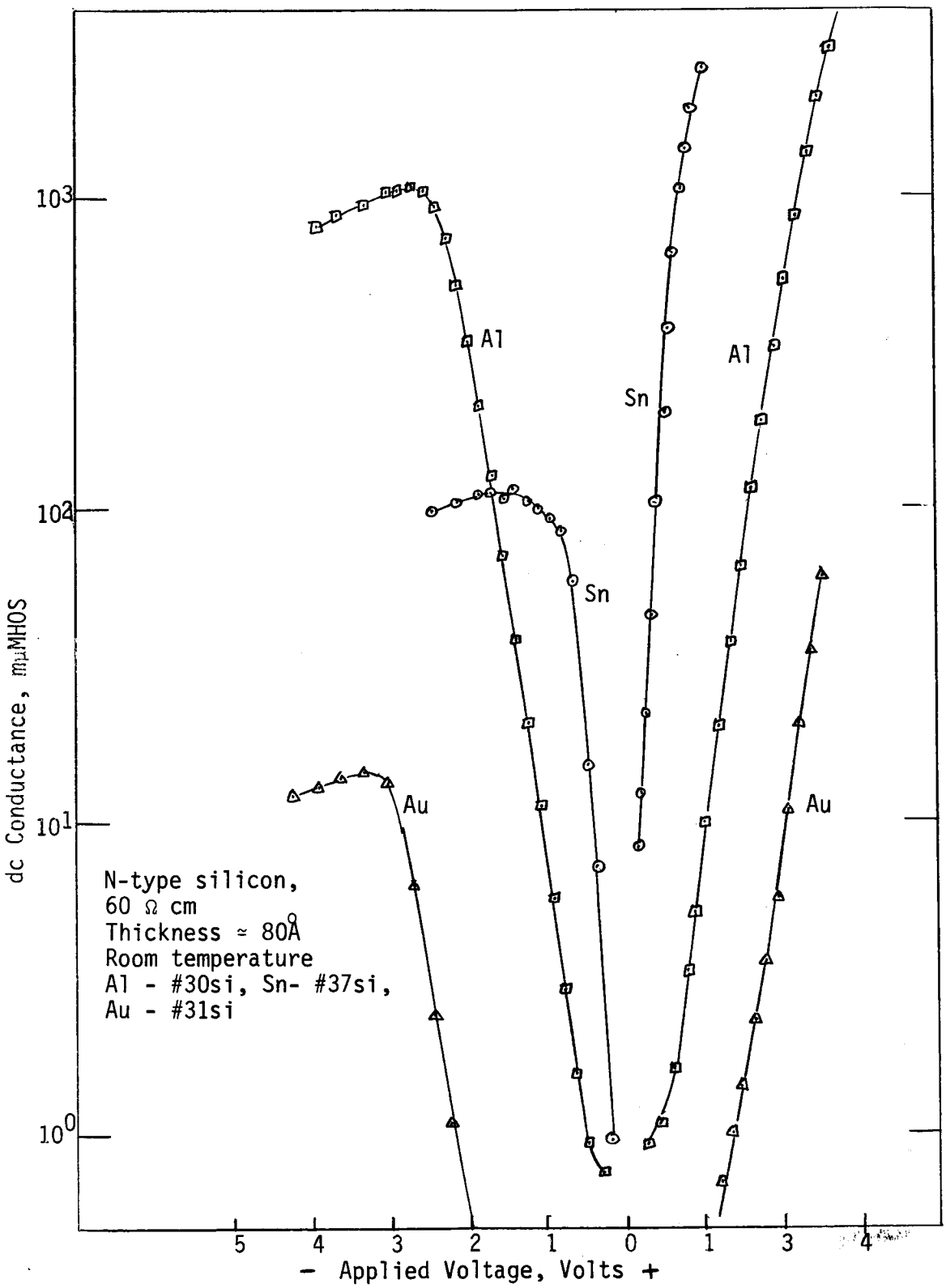

Figure 47. Effect of field plate work function on conductance curves.

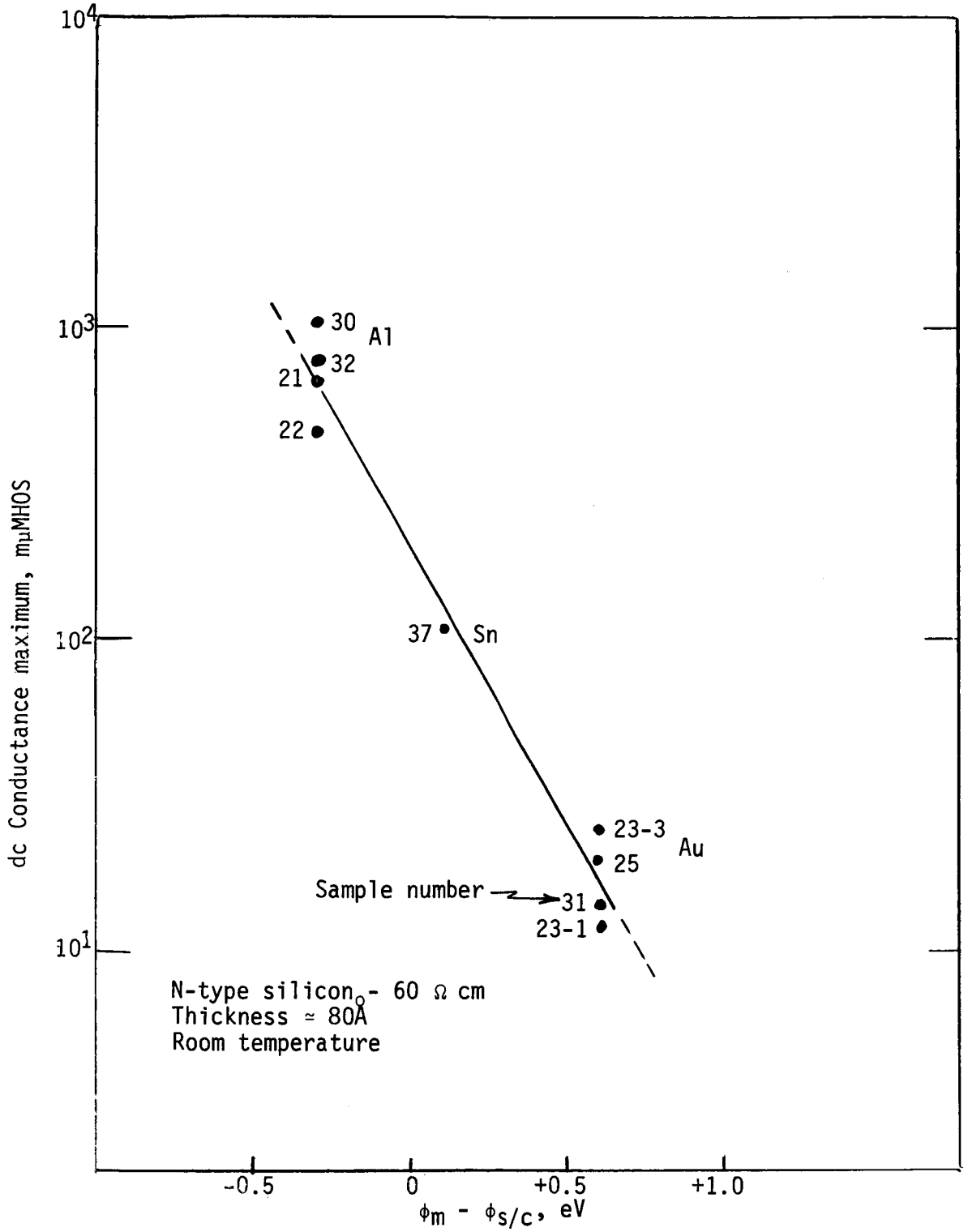

Figure 48. Conductance maximum versus difference in work function.

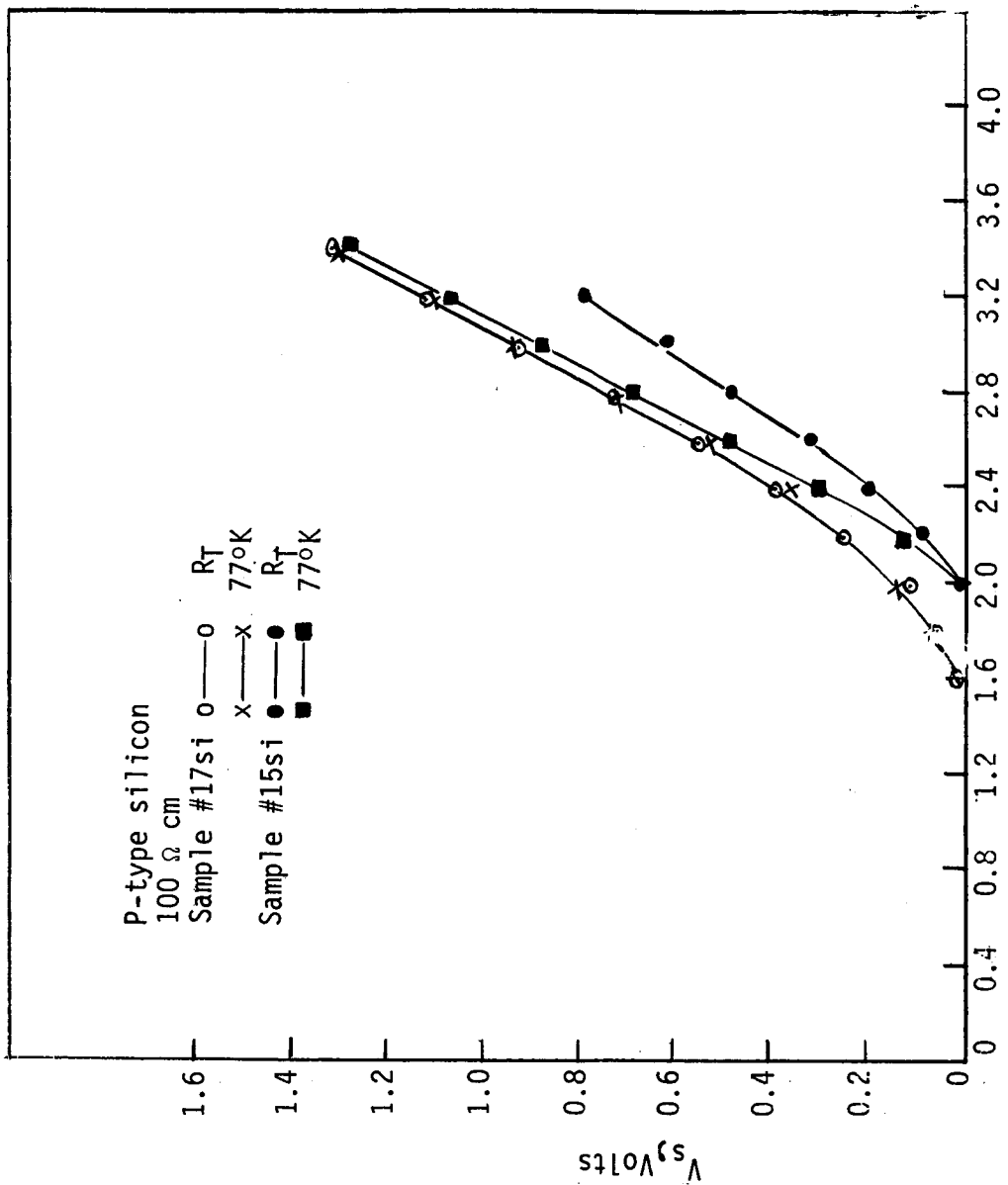

Figure 49. Temperature dependence of the voltage drop across si surface.

D. Impurity Distribution at the Silicon Surface

The variation of the depletion layer capacitance with voltage is dependent upon the impurity and defect distribution in the semiconductor as illustrated in Fig. 50 for an abrubt junction diode. A semiconductor surface is disturbed by many defects which penetrate a finite

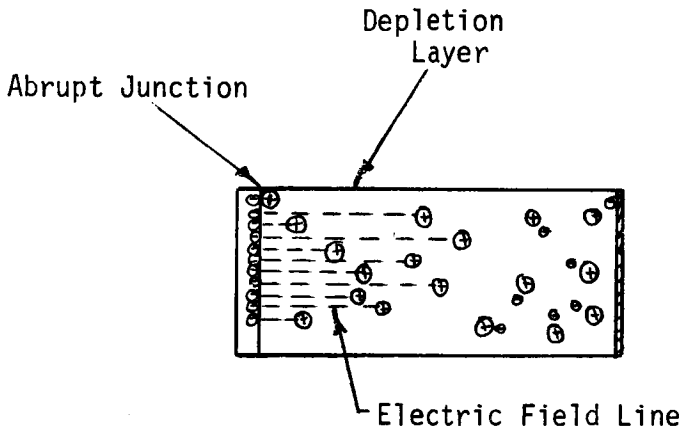

Figure 50. Impurity-defect distribution in a semiconductor.

depth into the semiconductor bulk. These defects may cause a non-homogeneous distribution of localized states in the bulk near the surface. The MIS tunneling junction offers a possible experimental method of determining this distribution. The analysis which follows first discusses abrupt PN junctions and thick insulator MOS structures. This is followed by an analysis of thin MIS structures which utilizes the point of tunneling saturation to determine the voltage at which the surface states are completely filled.

For an abrupt junction PN diode, Schottky[64] found that the reciprocal depletion layer capacitance increased linearly with the square root of the voltage across the layer. This square root

relationship has been verified many times, e.g. Giacoletto.[65] Garrett and Brattain[66] point out that the assumptions which produce the square root dependence are clearly met by a reversed biased PN junction but not completely by the surface of a semiconductor. Fig. 51 is a plot of $(1/C_{sp})^2$ versus applied voltage for the N-type MIS capacitance-voltage curve of Fig. 39. C_{sp} is the space charge (depletion) capacitance calculated from the measured capacitance using the following equivalent circuit:

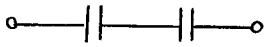

C_i C_{sp} , C_i = Insulator capacitance.

If the depletion layer followed a square root relationship, as does an abrupt PN junction, then the curve of Fig. 51 would be a straight line. Lehovec, et al[37] and Terman[36] reason that the depletion layer capacitance of an MIS structure follows the square law relationship but the charge which collects in the surface states prevents the manifestation of this fact in a simple $(1/C_{sp})^2$ versus applied voltage plot. In a back-biased PN junction all of the applied voltage appears across the depletion region. In the MIS structure, however, the applied voltage is divided between the insulator and the depletion layer. How the voltage divides depends upon how the charge collects in the surface states. Lehovec assumes the MIS equivalent circuit to be:

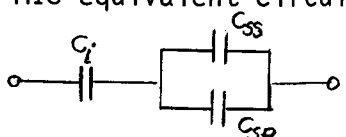

where: C_i = the insulator capacitance

C_{sp} = the space charge capacitance

C_{ss} = the capacitance associated with the charge collected in the surface states.

If the total capacitance is measured at a high frequency, the charge in

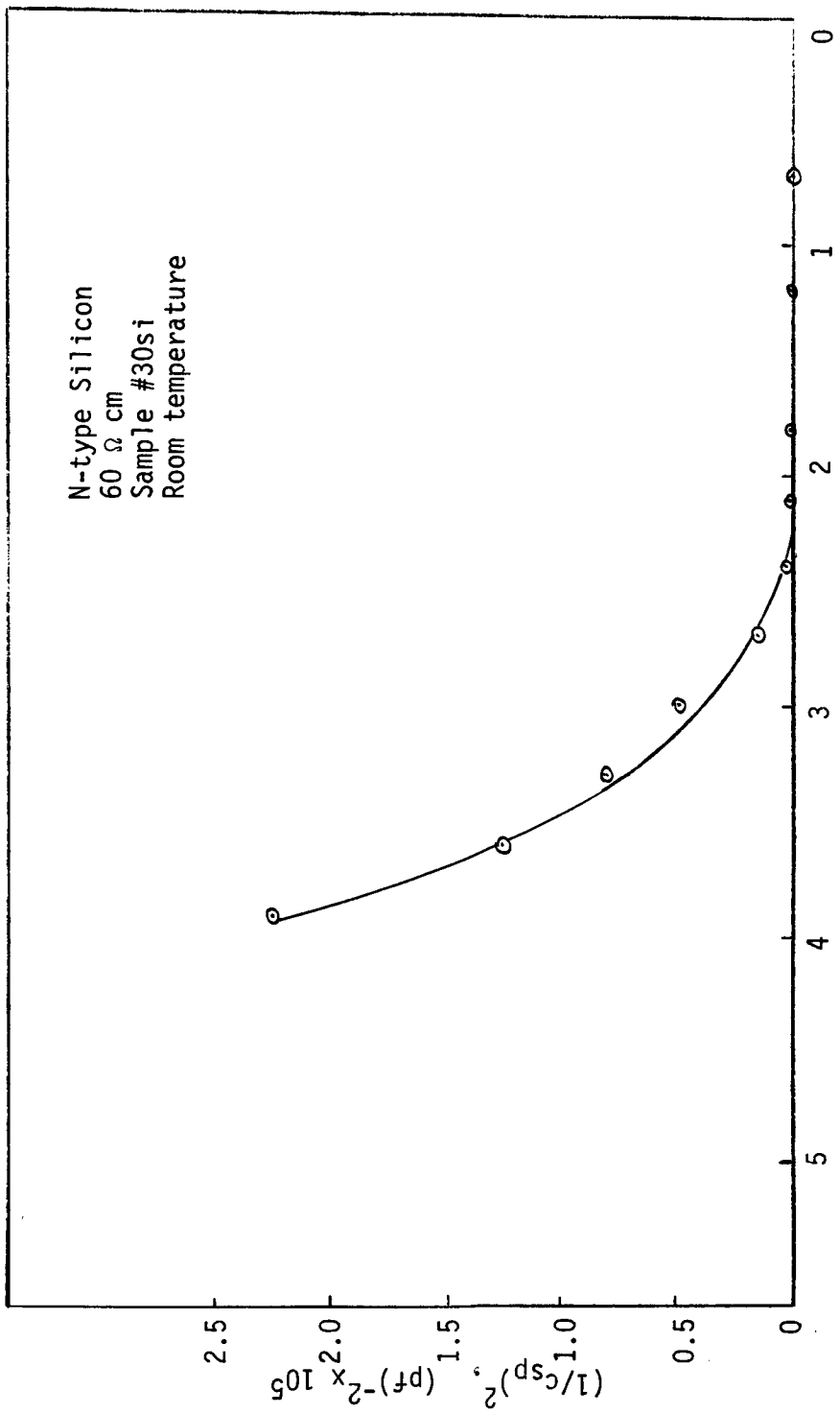

Figure 51. Square of the reciprocal depletion layer capacitance versus applied voltage.

the surface states cannot follow the ac field, hence the contribution of the surface state to the total capacitance is not known with confidence. However, Lehovec assumes the high frequency equivalent circuit to be:

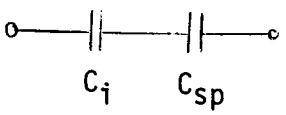

The measured capacitance, C_m, is:

(39) $$\frac{1}{C_m} = \frac{1}{C_i} + \frac{1}{C_{sp}} \quad \text{and} \quad C_{sp} = \frac{C_m C_i}{C_i - C_m}$$

Lehovec then assumes a form of the Garrett and Brattain square root equation (which assumes a homogeneous distribution of impurities).

(40) $$C_{sp} = \left(\frac{\varepsilon n_o e^2}{2kT}\right)^{1/2} \left\{ \frac{1 - \exp\left(\frac{eV_{sp}}{kT}\right)}{\left[\frac{-eV_{sp}}{kT} - 1 + \exp\left(\frac{eV_{sp}}{kT}\right)\right]^{1/2}} \right\}$$

where: V_{sp} = voltage across the space charge region

n_o = bulk electron concentration

e = electronic charge

ε = the dielectric constant.

Note that V_{sp} is negative which leads to Eq. (41) for $\frac{eV_{sp}}{kT} >> 1$.

(41) $$C_{sp} = \left(\frac{\varepsilon n_o e}{2}\right)^{1/2} V_{sp}^{-1/2}$$

From Eqs. (39) and (40) the voltage drop across the depletion layer can be calculated. With V_{sp} known, the space charge, Q_{sp}, can be subtracted from the total charge. This difference is attributed to the charge collected in the surface states.

Since the square root depletion layer equation is known to be valid for depletion layers within the bulk silicon, Lehovec's formulation

seems reasonable for a depletion layer which has penetrated the bulk. This permits calculation of the surface state charge as a function of applied voltage. However, surface defects may penetrate the bulk silicon and create a non-homogeneous distribution of localized states which will give rise to a non-square root C-V relationship. At low voltage the impurity distribution analysis is complicated by the collection of charge in surface states. At higher voltage the surface states are filled and the C-V relationship is directly related to the impurity and defect distribution. The dc voltage at which the surface states are fully charged can be obtained for thin insulator MIS structures from a tunneling current curve for the same sample. The point of current saturation corresponds to the point of filled surface states and can be found by the method of Fig. 43a. For sample #30si, the voltage at saturation, V_s, is 2.4 volts. Subtracting V_s from the applied voltage, V_A, and plotting (V_A-V_s) versus $1/C_{sp}$ on a log-log scale (Fig. 52) yields the relation:

$$\frac{1}{C_{sp}} = B(V_A-V_s)^{0.8} \tag{42}$$

where: B = constant

V_A = applied voltage

V_s = saturation voltage

C_{sp} = depletion layer capacitance

Giacoletto[67] analyzed the C-V relationship for abrupt junction diodes with an arbitrary impurity distribution. Using Giacoletto's results, the impurity-defect distribution at the silicon surface of the MIS structure can be found. The analysis proceeds as follows:

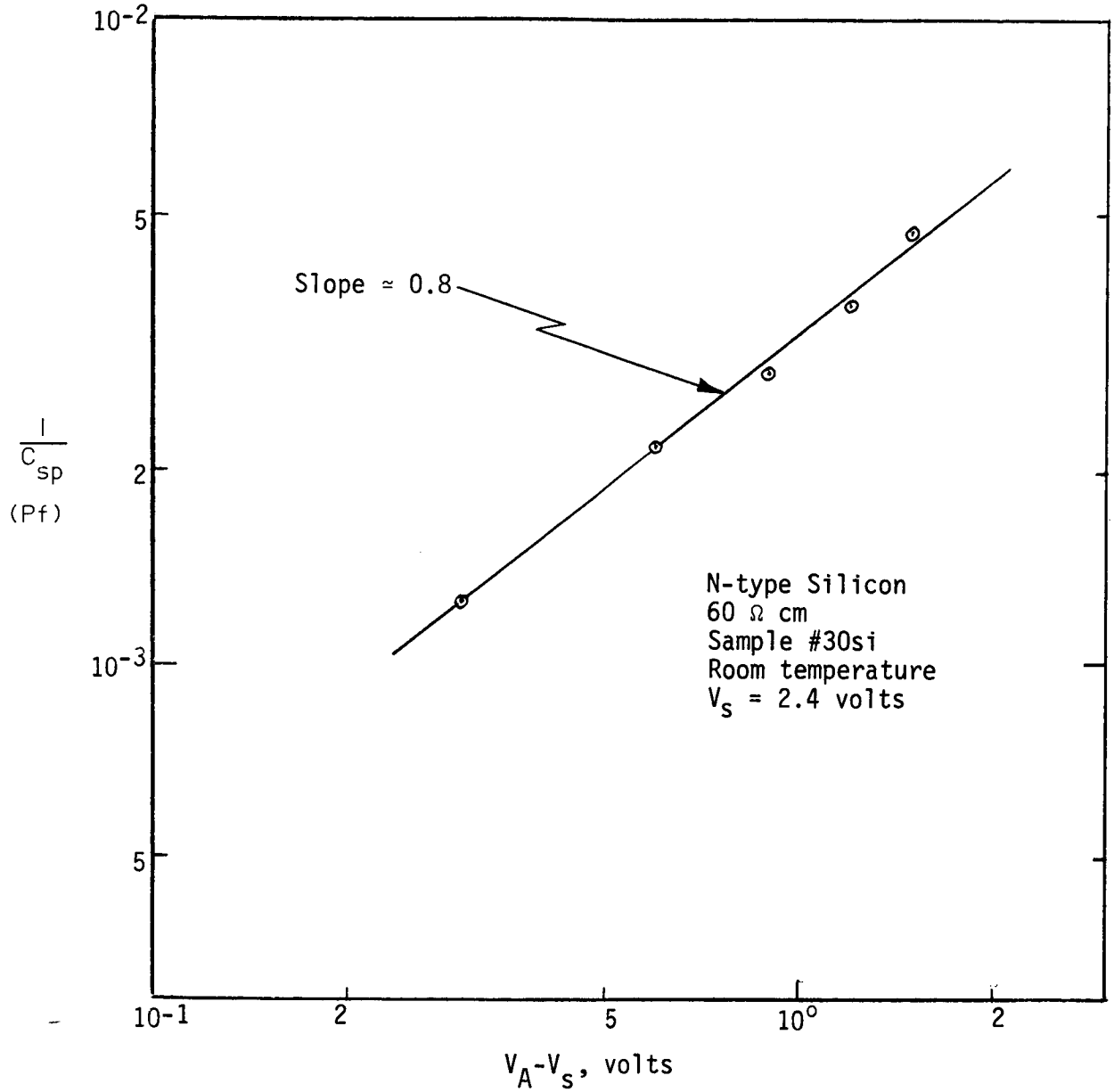

Figure 52. Reciprocal depletion layer capacitance versus depletion layer voltage.

(43) $$\frac{1}{C_{sp}} = B(V_A - V_S)^{\alpha} = \frac{W}{A\varepsilon}$$

where: W = depletion layer width

A = area

ε = dielectric constant

α = slope of the log-log C-V curve.

From Eq. (43)

(44) $$V_A - V_S = \left(\frac{W}{BA\varepsilon}\right)^{1/\alpha}$$

Giacoletto's expression for the impurity distribution, I(x), in the x direction is:

(45) $$I(x) = \frac{\varepsilon}{en_i} \quad \frac{d(V_A - V_S)}{dW}\Big|_{W = x}$$

where: e = electronic charge

n_i = intrinsic electron density.

Substituting Eq. (44) into Eq. (45) yields:

(46) $$I(x) = \frac{\varepsilon}{en_i}\left(\frac{1}{BA\varepsilon}\right)^{1/\alpha}(x)^{1/\alpha - 2} = \text{constant}\,(x)^{1/\alpha - 2}$$

From Fig. 52, α = 0.8. Therefore the impurity-defect distribution for sample #30si is, I(x) = constant $x^{-0.75}$, which is sketched in Fig. 53.

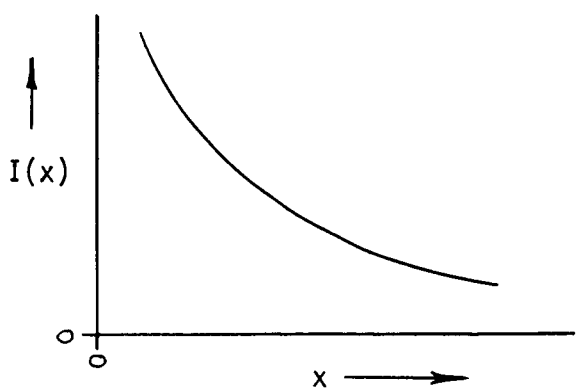

Figure 53. Impurity distribution of sample #30si.

The surface is shown to have a high impurity-defect density. This density decreases with penetration into the bulk. It is expected that I(x) would approach a constant at a sufficient distance from the surface where $\alpha = 1/2$ and $I(x) = \text{cont.} x^{\frac{1}{1/2}-2} = \text{const.}$

The above solution is dependent upon the choice of V_s which determines the exponent α. Also the location of $x = 0$ is not known. However, the above method seems to be valid and opens the door to a means of investigating impurity-defect distributions at a semiconductor surface. The method may be particularly useful in examining the MIS system with a thermally grown oxide since the oxidation process can change the surface doping density by diffusion redistribution of the impurities and by impurity rejection from the oxide.[68] It may also be possible to determine the depth of surface damage by correlating the voltage at which the capacitance begins to follow the square root law relation.

CHAPTER IV

Experimental Techniques

A. Formation of the Polymer Film

The formation of a thin pin-hole-free insulator is essential to successful tunneling experiments. There are several methods of forming a thin insulator, e.g., oxide growth and vapor deposition. The parameters of vapor deposited insulators, such as SiO, are difficult to control and the films often contain pin holes. Grown oxides depend upon the substrate material and therefore comparison of results on different substrate materials is difficult. A polymer film was chosen as the insulator for this research. It forms easily on a variety of substrates with a great deal of control of the thickness and uniformity.

K. M. Poole[56] describes the process by which organic molecules polymerize in a beam of electrons. The polymerization process begins when low energy electrons break the bonds between radicals of an organic molecule. Both single and double-ended radicals form. The double-ended radicals have two unsaturated bonds and are the building blocks which join together to form long chains. The single-ended radicals have only one unsaturated bond and cause the chains to terminate, thus impeding the polymerization process. Fig. 54 illustrates this building and termination diagramically.

To form a solid polymer film on a substrate consider the diagram of Fig. 55.

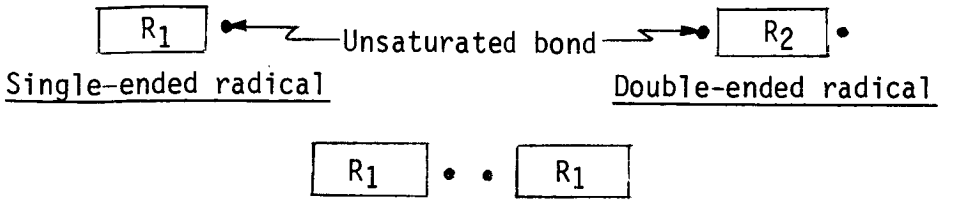

Two single-ended radicals which by necessity are terminated at both ends.

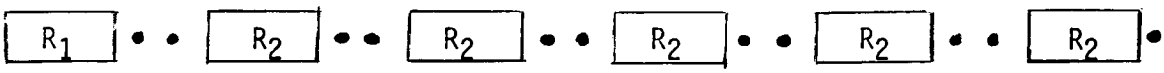

Chain of double-ended radicals terminated at one end by a single-ended radical.

Figure 54. The continuation and termination of radicals chains.

To form a solid polymer film on a substrate consider the diagram of Fig. 55.

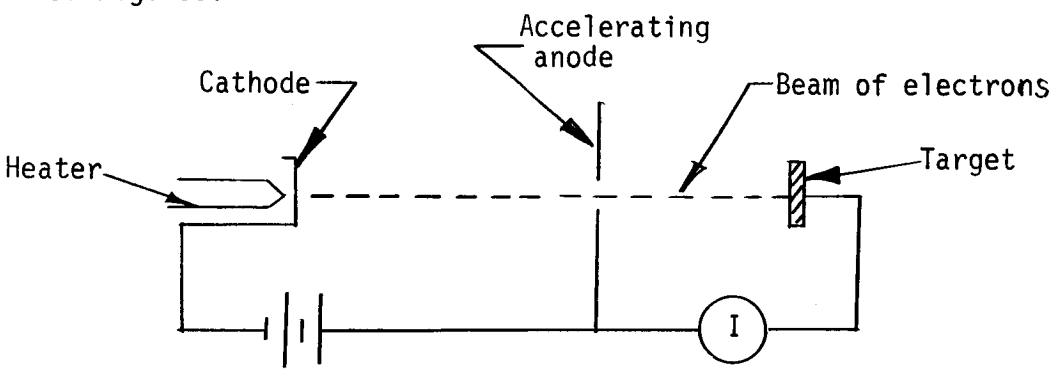

Figure 55. Electrical circuit diagram of electron beam.

First, organic molecules adsorb on the substrate target contained in a vacuum chamber. The beam of electrons strike the substrate forming free radicals. Many of the single-ended radicals, such as methane, are pumped out of the vacuum chamber. The heavier double-ended radicals proceed to form long chains, which cross link to form a solid film.

Too large an accelerating potential strips hydrogen (a single-ended radical) off the organic molecules. The hydrogen will either terminate the polymerization process at one end of the chain or pass out

of the vacuum chamber. In either case an insulating film does not form because the film is destroyed as fast as it is formed. A darkening of the film caused by the carbon residue accompanies this film destruction.

Ennos[57] investigated sources of organic molecules in a vacuum chamber. He found that pump oils, vacuum greases, rubber gaskets, machined metal surfaces, and any material which had been touched by a bare hand produced organic vapors in the vacuum which can be polymerized by a beam of low energy electrons to form a solid insulator. Ordinary grease removers, e.g., ether or aqueous detergent solutions, were found to be ineffective in eliminating contamination from metals.

R. W. Christy[58] studied the formation rate of polymerized Dow Corning 704 silicon diffusion pump oil films. These films have excellent insulating properties. The rates of film formation depend strongly on the partial pressure of the oil but only slightly on the total pressure. The films grow linearly with time. The rate of film formation does not depend upon electron energy below the self-destruction level. A plot of formation rate, R, versus target current density, J, for three substrate temperatures appears in Fig. 56.

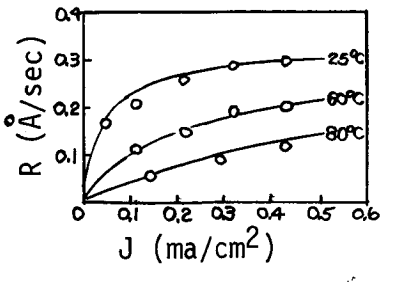

Figure 56. Rate of film formation as a function of target current (from Christy[58]).

H. T. Mann[59] and R. W. Christy[52] reported electrical properties of polymer films of thickness 50 to 2500 Å made from Dow-Corning 704 diffusion pump oil. A process similar to that described by Mann and Christy formed the insulator in the tunneling investigation presented in this paper.

Construction of fifty-four (54) different metal-polymer-metal samples developed the technique and determined the polymer film properties. Considerable effort to understand the technology of the film formation and the parameters which effect the film properties appear summarized below with a description of the apparatus used and a discussion of the procedure followed in forming the polymer films.

The formation of the polymer films and the deposition of the contacting metal electrodes occurred in a vacuum. The vacuum chamber (Plate I) is a 24" glass bell jar pumped by an eight (8) inch diameter, three (3) stage diffusion pump using Dow Corning 704 oil. The vacuum pressure of 1 to 5 x 10^{-5} Torr required approximately one hour pumping time. A three station evaporation apparatus (Plates II and III) allowed the construction of metal-polymer-metal devices without opening of the vacuum chamber. The apparatus used glass evaporation shields to prevent the evaporant from coating the bell jar and other devices contained within the chamber. Alignment pins provided a means of aligning the metal masks and the substrate at the three stations. All of the machined parts to be placed in the vacuum chamber received a mechanical polish and a chemical etch to remove the outer skin of metal. This cleaning reduces outgasing and prevents organic contamination. All tools were thoroughly cleaned and white gloves were worn whenever handling of the vacuum apparatus.

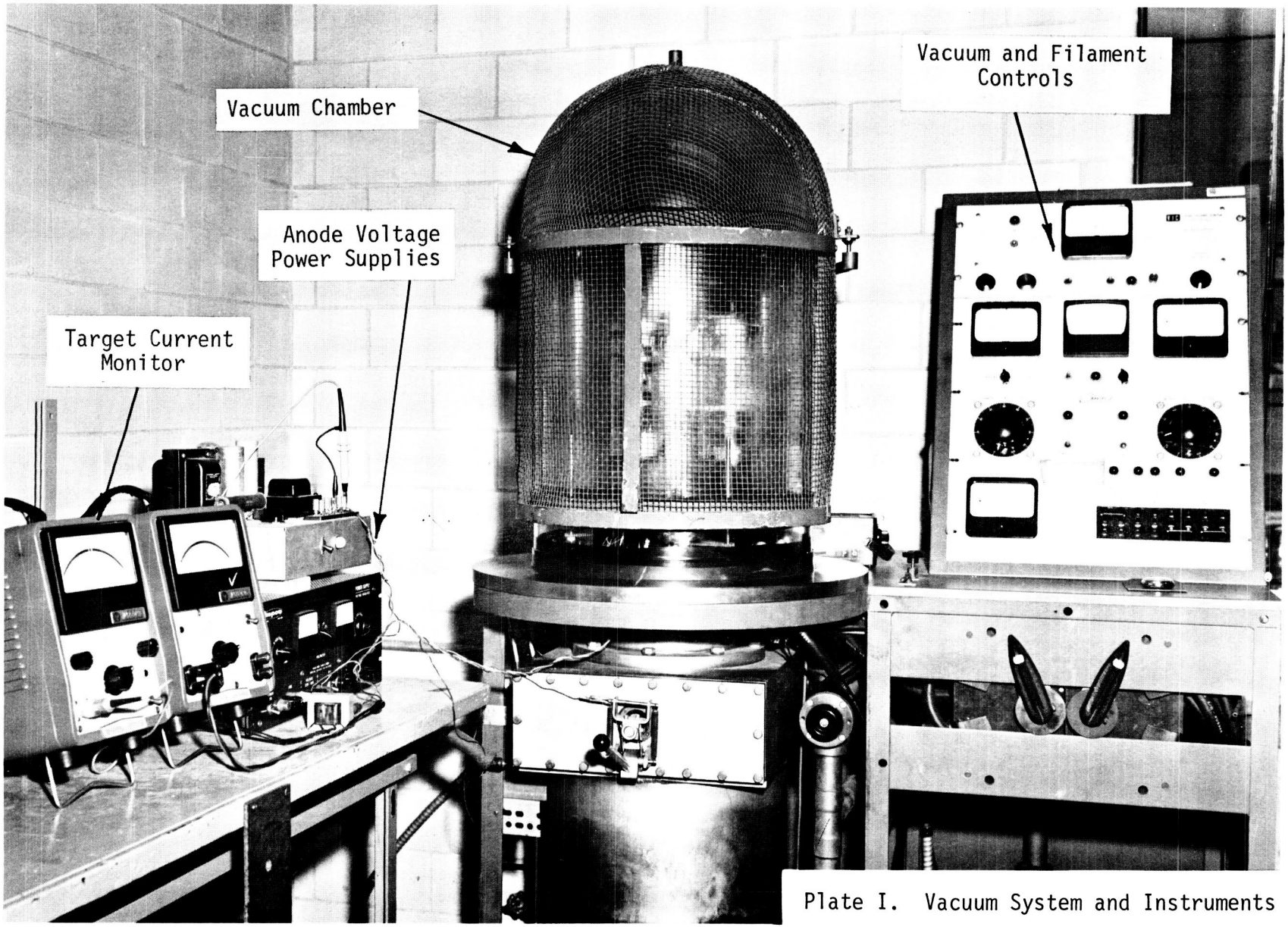

Plate I. Vacuum System and Instruments

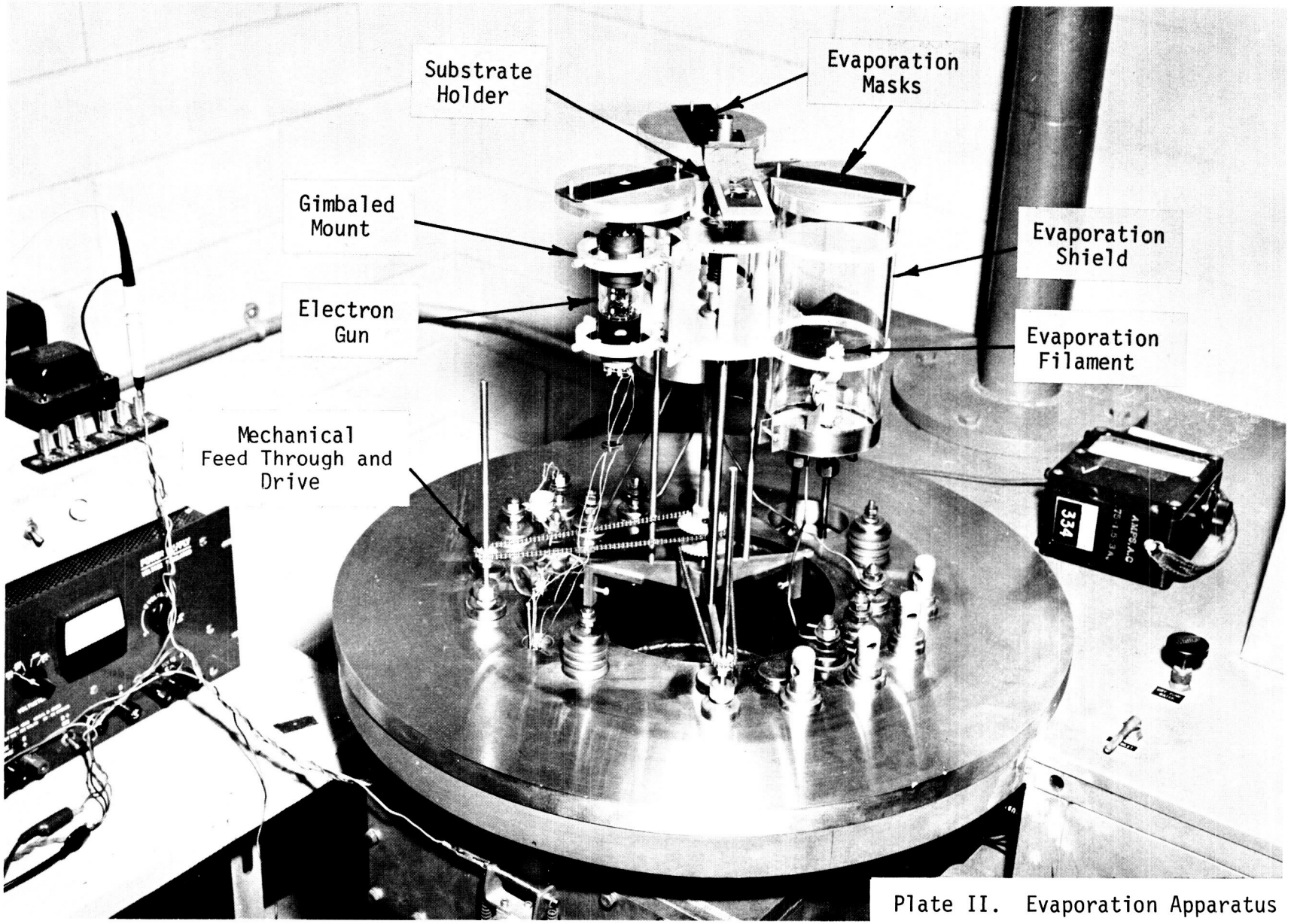

Plate II. Evaporation Apparatus

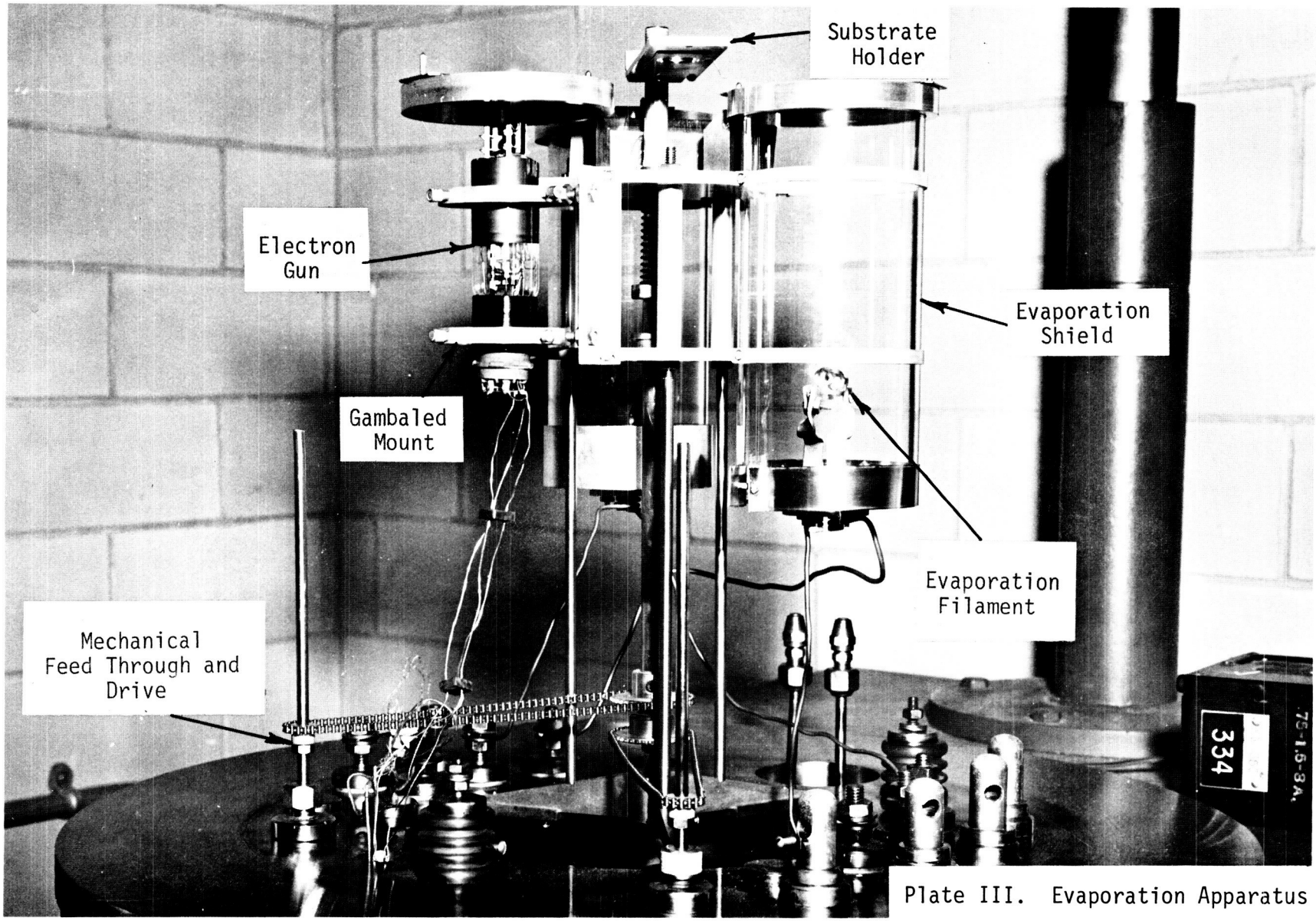

Plate III. Evaporation Apparatus

A 902A cathode ray tube with the upper portion of the tube removed served as the source of electrons for the polymerization process. The unfocused electron beam formed a circular spot approximately 5 mm in diameter. The focusing anode, accelerating anode, and all four deflection plates were placed at the same potential. The substrate potential exceeded that of the anode to collect the secondary electrons. Fig. 57 shows the electrical connections of the CRT circuit.

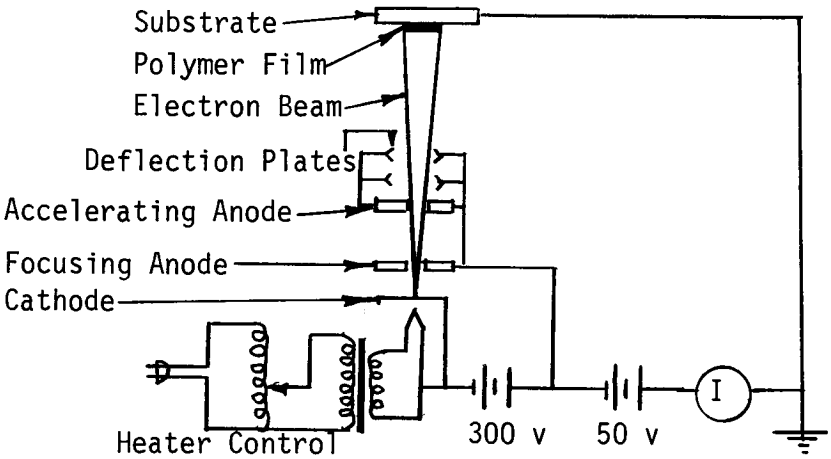

Figure 57. Cathode ray tube circuit.

A gimbaled mount held the CRT. To align the beam of electrons, place the phosphor face of the tube at the substrate position and evacuate the bell jar. Turning on the tube allowed noting the relative position of the spot on the phospher screen and an alignment substrate. With the tube turned off, open the bell jar and adjust the CRT position. Again evacuate the system and note the position of the spot. Continue this procedure until alignment is achieved.

A total accelerating voltage of 350 volts produced a good polymer film. A 400 volt potential produced a dark film which is a poor insulator. Controlling the heater voltage held the target current constant at 1.75 μamps. A minimum current of 0.5 μamps was required to

form an insulating film. Before the accelerating potentials were turned on, the tube was preheated for 5 to 10 minutes at 9 volts to reactivate the cathode which is contaminated by the exposure to air. Back-streaming from the diffusion pump provides an adequate supply of diffusion pump oil to produce a polymer film. However, placing an added source of DC 704 oil in a crucible in the vacuum chamber provides better control of the film formation. A crucible with a surface area of 4 cm^2 heated to 60°C at a distance of 40 cm from the substrate was used as the extra oil source. Under these conditions (350 volts, 1.75 μamps and added oil source) the film formation rate was approximately 6.7Å/min.

B. Physical Properties of the Polymer Film

The polymer films adhere tenaciously to the substrate. They cannot be removed by pulling with scotch tape, by rubbing with a non-abrasive cloth, or heating to 200°C. The polymer is not soluble in methanol, acetone, KMER striper or boiling trichlorethylene. Since the polymer very strongly adheres to even passively cleaned substrates, it is believed that the adsorbed organic molecules which form a surface layer of contamination are polymerized. If this is the case then the polymer is held by strong chemical type forces. Thus, the polymerization would be self-cleaning. However, the properties of the polymer would change if very much surface contamination were encountered.

Plate IV is a picture of a 900Å thick polymer film on a silicon substrate taken in white light at a magnification of 8X.

Plate V is a picture taken through an interferometer of a 900Å thick polymer film on optically flat glass. The polymer is covered with 700Å of aluminum which provides the highly reflective surface required by the interferometer.

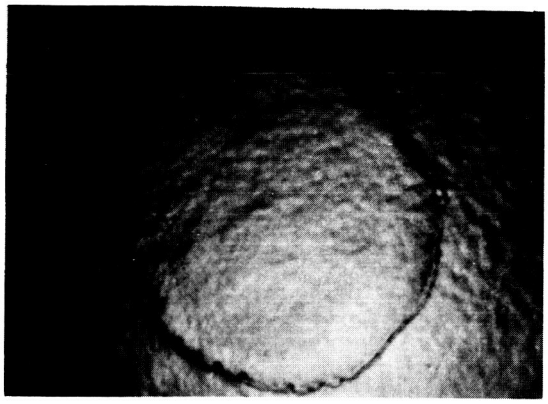

Plate IV. 900Å polymer film on a silicon substrate, white light, 8X.

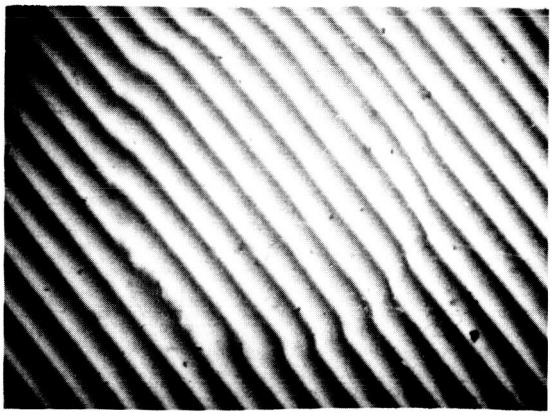

Plate V. 900Å polymer film on optically flat glass covered by 700Å of aluminum.

The straightness of the interference fringes across the polymer is indicative of the uniformity of the film.

C. Electrical Properties of the Polymer Film

1. Construction of MIM Devices

Experiments performed on aluminum-polymer-aluminum capacitors determined the electrical properties of the polymer film. These capacitors consisted of a vapor deposited aluminum base stripe on optically flat glass, a polymer film over part of the stripe, and cross stripe of aluminum to form the top electrode. Fig. 58 illustrates the finished capacitor.

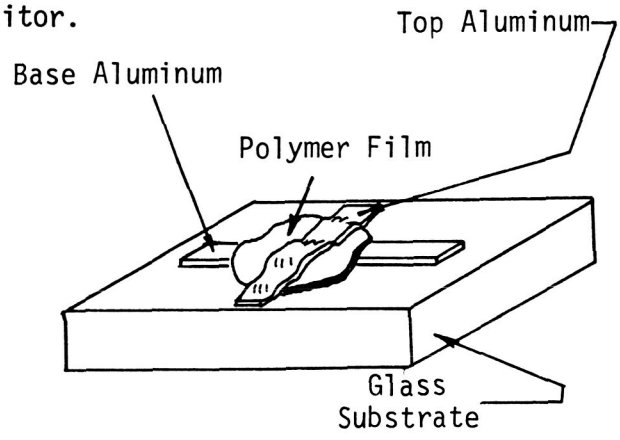

Figure 58. Metal-polymer-metal capacitor.

The interference pattern of Plate VI (20X magnification) shows the contours of the capacitor.

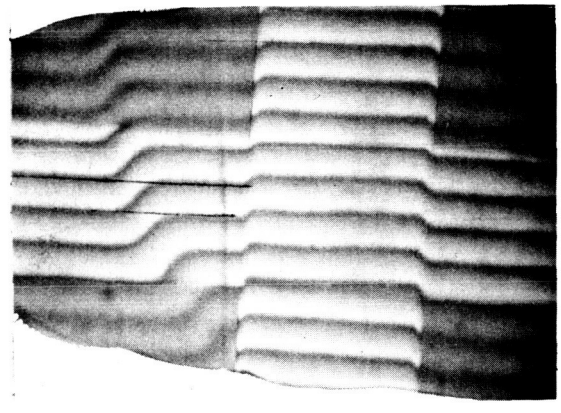

Plate VI. Contours of MIM capacitor.

The aluminum stripes are 1.2mm wide and approximately 700Å thick. A 3 strand, 5 coil tungsten filament (R. D. Mathis #F4-3-030a) 10 cm from the substrates evaporated the aluminum. The resistance of the aluminum stripes is only a few ohms and therefore did not affect the electrical measurements. No edge currents exist since the polymer extends beyond the edges of the aluminum. The three steps required in constructing the capacitors were performed without opening the vacuum chamber.

2. Dielectric Constant

The dielectric constant of the polymer film was determined by measuring the capacitance, area, and thickness of six Al- polymer - Al capacitors which had thickness between 1000 and 4000Å and then plotting the capacitance per unit area as a function of reciprocal polymer thickness, Fig. 59 . A least squares fit of a straight line through the points yields a dielectric constant of 2.8 which is the same as found by Christy for similar polymer films. The method described above averages out the measurement errors. After determination of the dielectric constant, capacity measurements permitted, calculation of the polymer thickness. The dielectric strength of the polymer is about 5×10^6V/cm.

To make electrical measurements the capacitor samples were mounted in a jig and placed in a small vacuum chamber which was pumped to 100 microns absolute pressure. The room temperature capacity of the samples was measured at 1, 10 and 100 KHz by a GR1615A capacitance bridge shown in Plate VII. Following the room temperature test, the capacity was measured with the sample immersed in liquid nitrogen (77°K). The results of this test are shown in Fig. 60. The capacitance is approximately independent of frequency and temperature in the ranges tested. The capacitance was measured to three significant figures.

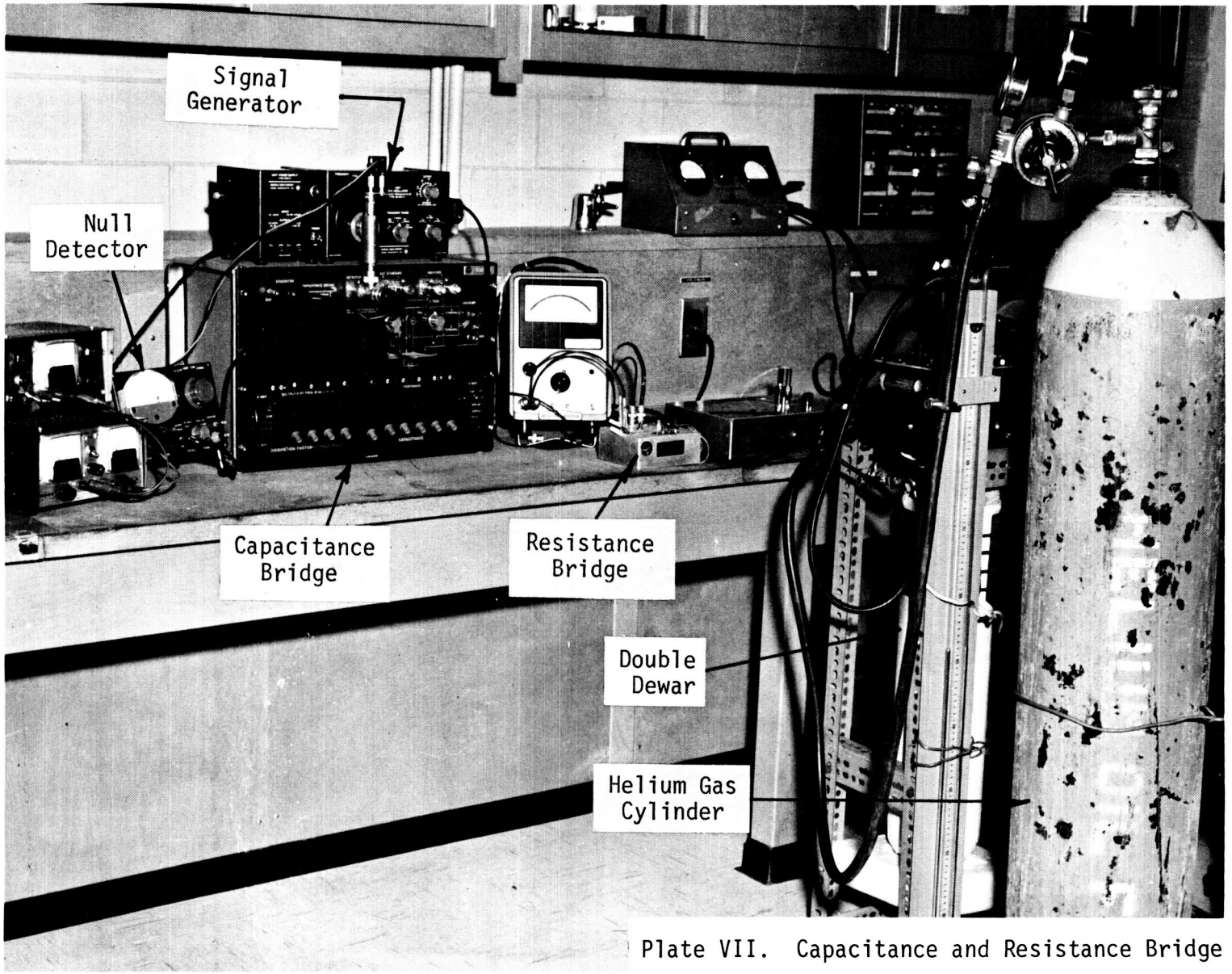

Plate VII. Capacitance and Resistance Bridge

The area of the capacitors was measured with a calibrated eye piece microscope at a magnification of 20X. The small penumbra of the aluminum stripes assured accurate measurement of the stripe width.

Polaroid pictures taken through an interferometer illuminated by a sodium lamp (λ = 5900Å) provided a means of determining the thickness of the polymer films. The width of the fringes prevents accurate thickness measurement. To average the thickness, measurement was made of several fringes on several photographs. Thin polymers presented the greatest difficulty in measurement of the thickness as shown in the two examples of Plate VIII. This error in the thickness determination causes the scatter in the points of Fig. 59.

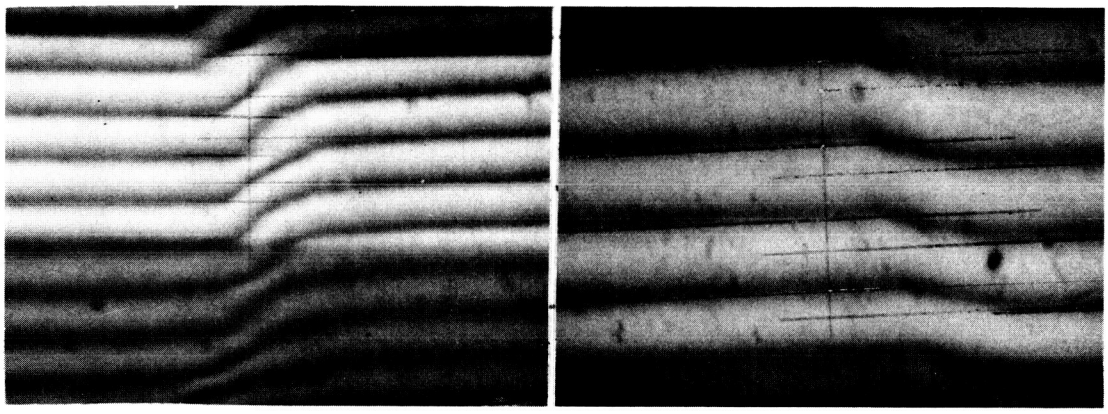

Plate VIII. Interference fringes for insulator thickness determination.

3. Voltage-Current Characteristics

V-I curves for MIM tunneling junctions of thickness between 67 and 200Å appear in Fig. 30 of Chapter III. These MIM characteristics serve as the basis for interpreting MIS data. MIS and MIM tunneling are compared in Chapters II and III. The following discussion covers aging, insulator thickness and temperature dependence of the MIM V-I characteristics.

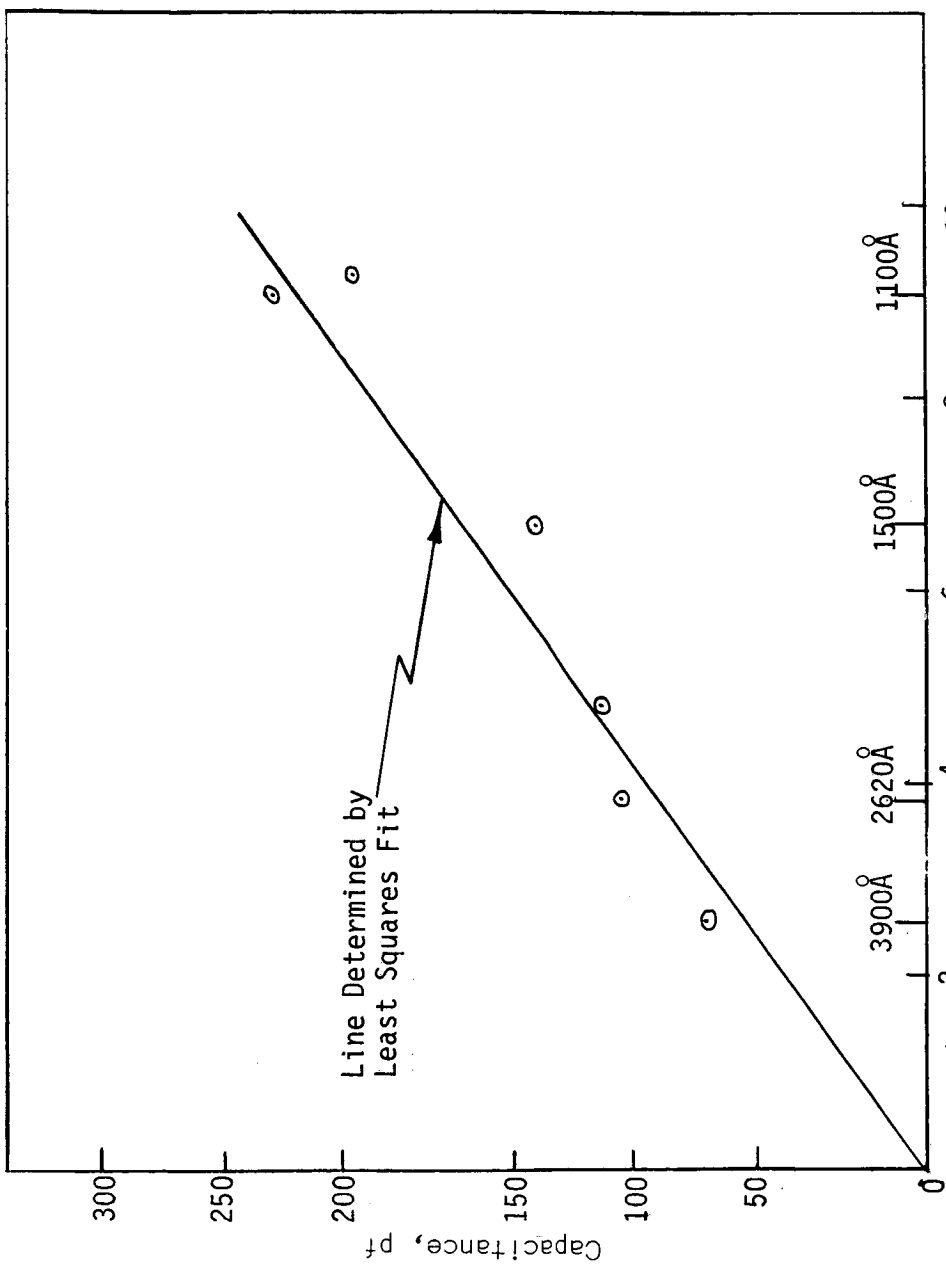

Figure 59. Polymer dielectric constant determination.

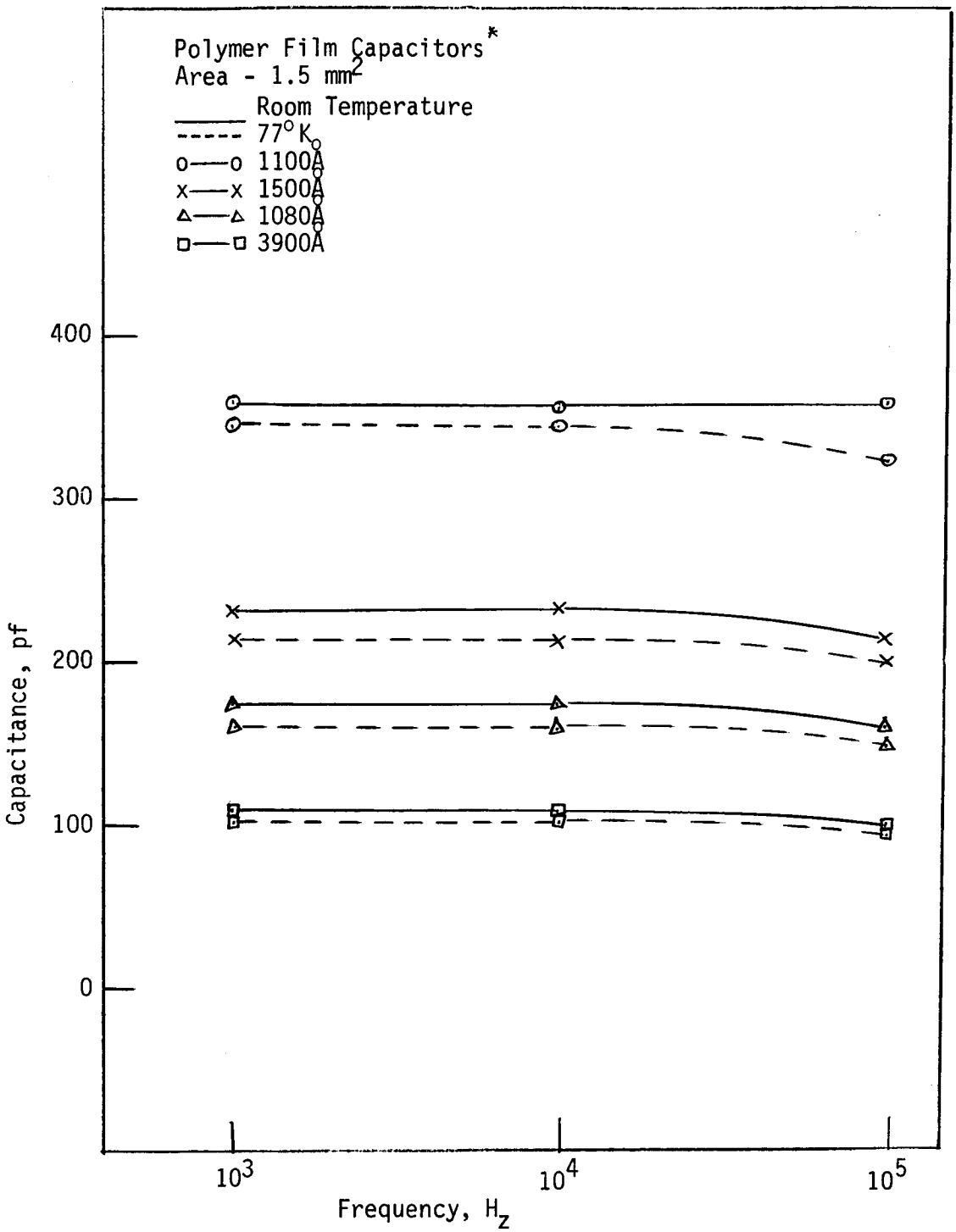

Figure 60. MIM capacitance variation with frequency.

Chapter III points out the strong dependence of MIM tunneling current upon insulator thickness. Current versus thickness at room temperature appears in Fig. 61. In agreement with theory the current decreases exponentially with thickness. For thickness greater than 125Å the current levels off and tends to become independent of thickness which indicates the tunneling currents give way to another current mechanism such as Schottky emission. The small difference in the V-I curves of Fig. 62 for reversed voltage polarity indicates a slight asymmetry of the tunneling barrier.

Stratton[18] and Simmons[14] predict the MIM tunneling current to decrease with the square of absolute temperature. Hartman[61] and Chow[62] verified this on Al - Al_2O_3 - Al and Be - BeO - Au respectively. To determine the temperature dependence of an Al - polymer - Al junction, an 80Å thick sample was tested from room temperature to 80°K. The sample was placed in the inner Dewar of a double Dewar system, illustrated in Fig. 63. The Dewar containing the sample was pumped out with a rotary vacuum pump and then back-filled with Helium gas. This prevented the condensation of water on the sample. The outer Dewar was then filled with liquid nitrogen (77°K). As the sample cooled down, the MIM current was measured at 1.35 volts. Cooling from room temperature to 77°K required approximately three hours. The sample temperature was measured with a copper-constantan thermocouple with an ice water reference. The results of this test are shown in Fig. 64. A line with a slope of 2 drawn through the data points shows good agreement with the theoretical prediction. I(0) was determined by plotting the tunneling current as a function of temperature on a linear scale graph and extrapolating to T = 0°K. The

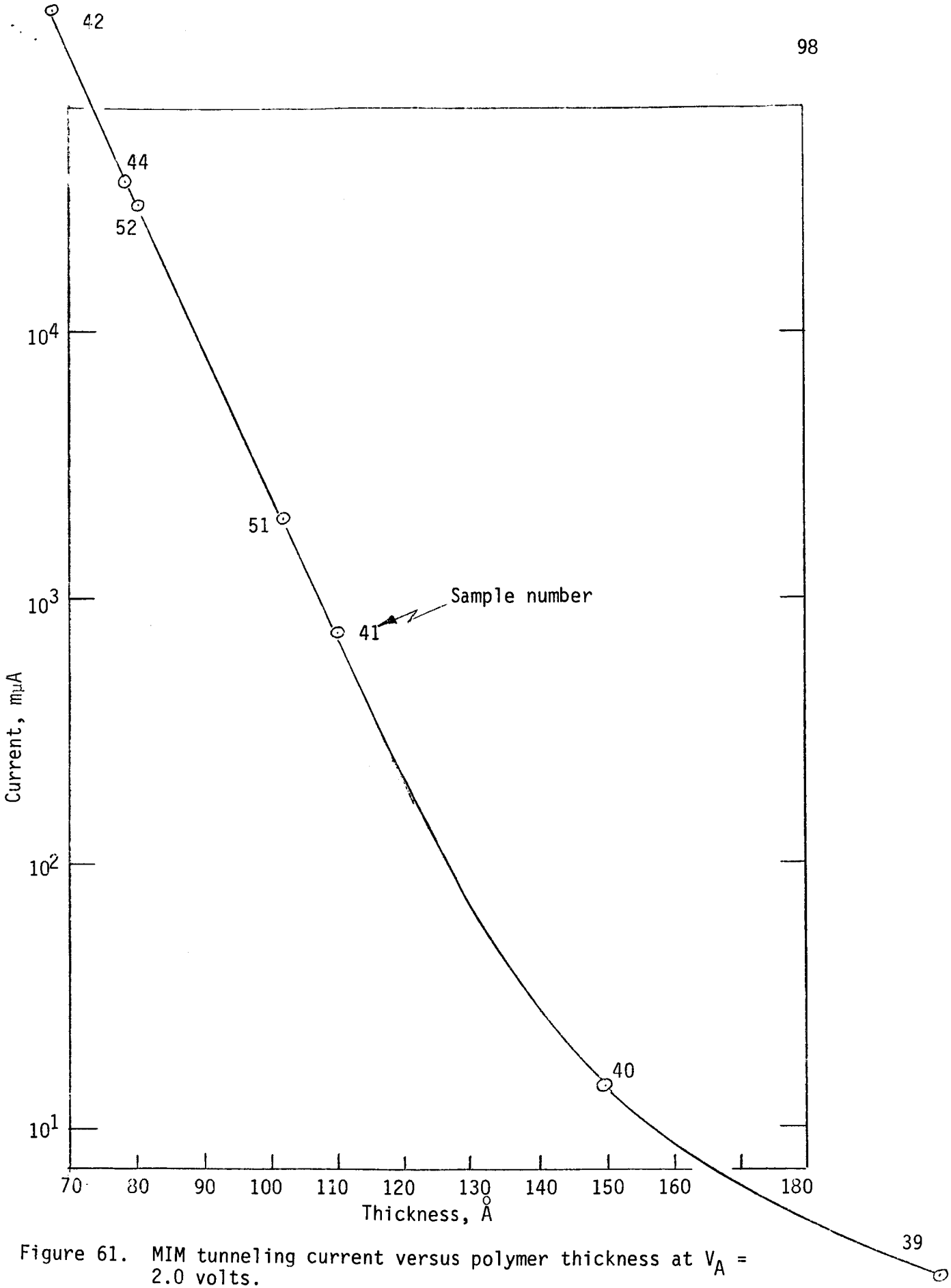

Figure 61. MIM tunneling current versus polymer thickness at V_A = 2.0 volts.

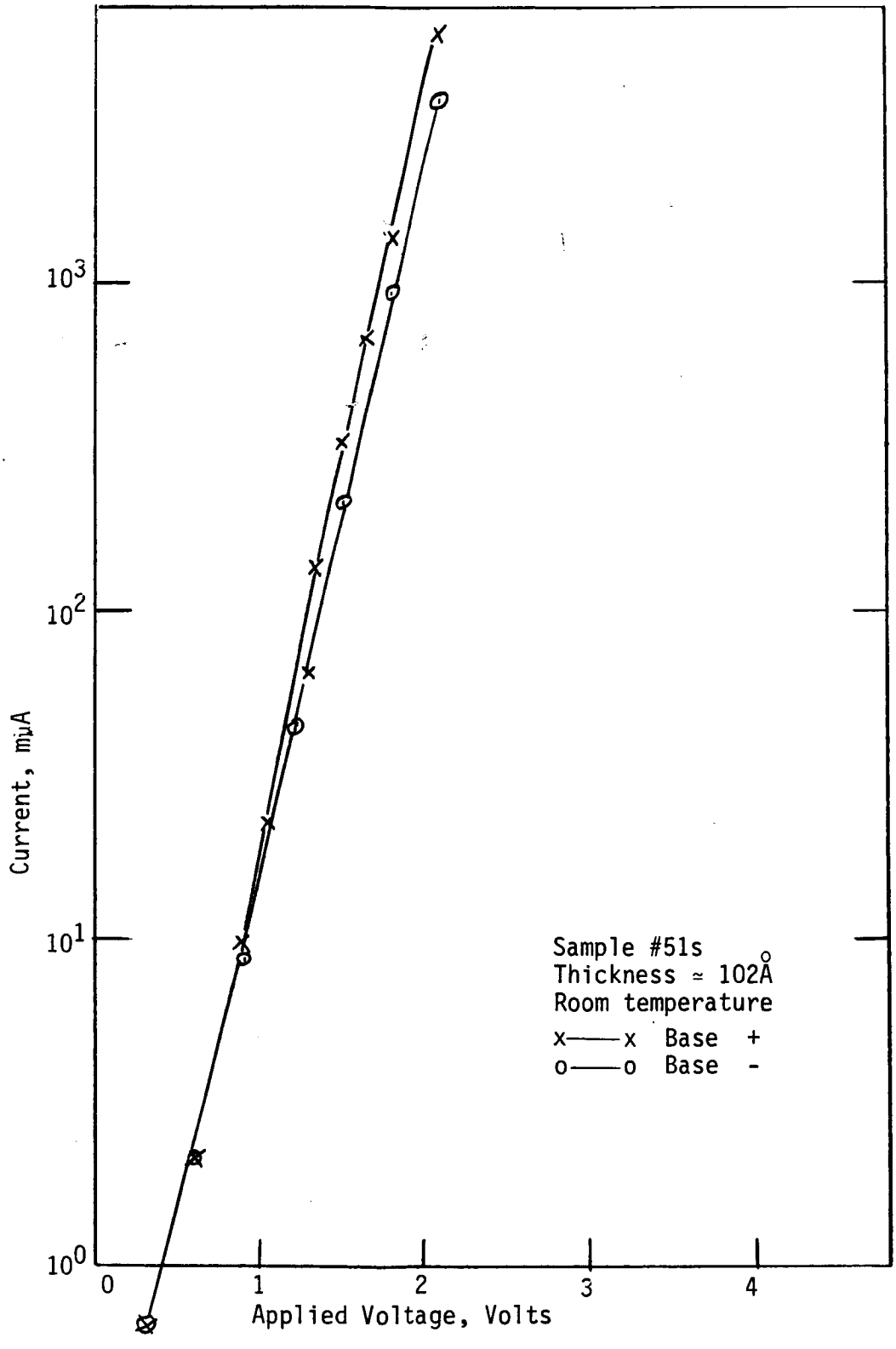

Figure 62. Symmetry of MIM tunneling current.

Log - Log graph of Fig. 64 is obtained by subtracting I(0) from the total current I(T).

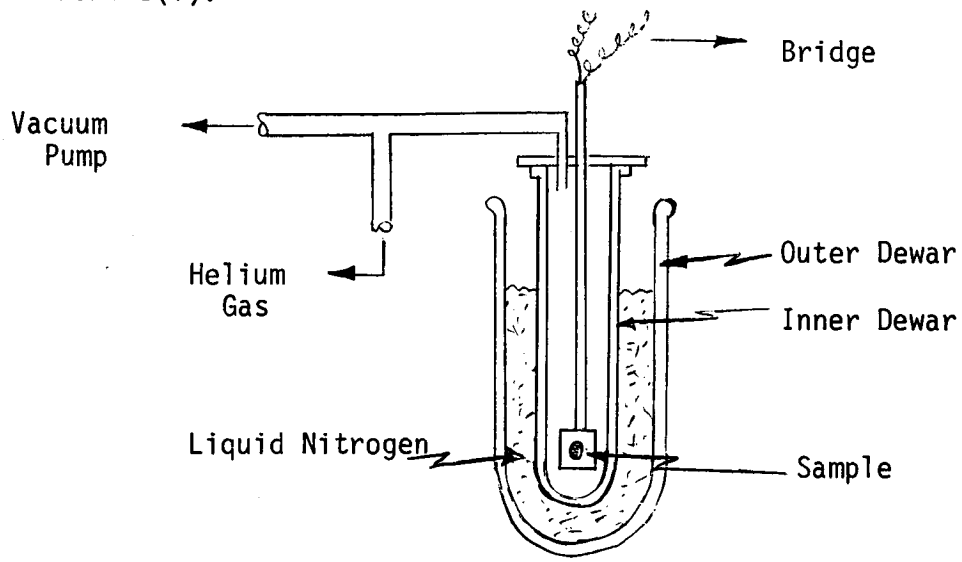

Figure 63. Double Dewar temperature apparatus.

The effects of aging are illustrated by Fig. 65. Very little change in the V-I characteristics occurs in a vacuum (100 microns) but aging in air reduces the exponential rise of current with voltage. No aging of the sample occurred after three and one-half hours in liquid nitrogen.

D. MIS Devices

1. Construction of MIS Devices

A single crystal silicon boule was cut into 20 mil wafers with a diamond wheel. The wafers were lapped with #240, #400, and #600 grit. The polished silicon was then etched in CP-4 for 90 seconds and stored in air after rinsing with deionized water. To clean the silicon for construction of MIS devices, the silicon was first washed with non-ionic detergent and rinsed with deionized water and methanol. The silicon was then boiled in trichloroethylene for 10 minutes, rinsed with running

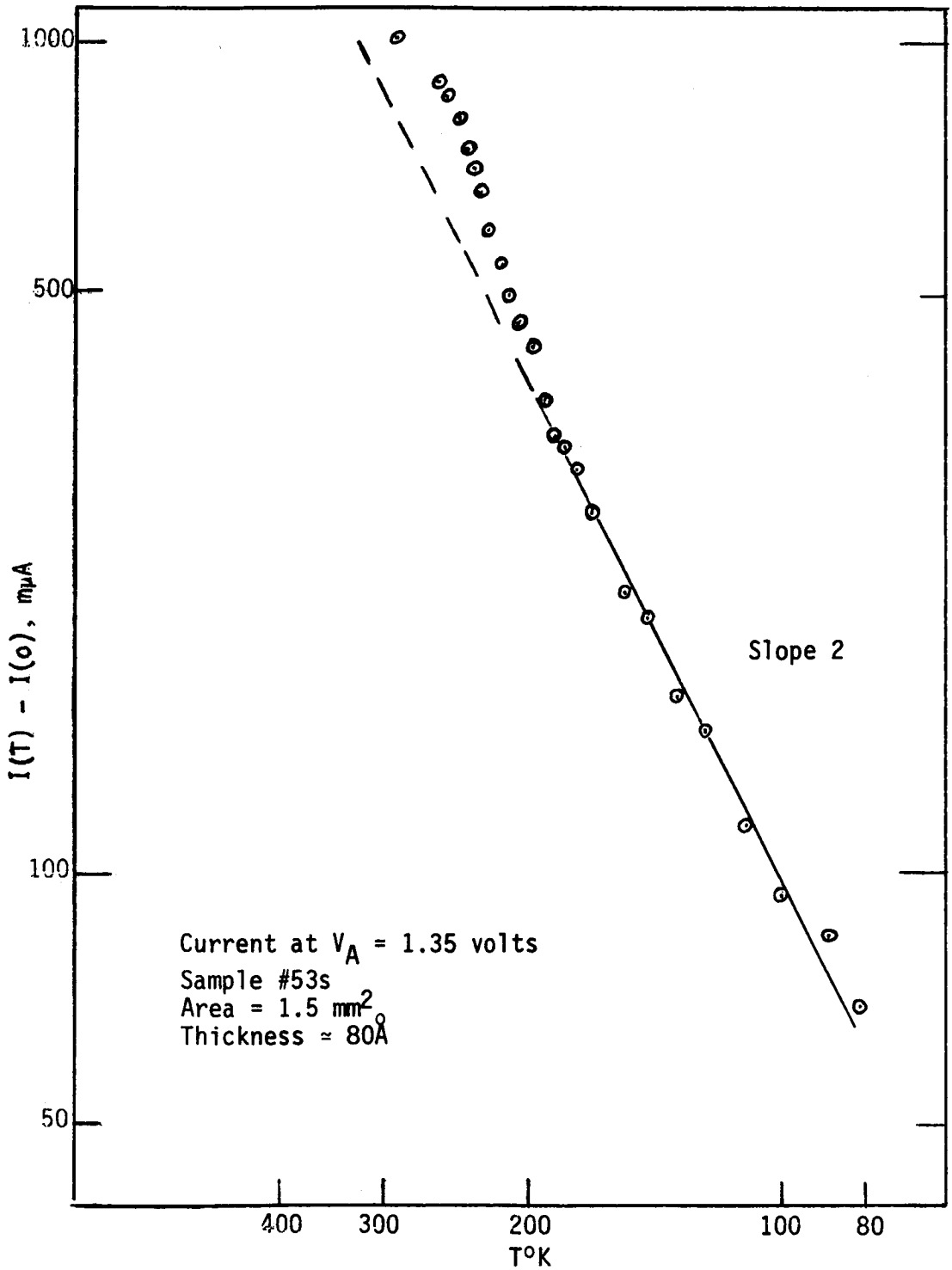

Figure 64. Temperature dependence of MIM tunneling current, V_A = 1.35.

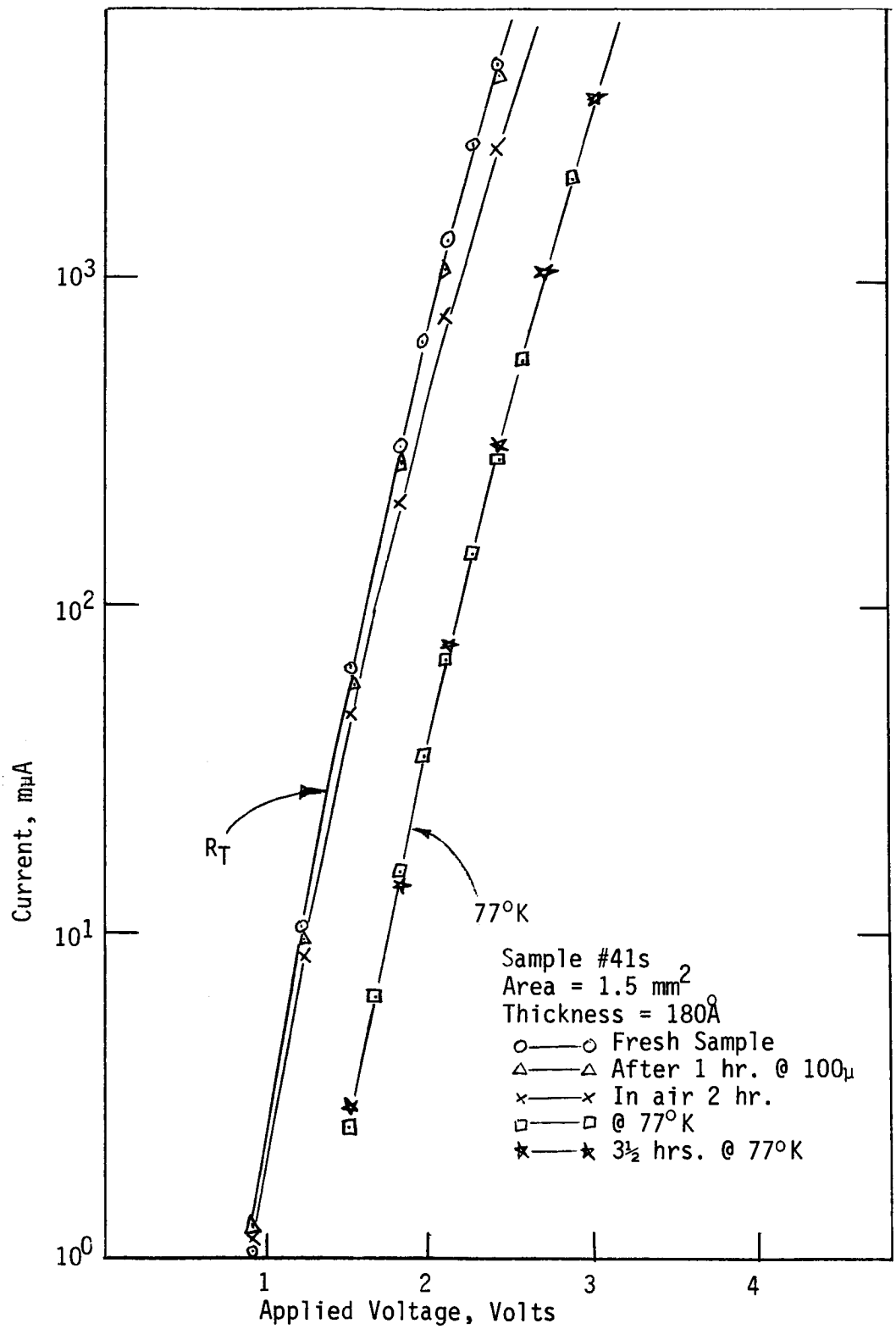

Figure 65. MIM aging at room temperature and 77°K.

methanol and placed wet in the vacuum chamber. The methanol evaporated in the vacuum of the roughing pump. When the bell jar pressure reached the mid-10^{-4} torr range, the extra oil source was heated to 60°C. The bell jar was pumped for approximately one hour at which time the pressure was below 5 X 10^{-5} torr. Storing the substrate in the vacuum before polymerization for more than three hours allows a large deposit of adsorbed oil to collect and a good insulating film does not form. The electron gun was preheated for five to ten minutes before polymerization was begun. After the polymer was formed on the silicon, three metal dot field plates (0.85 mm^2) were vapor deposited through a stainless steel mask. The sample was allowed to stand about 15 minutes in the vacuum to allow the deposited metal to anneal and order itself. The ordering of the metal tends to reduce the porosity of the metal and slows down the penetration of oxygen and water vapor after the sample is removed from the vacuum. Gold was deposited on the back side of P-type samples to form an ohmic contact. In-Ga paste was used as the ohmic contact metal an N-type.

2. Testing of the MIS Devices.

After construction, the MIS devices were placed in the holder shown in Plate X and illustrated in Fig. 66. A brass point with a small ball of In-Ga paste on the end made contact with the field plate without disturbing the polymer film. A small spring held the wafer in contact with the base plate. Capacitance and current were measured by the method described for MIM samples. Each sample was tested for photovoltaic effects which is indicative of an incomplete insulator. Most of the samples were electrically stable and good reproducable data was obtained. Unstable samples were discarded.

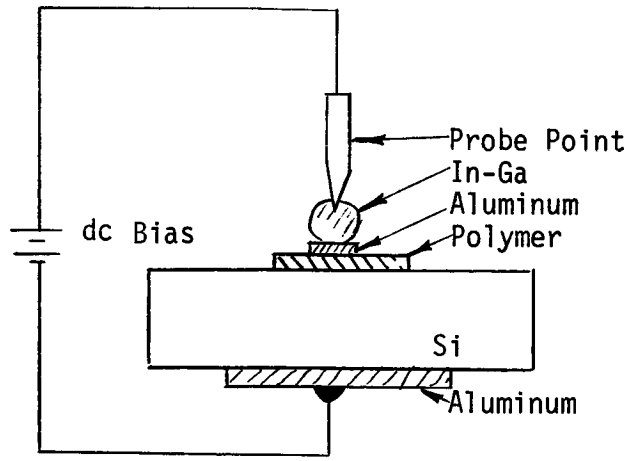

Figure 66. Metal-polymer-semiconductor (MIS) construction.

3. Comparison of Al-Polymer-Si and Al-SiO_2-Si Capacitance Curves

Before investigating thin insulator MIS tunneling, twelve thick insulator samples were constructed in order to determine the surface state density which resulted with the polymer insulator. The results were compared with grown oxide samples. Fig. 67 presents C-V data for both a polymer and oxide insulator on 60 ohm - cm N-type silicon. The oxide was grown with wet nitrogen.[63] The curves have the same general shape, but there is a vast difference in the voltage required to reduce the capacitance. This is partially accounted for by the difference in thickness, dielectric constant and area of the two dielectrics. However, the difference in the surface state density is the major cause of the voltage offset. The surface state density is calculated by:

$$N_S = \frac{Q}{eA} = \frac{CV}{eA} \quad ,$$

where: V = applied voltage at flat band
C = capacitance at V = 0
A = field plate area
e = electronic change.

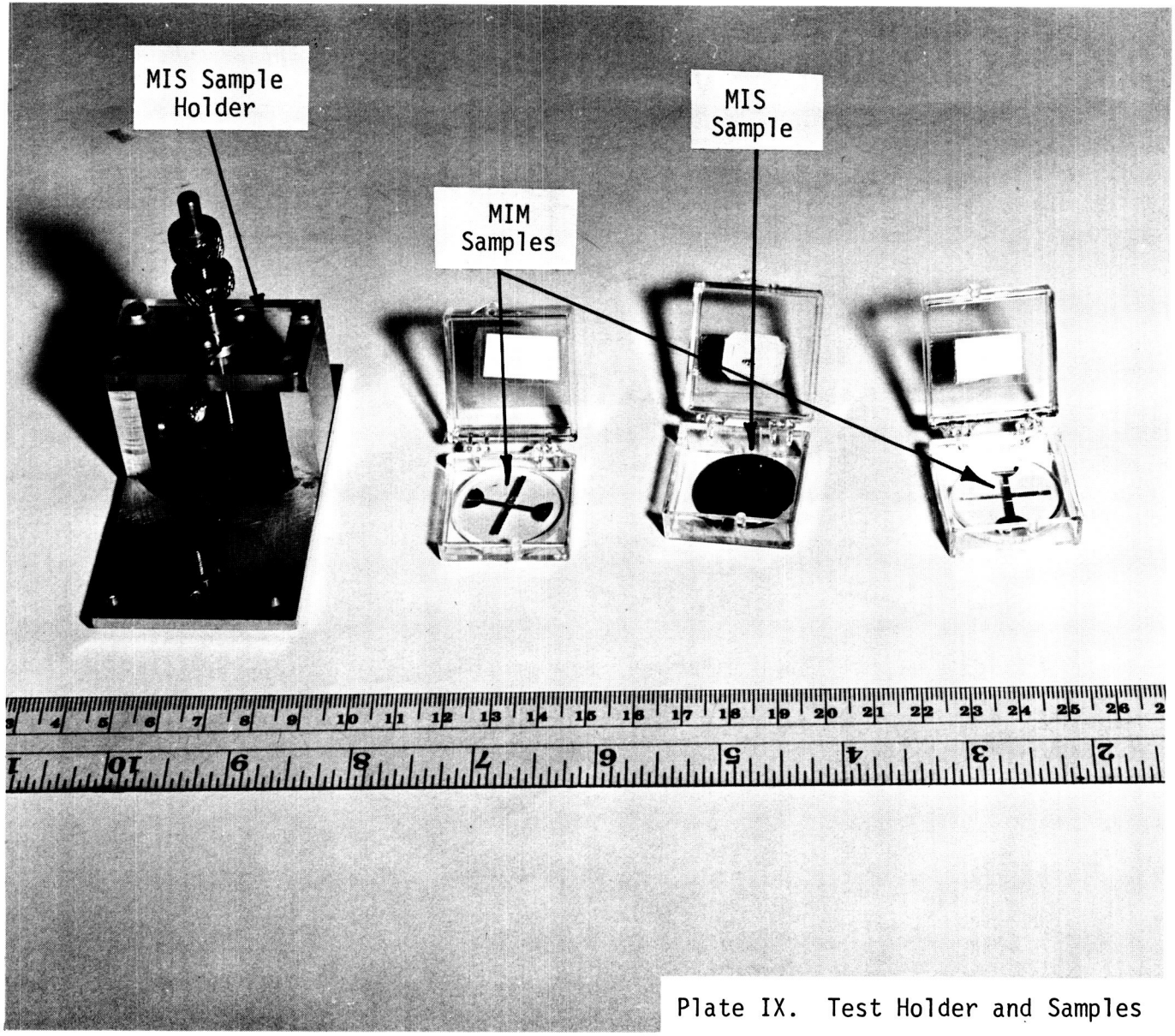

Plate IX. Test Holder and Samples

The thick polymer samples demonstrate that an insulating film is formed on silicon and that C - V data is consistent with the well established MOS system, although the surface state density is a factor of 10 higher. The surface state density of grown oxide samples is strongly dependent upon the method of sample preparation. Surface state densities as high as 10^{13} and as low as 10^{11} are reported by other investigators.[37] The surface state density with polymer films lies above the average grown oxide sample but below the maximum reported.

Fig. 68 gives the C-V curve for a P-type silicon sample. This is also consistent with published MOS data.

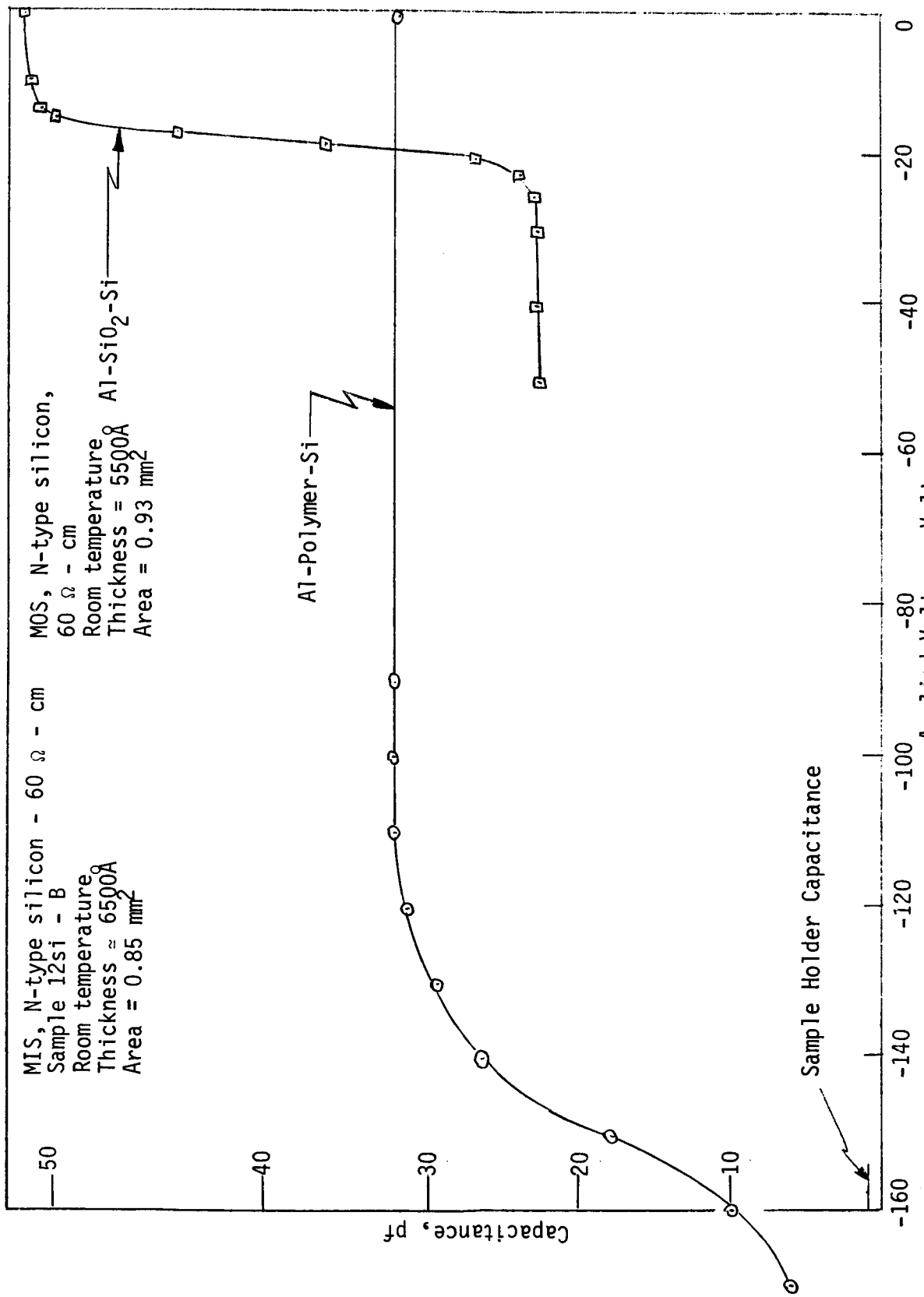

Figure 67. N-type MIS and MOS capacitance-voltage curves.

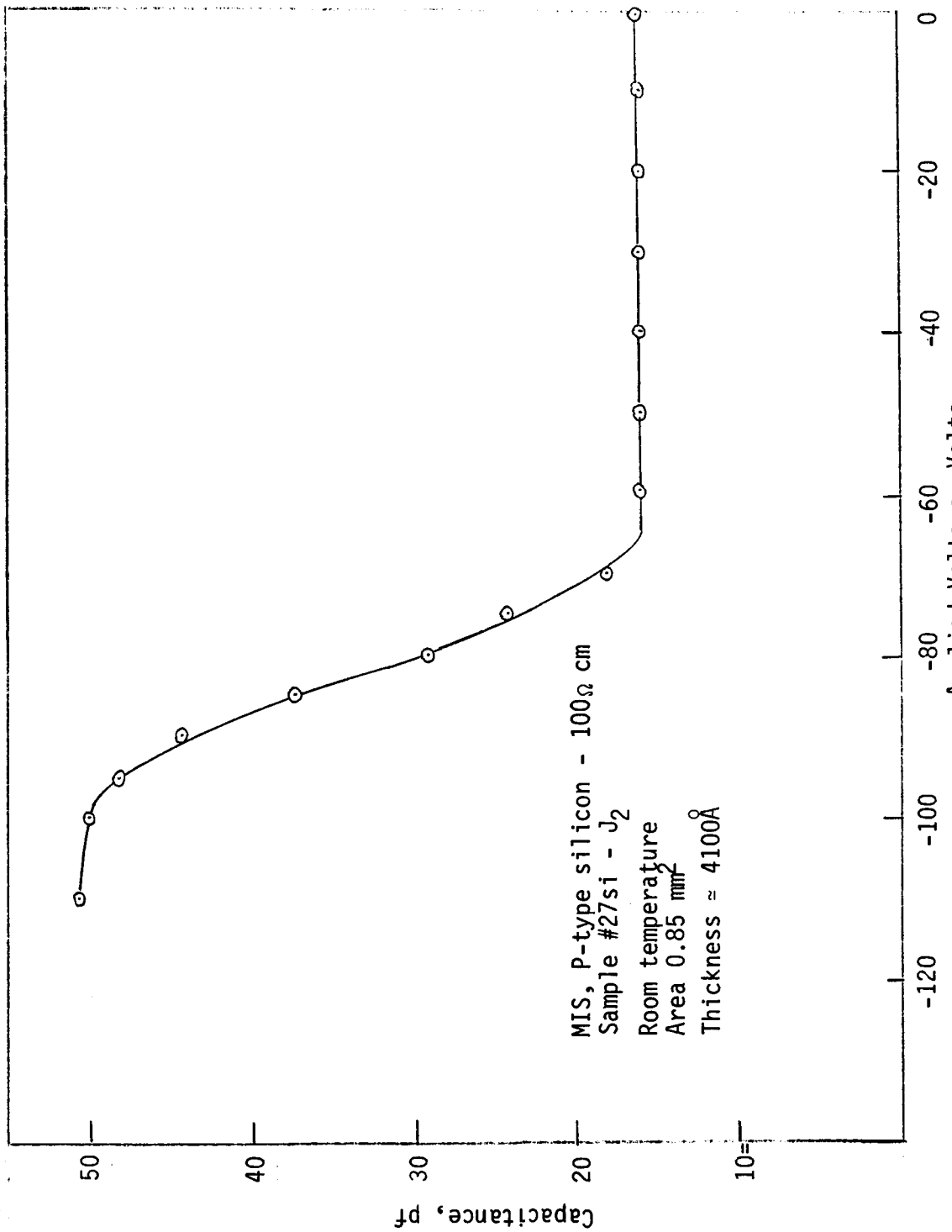

Figure 68. P-type MIS capacitance-voltage curve.

CHAPTER V

Summary of Conclusions and Recommendations for Further Research

A. Conclusions

This research investigated the general properties of tunneling between silicon and a metal separated by a thin polymer insulator. This section summarizes the various conclusions which appear throughout the text of this paper.

Surface states have been shown to play an important role in the entire MIS tunneling process. They provide an abundance of states which give the silicon a metallic-like surface. The voltage-current properties of the MIS tunneling are best described in terms of the electric field within the insulator which is controlled by the location of the terminating charge within the silicon. At low applied voltage the ionized surface states terminate the electric field lines and cause the insulator field to increase as in the case of MIM tunneling. When the surface states are fully ionized, an increase in the applied voltage creates either an accumulation or depletion layer on the silicon surface depending upon the conductivity type of the silicon and the polarity of the applied voltage. When the accumulation layer forms, then the insulator field and the tunneling current increase as before since the accumulated charge collects at the silicon surface. When a depletion layer forms, then the electric field terminates on dopant states within the silicon bulk. As a result the insulator field and the tunneling current level off.

To describe MIS tunneling, Stratton's MIM tunneling equation requires modifications which take into account the forbidden band of the silicon and the conservation of momentum of the transistion. These modifications do not change the form of the MIM equation but decrease the constants and replace the independent variable, V_A, by a reduced voltage, $V_A - V_G$.

Experimentally, the MIS tunneling current increases with applied voltage in an exponential manner as predicted by the modified Stratton equation. However, an asymmetric current saturation occurs which is dependent upon the polarity of the applied voltage and the conductivity type of the silicon. Plotting the voltage-current characteristics on a semi-logarithmic graph demonstrates the exponential nature of the tunneling current and indicates that the current saturation is a separate mechanism from that of tunneling. This mechanism has been shown to be the penetration of the electric field into the silicon bulk which occurs when the surface states are exhausted and a depletion layer forms. The establishment of the basic role of the surface states is of major importance for it not only explains current saturation, but also provides a means of examining the surface states and allows determination of the effect of variation of the physical parameters.

Application of Gauss' law determines the effect of insulator thickness and work function of the field plate metal upon the saturated current level. The saturated current level is independent of the insulator thickness, but exponentially dependent upon the field plate work function. Temperature dependence does not lend itself to rigorous analysis, but the reduction of tunnel efficiency is seen to be the major temperature effect.

B. Recommendations

This research generated several interesting ideas which seem worthy of further consideration. These ideas are:

(1) Study surface states with the tunneling saturation method.

(2) Study tunneling into other single crystal and vapor deposited semiconductors.

(3) Study tunneling in semiconductor-insulator-semiconductor structures (SIS).

(4) Determine the relative work function of metals and semiconductors with the tunneling saturation.

(5) Construct and investigate a triode with a MIMS structure. The MIM forms the emitter and the MS forms the collector.

(6) Investigate electroluminescence in CdS and GaAs using the MIS structure.

A P P E N D I X I

Analysis of Resistance Bridge

A resistance bridge simultaneously measured the tunneling current and voltage of the samples. An analysis of the bridge is given below.

The bridge is balanced at open circuit. The resistance of voltmeter 2 is one arm of the bridge. When an unknown resistance is placed in the circuit, the bridge is unbalanced. The voltage, across the bridge, $V_1 - V_2$, is proportional to the current through the unknown resistance and the voltage, V_2, is the voltage applied across the resistance.

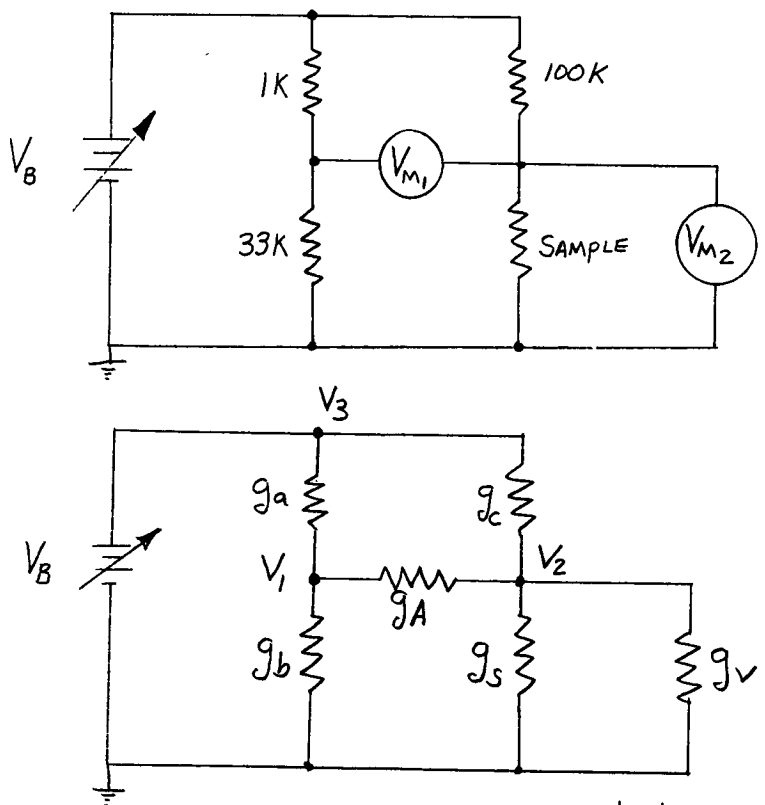

g_A - conductance of ammeter

g_V - conductance of voltmeter

g_S - conductance of sample

V_B - Voltage supply

Figure 65. Circuit of resistance bridge

The three node equations are:

$$(1)\quad (V_1 - V_3)\, g_a + (V_1 - V_2)\, g_A + V_1 g_b = 0$$

$$(2)\quad (V_2 - V_3)\, g_c + V_2 g_s + V_2\, g_v - (V_2 - V_1)\, g_A = 0$$

$$(3)\quad V_3 = V_B.$$

Combining and solving for V_1 and V_2 yields

$$(4)\quad V_1 = V_B \frac{g_a g_2 + g_A g_c}{g_1 g_2 + g_A^2} \qquad \text{Where } g_2 = g_c + g_s + g_v - g_A$$

$$(5)\quad V_2 = V_B \frac{g_c g_1 + g_A g_a}{g_1 g_2 + g_A^2} \qquad \text{and } g_1 = g_a + g_A + g_b$$

The voltage across the bridge then is:

$$(6)\quad V_1 - V_2 = V_4 = V_B \left[\frac{g_a g_2 + g_A g_c - g_c g_1 + g_A g_a}{g_1 g_2 + g_A^2} \right].$$

Since the bridge is balance at open circuit,

$$(7)\quad g_a / g_b = g_c / g_v.$$

Hence

$$(8)\quad V_4 = V_B \frac{g_a g_s}{g_1 g_2 + g_A^2}.$$

The current of the unknown resistance is

$$(9)\quad I = V_2 g_s = V_B \left[\frac{g_c g_s - g_A g_a}{g_1 g_2 + g_A^2} \right] g_s$$

and

$$(10)\quad \frac{V_B}{g_1 g_2 + g_A^2} = \frac{I_s}{g_s (g_c g_1 - g_A g_a)}.$$

Substituting (10) into (8) gives the bridge voltage in terms of the unknown current:

$$(11)\quad V_4 = \frac{g_a I_s}{g_c g_1 - g_A g_a}.$$

Solving for I_s,

$$(12)\quad I_s = \frac{g_c g_1 - g_A g_a}{g_a} V_4 = KV_4$$

$$\text{Where } K = \frac{g_c g_1 - g_A g_a}{g_a}$$

Therefore it is shown that V_4 is proportion to I_s.

For the circuit of Fig. 65,

$K = 11.3\ \mu A/volt.$

The bridge was tested with known resistances of valve from 10k to 680 meg ohms. The accuracy was better than 5% on all resistances. The leakage resistance of the bridge varied from day to day, but was of the order of 1000 meg ohms.

A P P E N D I X II

Calculations of Stratton's Equation

Calculation of Stratton's Equation to Fit MIM Polymer Sample #53S

$$I = \frac{2\pi C_{10} kT}{\text{Sin}\ (\pi C_{10} kT)}\ I_o \exp\ (-b_{12}V^2)\ \sinh\ (\frac{C_{10}}{2}\ V)$$

$C_{10} = 16.4$

$b_{12} = 1.0$

$I_o = 0.088 m\mu\ A$

V	V^2	$\exp(-b_{12}V^2)$	8.2V	sinh(8.2V)	$e^{-b_{12}V^2}$ sinh(8.2V)	I
0.12 volts	0.0144	0.99	0.985	1.15	1.14	$2.74 \times 10^{-1} m\mu A$
0.2	0.04	0.96	1.64	2.48	2.38	5.72
0.3	0.09	0.91	2.46	5.81	5.28	1.27×10^{0}
0.4	0.16	0.85	3.27	13.05	11.1	2.67
0.5	0.25	0.77	4.09	30.0	23.1	5.55
0.6	0.36	0.70	4.91	68.0	47.6	1.14×10^{1}
0.7	0.49	0.61	5.73	155	94.5	2.27
0.8	0.64	0.53	6.55	350	185	4.44
0.9	0.81	0.44	7.37	800	352	8.46
1.0	1.00	0.37	8.20	1,800	665	1.60×10^{2}
1.1	1.21	0.30	9.05	4,000	1,200	2.88
1.2	1.44	0.24	9.85	9.500	2,280	5.48
1.3	1.69	0.18	10.6	20,000	3,600	8.65
1.4	1.96	0.14	11.5	49,000	6,850	1.65×10^{3}
1.5	2.25	0.105	12.3	110,000	11,600	2.79
1.6	2.56	0.077	13.1	244,000	18,000	4.52
1.7	2.89	0.055	13.9	540,000	29,700	7.15

Calculation of Stratton's Modified Equation to Fit N-Type MIS Polymer

Sample #30si

V_G = 0.2 volts, C_{10} = 14, b_{12} = 0.9, I_o = 0.04 mμA

V	$V-V_G$	$(9)(V-V_G)^2$	$e^{-b_{12}(V-V_G)^2}$	$7(-V_G)$	$\sinh 7 (V-V_G)$	$e^{-}(\ )\sinh(\ )$	I
0.3	0.1	0.0009	1.00	0.7	0.76	0.76	7.6×10^{-2} mμA
0.5	0.3	0.081	0.92	2.1	4.0	3.7	3.7×10^{-1}
0.7	0.5	0.225	0.80	3.5	16	12.8	1.28×10^{0}
0.9	0.7	0.44	0.64	4.9	67	43	4.3
1.2	1.0	0.90	0.41	7.0	548	225	2.25×10^{1}
1.5	1.3	1.52	0.22	9.1	4,500	990	9.9
1.8	1.6	2.50	0.082	11.2	37,000	3,050	3.05×10^{2}
2.1	1.9	3.25	0.039	13.3	300,000	11,700	1.17×10^{3}
2.4	2.3	4.35	0.013	15.4	2,420,000	31,400	3.14
2.7	2.5	5.60	0.0037	17.5	19,800,000	73,500	7.35

Bibliography

1. R. C. Jaklevic, D. K. Donald, J. Lambe, and W. C. Vassell, Injection Electroluminescence in CdS by Tunneling Films, Appl. Phys. Letters 2, 7, January 1963.

2. P. V. Gray, Observation of Surface and Impurity States in Silicon by Oxide Tunneling, Phys. Rev. Letters 9, 302, October 1962.

3. P. V. Gray, Tunneling from Metal to Semiconductor, Phys. Rev. 140, A179, October 1965.

4. L. Esaki and P. J. Stiles, Study of Electronic Band Structure by Tunneling Spectroscopy: Bismuth, Phys. Rev. Letters 14, 902, May 1965.

5. L. Esaki and P. J. Stiles, New Type of Negative Resistance in Barrier Tunneling, Phys. Rev. Letters 16, 1108, June 1966.

6. L. L. Chang, L. Esaki and F. Jona, Electron Tunneling from Metal to InSb, Appl. Phys. Letters 9, 21, July 1966.

7. L. Esaki and P. J. Stiles, BiSb Alloy Tunnel Junctions, Phys. Rev. Letters 16, 574, March 1966.

8. R. L. Ramey, Physical Electronics, p 163, Wadsworth Publishing Co., Belmont, Calif. 1961.

9. J. L. Moll, Physics of Semiconductors, McGraw-Hill, N. Y., 1964.
   a) p 241
   b) p 242
   c) p 252
   d) p 248

10. C. W. Sherwin, Introduction to Quantum Mechanics, p 141; Holt, Rinehart and Winston, N. Y. 1960.

11. S. R. Pollock and C. E. Morris, Electron Tunneling through Asymmetric Films of Thermally Grown Al_2O_3, J. Appl. Phys. 35, 1503, May 1963.

12. B. A. Politzer, Comparison of a Numberical Method and the WKB Approximation in the Determination of Transmission Coefficients for Thin Insulating Films, J. Appl. Phys. 37, 279, January 1966.

13. A. Messiah, Quantum Mechanics, p 231. North Holland Publishing Co., N. Y., 1961.

14. J. G. Simmons, Generalized Formula for the Electric Tunneling Effect between Similar Electrodes Separated by a Thin Insulating Film, J. Appl. Phys. 34, 1793, June 1963.

15. R. Holm, The Electric Tunnel Effect Across Thin Insulator Films in Contact, J. Appl. Phys. 22, 569, May 1951.

16. N. Goldberg and S. R. Pollock, Oscillatory Tunneling Current Through Thin Film Insulating Barriers in a Magnetic Field, J. Appl. Phys. 34, 3556, December 1963.

17. C. K. Chow, On Tunneling Equations of Holms and Stratton, J. Appl. Phys. 34, 2490, August 1963.

18. R. Stratton, Volt-Current Characteristics for Tunneling Through Insulating Films, J. Phys. Chem. Solids 23, 1177, 1962.

19. T. E. Hartman, Tunneling Through Asymmetric Barriers, J. Appl. Phys. 35, 3283, November 1964.

20. J. G. Simmons, Generalized Thermal J-V Characteristic for the Electric Tunnel Effect, J. Appl. Phys. 35, 2655, September 1964.

21. D. Meyerhoffer and S. A. Ochs, Current Flow in Very Thin Films of Al_2O_3 and BeO, J. Appl. Phys. 34, 2535, September 1963.

22. E. L. Murphy and R. H. Good Jr., Thermionic Emission, Field Emission, and the Transition Region, Phys. Rev. 102, June 1956.

23. A. H. Wilson, Proc. Roy. Soc. A, B6, 987.

24. N. F. Mott, The Theory of Crystal Rectifiers, Proc. Roy. Soc. A, 171, 27.

25. Miss C. C. Dilworth, The Influence of Surface Films on the Electrical Behavior of Contacts, Proc. Phys. Soc. 60, 315, 1948.

26. J. Bardeen, Tunneling from a Many-Particle Point of View, Phys. Rev. Letters 6, 57, January 1962.

27. W. A. Harrison, Tunneling from an Independent-Particle Point of View, Phys. Rev. 123, 85, July 1961.

28. G. J. Unterkofler, Theoretical Curves of Tunneling Resistivity vs Voltage, J. Appl. Phys. 34, 3143, October 1963.

29. J. G. Simmons, Intrensic Fields in Thin Insulating Films Between Dissimilar Electrodes, Phys. Rev. Letters 10, 10, January 1963.

30. A. C. Fischer and H. I. Moss, Tunnel-Injection Electroluminescence, J. Appl. Phys. 34, 2112, July 1963.

31. D. D. O'Sullivan and E. C. Malarkey, High-Current-Density Injection Electroluminescence in Cadmium Sulfide, Appl. Phys. Letters 6, 5, January 1965.

32. A. S. Groves, E. H. Snow, B. E. Deal, and C. T. Sah, Simple Physical Model for the Space-Charge Capacitance of Metal-Oxide-Semiconductor Surface, D. Appl. Phys. 35, 2458, August 1964.

33. D. V. Geppert, Theoretical Shape of Metal-Insulator Potential Barrier, J. Appl. Phys. 34, 490, March 1963.

34. D. V. Geppert, Experimental Determination of the Shape of Metal-Insulator-Metal Potential Barriers, J. Appl. Phys. 35, 2151, July 1964.

35. N. Goldberg and S. R. Pollock, Effect of Band Structure on Tunneling Currents, J. Appl. Phys. 37, 446, January 1965.

36. I. M. Terman, An Investigation of Surface States at a Silicon/ Silicon Oxide interface Employing-Metal-Oxide-Silicon Diode, Solid State Elect. 5, 285, 1962.

37. K. Lehovec, A. Slobodskoy, and J. L. Sprage, Field Effect-Capacitance Analysis of Surface States on Silicon, Phys. Status. Sod. 3, 447, 1963.

38. S. R. Hofstein and G. Warfield, Physical Limitations of the Frequency Response of a Semiconductor Surface Inversion Layer, Solid-State Electronics 8, 321, 1965.

39. C. K. Chow, Effect of Insulating Film-Thickness Nonuniformity on Tunnel Characteristics, J. Appl. Phys. 34, 2599, September 1963.

40. C. A. Mead, Anomalous Capacitance of Thin Dielectric Structure, Phys. Rev. Letters 6, 545, May 1961.

41. J. C. Penley, A Note on the Anomalous Capacitance of Thin Dielectric Structures, J. Appl. Phys. 33, 2906, September 1962.

42. H. Y. Ku and F. G. Ullman, Capacitance of Thin Dielectric Structures, J. Appl. Phys. 35, 265, February 1964.

43. O. L. Nelson and D. E. Anderson, Potential Barrier Parameters in Thin-Film Al-Al_2O_3 - Metal Diodes, J. Appl. Phys. 37, 77, January 1966.

44. A. J. Dekker, Solid State Physics, Prentice-Hall, Englewood Cliffs, N. J. 1957.

45. J. C. Fisher and I. Giaever, Tunneling Through Thin Insulating Layers, J. Appl. Phys. 32, 172, February 1961.

46. A. Many, Y. Goldstein, and N. B. Grover, Semiconductor Surfaces, North-Holland Publishing Co., Amsterdam, 1965.
a) P - 134
b) P - 189
c) P - 137

47. H. K. Henisch, Rectifying Semi-conductor Contacts, Oxford University Press, London, 1957.
a) P - 182
b) P - 184

48. L. Esaki, J. Phys. Soc. Japan, 8, 347, 1953.

49. R. Williams, Photoemission of Electrons from Silicon into Silicon Dioxide, Phys. Rev. 140, A569, October 1965.

50. L. P. Hunter (Editor), Handbook of Semiconductor Electrons. 2nd Edition Section 8, page 10, 1956.

51. P. V. Gray, Tunneling from Metal to Semiconductor, Doctoral Dissertation, University of Illinois, 1962.

52. R. W. Christy, Electrical Properties of Thin Polymer Films. Part II. Thickness 50 - 150 Å, J. Appl. Phys. 35, 2179, July 1964.

53. Reference Data for Radio Engineers, 4th edition, Federal Telephone and Radio Corp. p 66.

54. P. M. Marcus, Calculation of the Capacitance of a Semiconductor Surface, with Application to Silicon, IBM Journal 8, 496, November 1964.

55. K. H. Zaininger and G. Warfield, Limitations of the MOS Capacitance Method for the Determination of Semiconductor Surface Properties, IEEE Trans. on Electron Devices ED-12, 179, April 1965.

56. K. M. Poole, Electrode Contamination in Electronic Optical Systems, Proc. Phys. Soc. B66, 541, 1953.

57. A. E. Ennos, The Sources of Electron-Inducted Contamination, in Kinetic Vacuum Systems, Brit. J. Appl. Phys. 5, 27, 1954.

58. R. W. Christy, Formation of Thin Polymer Films by Electron Bombardment, J. Appl. Phys. 31, 1680, September 1960.

59. H. T. Mann, Electrical Properties of Thin Polymer Films. Part I. Thickness 500-2500 Å, J. Appl. Phys. 35, 2173, July 1964.

60. J. G. Simmons, Electric Tunnel Effect between Dissimilar Electrodes Separated by a Thin Insulating Film, J. Appl. Phys. 34, 2581, September 1963.

61. T. E. Hartman and J. S. Chivian, Electron Tunneling Through Thin Aluminum Oxide Films, Phys. Rev. 134, A1094, May 1964.

62. C. K. Chow, Temperature Dependence of BeO Tunneling Structures, J. Appl. Phys. 34, 2918, September 1963.

63. J. R. Yeargan, D. R. Harbison, and H. L. Taylor, MOS Capacitance Dissipation Properties, Southwestern IEEE Conference Record (1966).

64. J. Joffe, Schottky's Theories of Dry Solid Rectifiers, Electrical Communication 22, 217, 1945.

65. L. J. Giacoletto and J. O'Connell, A Variable Capacitance Germanium Junction Diode for UHF, RCA Reviews 17, 68, March 1956.

66. C. G. B. Garrett and W. H. Brattain, Physical Theory of Semiconductor Surfaces, Phys. Rev. 99, 376, July 1955.

67. L. J. Giacoletto, Junction Capacitance and Related Characteristics Using Graded Impurity Semiconductors IRE Trans., ED 4, 207, 1957.

68. M. M. Atalla, E. Tannbaum, E. J. Scheiber, Stabilization of Silicon Surfaces by Thermally Grown Oxides, Bell System Tech. J. 38, 749, May 1959.

Security Classification

DOCUMENT CONTROL DATA - R&D

(Security classification of title, body of abstract and indexing annotation must be entered when the overall report is classified)

1. ORIGINATING ACTIVITY (Corporate author)	2a. REPORT SECURITY CLASSIFICATION
Laboratories for Electronics and Related Science Research The University of Texas, Austin 78712	Unclassified
	2b. GROUP

3. REPORT TITLE

TUNNELING BETWEEN A METAL AND SILICON SEPARATED BY A POLYMER INSULATOR

4. DESCRIPTIVE NOTES (Type of report and inclusive dates)

Technical Report No. 25 September 15, 1966

5. AUTHOR(S) (Last name, first name, initial)

Wilmsen, Carl W.
Hartwig, William H.

6. REPORT DATE	7a. TOTAL NO. OF PAGES	7b. NO. OF REFS
September 15, 1966	123	30

8a. CONTRACT OR GRANT NO.	9a. ORIGINATOR'S REPORT NUMBER(S)
AR-AFOSR 766-66 b. PROJECT NO.	JSEP Technical Report No. 25
c.	9b. OTHER REPORT NO(S) (Any other numbers that may be assigned this report)
d.	

10. AVAILABILITY/LIMITATION NOTICES

Qualified requesters may obtain copies of this report from DDC

11. SUPPLEMENTARY NOTES	12. SPONSORING MILITARY ACTIVITY
Includes Research monitored by the Dept. of Defense's Joint Services Electronics Program through the Tech. Advisory Committee (U.S. Army, Navy, and Air Force), with partial support by the NASA Grants 8-11235 and NGR 44-012-043	U.S. Air Force Office of Scientific Research, Washington, D.C. 20333, and others.

13. ABSTRACT This research investigates tunneling between a metal and silicon separated by an insulator (MIS structure) and develops a model describing the MIS current-voltage characteristics. Analysis shows that any model for MIS tunneling must consider the density of surface states and the formation of a depletion or accumulation layer in the silicon. The model shows that the electric field in the insulator controls the MIS current while the charge distribution in the silicon determines the insulator field.

For the experimental results presented in this report a polymerized silicone film formed the insulator. After establishing the technique of forming the polymer, metal - insulator (MIM) junctions enabled study of the electrical properties of the polymer and characterization of MIM tunneling currents. The MIM characteristics permitted comparative analysis with MIS structures.

The experimental MIS curves on both N and P type silicon show the exponential dependence of current on voltage and they indicate that the mechanisms for MIM and MIS tunneling are quite similar. An asymmetric saturation of the MIS tunneling occurs. This is shown to be caused by the formation of a depletion layer on the semiconductor which forms after completely charging the surface states. Experimental evidence verified this model. The distinct roles played by the surface states, the depletion layer, insulator thickness, temperature and the work function of the field plate metal appears in the analysis.

DD FORM 1 JAN 64 1473

Security Classification

14. KEY WORDS	LINK A		LINK B		LINK C	
	ROLE	WT	ROLE	WT	ROLE	WT
Tunneling Semiconductor Surface States Thin Films MOS Structures						

INSTRUCTIONS

1. ORIGINATING ACTIVITY: Enter the name and address of the contractor, subcontractor, grantee, Department of Defense activity or other organization *(corporate author)* issuing the report.

2*a*. REPORT SECURITY CLASSIFICATION: Enter the overall security classification of the report. Indicate whether "Restricted Data" is included. Marking is to be in accordance with appropriate security regulations.

2*b*. GROUP: Automatic downgrading is specified in DoD Directive 5200.10 and Armed Forces Industrial Manual. Enter the group number. Also, when applicable, show that optional markings have been used for Group 3 and Group 4 as authorized.

3. REPORT TITLE: Enter the complete report title in all capital letters. Titles in all cases should be unclassified. If a meaningful title cannot be selected without classification, show title classification in all capitals in parenthesis immediately following the title.

4. DESCRIPTIVE NOTES: If appropriate, enter the type of report, e.g., interim, progress, summary, annual, or final. Give the inclusive dates when a specific reporting period is covered.

5. AUTHOR(S): Enter the name(s) of author(s) as shown on or in the report. Enter last name, first name, middle initial. If military, show rank and branch of service. The name of the principal author is an absolute minimum requirement.

6. REPORT DATE: Enter the date of the report as day, month, year; or month, year. If more than one date appears on the report, use date of publication.

7*a*. TOTAL NUMBER OF PAGES: The total page count should follow normal pagination procedures, i.e., enter the number of pages containing information.

7*b*. NUMBER OF REFERENCES: Enter the total number of references cited in the report.

8*a*. CONTRACT OR GRANT NUMBER: If appropriate, enter the applicable number of the contract or grant under which the report was written.

8*b*, 8*c*, & 8*d*. PROJECT NUMBER: Enter the appropriate military department identification, such as project number, subproject number, system numbers, task number, etc.

9*a*. ORIGINATOR'S REPORT NUMBER(S): Enter the official report number by which the document will be identified and controlled by the originating activity. This number must be unique to this report.

9*b*. OTHER REPORT NUMBER(S): If the report has been assigned any other report numbers *(either by the originator or by the sponsor)*, also enter this number(s).

10. AVAILABILITY/LIMITATION NOTICES: Enter any limitations on further dissemination of the report, other than those imposed by security classification, using standard statements such as:

(1) "Qualified requesters may obtain copies of this report from DDC."

(2) "Foreign announcement and dissemination of this report by DDC is not authorized."

(3) "U. S. Government agencies may obtain copies of this report directly from DDC. Other qualified DDC users shall request through _____."

(4) "U. S. military agencies may obtain copies of this report directly from DDC. Other qualified users shall request through _____."

(5) "All distribution of this report is controlled. Qualified DDC users shall request through _____."

If the report has been furnished to the Office of Technical Services, Department of Commerce, for sale to the public, indicate this fact and enter the price, if known.

11. SUPPLEMENTARY NOTES: Use for additional explanatory notes.

12. SPONSORING MILITARY ACTIVITY: Enter the name of the departmental project office or laboratory sponsoring *(paying for)* the research and development. Include address.

13. ABSTRACT: Enter an abstract giving a brief and factual summary of the document indicative of the report, even though it may also appear elsewhere in the body of the technical report. If additional space is required, a continuation sheet shall be attached.

It is highly desirable that the abstract of classified reports be unclassified. Each paragraph of the abstract shall end with an indication of the military security classification of the information in the paragraph, represented as *(TS), (S), (C), or (U)*.

There is no limitation on the length of the abstract. However, the suggested length is from 150 to 225 words.

14. KEY WORDS: Key words are technically meaningful terms or short phrases that characterize a report and may be used as index entries for cataloging the report. Key words must be selected so that no security classification is required. Identifiers, such as equipment model designation, trade name, military project code name, geographic location, may be used as key words but will be followed by an indication of technical context. The assignment of links, rules, and weights is optional

GPO 886-551